KAUNAS UNIVERSITY OF TECHNOLOGY

TADAS DAMBRAUSKAS

SYNTHESIS AND FUNCTIONAL PROPERTIES OF α-C_2SH, KILCHOANITE AND HYDROXYLEDGREWITE

Doctoral dissertation
Technological Sciences, Chemical Engineering (T 005)

2019, Kaunas

This doctoral dissertation was prepared at Kaunas University of Technology, Faculty of Chemical Technology, Department of Silicate Technology during the period of 2015–2019. The studies were supported by the Research Council of Lithuania.

Scientific Supervisor:

Prof. Dr. Kęstutis Baltakys (Kaunas University of Technology, Technological Sciences, Chemical Engineering, T 005).

Doctoral dissertation has been published in:
http://ktu.edu

Editor:

Armandas Rumšas (Publishing Office "Technologija")

ISBN 978-609-02-1583-8

The bibliographic information about the publication is available in the National Bibliographic Data Bank (NBDB) of Martynas Mažvydas National Library of Lithuania.

KAUNO TECHNOLOGIJOS UNIVERSITETAS

TADAS DAMBRAUSKAS

α-C_2SH, KILCHOANITO BEI HIDROKSILEDGREVITO SINTEZĖ IR JŲ FUNKCINĖS SAVYBĖS

Daktaro disertacija
Technologiniai mokslai, Chemijos inžinerija (T 005)

2019, Kaunas

Disertacija rengta 2015–2019 metais Kauno technologijos universiteto Cheminės technologijos fakultete, Silikatų technologijos katedroje. Mokslinius tyrimus rėmė Lietuvos mokslo taryba.

Mokslinis vadovas:

Prof. dr. Kęstutis BALTAKYS (Kauno technologijos universitetas, technologiniai mokslai, chemijos inžinerija, T005).

Interneto svetainės, kurioje skelbiama disertacija, adresas:
http://ktu.edu

Redagavo:

Armandas Rumšas (leidykla "Technologija")

ISBN 978-609-02-1583-8

Leidinio bibliografinė informacija pateikiama Lietuvos nacionalinės Martyno Mažvydo bibliotekos Nacionalinės bibliografijos duomenų banke (NBDB).

Table of contents

Abbreviations 6
Introduction 7
1. Literature Review 10
1.1. Classification of calcium silicate hydrates 10
1.2. Synthesis, properties and structure of high basicity calcium silicates and calcium silicate hydrates 14
1.3. The application of calcium silicates and calcium silicate hydrates on environmentally friendly cementitious materials 22
2. Materials and Methods 25
3. Results and Discussion 31
3.1. Formation of α-C_2SH in $1.5CaO–(1-x)SiO_2 \cdot nH_2O–xAl_2O_3–H_2O$ suspensions at 175 °C and application as a precursor for binder material 31
3.1.1. Hydrothermal synthesis of α-C_2SH and α-C_2SH–Al 31
3.1.2. Thermal stability of α-C_2SH and α-C_2SH–Al 37
3.1.3. Hydration properties of BM based on α-C_2SH or α-C_2SH–Al 39
3.1.4. Hydration properties of BM based on α-C_2SH or α-C_2SH–Al and quartz sand 42
3.2. Formation of α-C_2SH in $1.75CaO–(1-x)SiO_2 \cdot nH_2O–xAl_2O_3–H_2O$ suspensions at 175 °C 48
3.3. Formation of α-C_2SH in $1.5CaO–(1-x)SiO_2 \cdot nH_2O–xAl_2O_3–H_2O$ suspensions at 200 °C and application as a precursor for binder material 52
3.3.1. Hydrothermal synthesis of α-C_2SH in a pure system 52
3.3.2. The influence of γ-Al_2O_3 on dibasic calcium silicates hydrates crystallization at 200 °C 58
3.3.3. Hydration peculiarities of α-C_2SH and quartz sample 68
3.4. Hydrothermal synthesis of kilchoanite and application as a precursor for binder material 72
3.4.1. Hydrothermal synthesis 72
3.4.2. Thermal stability 75
3.4.3. Hydration properties 78
3.5. Hydrothermal synthesis of hydroxyledgrewite and its properties 80
3.6. Microstructure of synthetic and calcined α-C_2SH, kilchoanite and hydroxyledgrewite 86
3.6.1. Microstructure of synthetic products 86
3.6.2. Microstructure of calcined products 90
4. Conclusions 94
References 95
List of scientific publications 106
Acknowledgments 109

Abbreviations

CSH – calcium silicate hydrate
C-S-H – semicrystalline type compounds C-S-H(I) and/or C-S-H(II)
C/S – the molar ratio of CaO and SiO_2
CA – calcium aluminate silicate and/or calcium aluminate
α-C_2SH – α-dicalcium silicate hydrate ($2CaO \cdot SiO_2 \cdot H_2O$)
α-C_2SH –α-dicalcium silicate hydrate sample without γ-Al_2O_3 additive
α-C_2SH-Al – α-dicalcium silicate hydrate sample with γ-Al_2O_3 additive
BM – binder material
OPC – ordinary Portland cement
EFCM – environmentally friendly cementitious material
BM-α – binder material based on α-C_2SH
BM-α-Q – binder material based on α-C_2SH and quartz
BM-α-Al – binder material based on α-C_2SH-Al
BM-α-Al-Q – binder material based on α-C_2SH-Al and quartz
BM-k-Q – binder material based on kilchoanite and quartz
BM-e – binder material based on hydroxiledgrewite and granite cutting waste
C_2S – dicalcium silicate ($2CaO \cdot SiO_2$)
XRD – X-ray diffraction analysis
QXRD – quantitative X-ray diffraction analysis
FT-IR – Fourier-transform infrared spectroscopy
STA – simultaneous thermal analysis
DSC – differential scanning calorimetry
QDSC – quantitative differential scanning calorimetry analysis
TG – thermogravimetry
w/s – water to solid ratio
SEM – scanning electron microscopy
TEM – transmission electron microscopy
C_P – specific heat capacity
S_a – surface area

Introduction

According to scholarly literature, in 2016, the global greenhouse gas emission reached about 49 Gt, and it still continues to grow, while the largest part (~65 %) of the greenhouse gas emitted through human activities is carbon dioxide. In fact, the cement industry accounts for approximately 4–6 % of global CO_2 emissions. This gas is released during limestone calcination and fuel combustion. Also, while manufacturing cement, a considerable quantity of energy (4.7–6.3 GJ/t) is used. For these reasons, the cement industry and the scientific community have been looking for alternative approaches in order to reduce the harmful effects on the environment. Seeking these goals, the cement industry not only uses alternative fuels, various additives and waste but also focuses on the development of new production technologies. However, the application of the above mentioned technologies can only partially reduce the negative effects on the environment. Thus it is generally recognized that, in order to reduce CO_2 emission and energy consumption, a new technologies for the development of environmentally friendly cementitious materials (EFCM) should be created and applied worldwide. The main feature of EFCM ("Celitement", "Solidia cement", "Calcium sulfoaluminate cement", "Magnesia-based cements," etc.) is that the energy consumption and the CO_2 emissions associated with cement production can be reduced within the range of 30–70 %. One of the most attractive ways to obtain EFCM is the production in a three-step process: 1) hydrothermal synthesis of higher basicity calcium silicate hydrate or calcium silicate (CaO/SiO_2 ratio from 1.25 to 2.0); 2) mechanochemical or thermal treatment of hydrothermal products together with siliceous raw materials such as sand, blast-furnace slag, glass, etc. or silica (usually 1:1); 3) cement curing in the water or CO_2 atmosphere. It is known that the properties of environmentally friendly cementitious materials depend on the mineral composition of products obtained during hydrothermal treatment. For these reasons, the synthesis, structure and chemistry of the above mentioned compounds have been studied by many scientists, yet their opinions seem to differ.

Recently, the synthesis and properties of dibasic calcium silicate hydrate – α-C_2SH –have regained interest because on its basis a new hydraulic cementitious material has been created. The synthesis of α-C_2SH is possible from lime and quartz/amorphous silica/silica acid mixtures or from dibasic calcium silicate (C_2S) polymorphs. According to several sources, α-C_2SH forms quite easily under hydrothermal conditions from CaO and silicic acid as the starting materials in the temperature range of 150–200 °C. Crystallization from quartz is very slow with the best results being obtained while using C_2S polymorphs as the starting material.

Kilchoanite, a polymorph of rankinite, can be used for the manufacturing of carbonatable calcium silicate cements. This compound could be prepared from mixtures of lime and quartz at 280–600 °C temperature and at 50–100 MPa pressure. In addition, by using the rapid heating method, γ-dicalcium silicate was formed as an initial product from mixtures of lime and silica acid, and it was replaced by kilchoanite and a small amount of $8CaO{\cdot}5SiO_2$ at 220–250 °C temperature.

Hydroxyledgrewite is the hydroxyl analogue of edgrewite, approved in 2012. Hydroxyledgrewite belongs to the nesosilicates or orthosilicates group; these silicates possess the lowest degree of polymerization possible, namely C-S-H phases with isolated silicon tetrahedra (Q0). Due to the similarities of the structures of hydroxyledgrewite and α-C_2SH, it may be possible to use it in alternative cementitious materials.

As a matter of fact, in the context of reducing environmental issues, economically attractive technologies for the synthesis of calcium silicates and/or calcium silicates hydrates, which can be used for the production of EFCM, are in great demand.

The aim of this work is to create an innovative preparation technique for the production of an environmentally friendly cementitious material which will combine the hydrothermal synthesis of calcium silicates and/or calcium silicates hydrates and their solid-state sintering at a low temperature.

The goals of this work are:

1) to investigate the influence of primary mixtures composition ($CaO/(SiO_2+Al_2O_3)$=1.5–2.25) and hydrothermal synthesis parameters on the formation processes of calcium silicates and calcium silicates hydrates;
2) to determine the effect of mechanochemical and thermal activation on the stability of synthesis products and their derivative physical and chemical properties;
3) to investigate the hydration mechanism and strength properties of binding materials prepared by using synthetic α-C_2SH, kilchoanite, hydroxyledgrewite and quartz.

Statements presented for defense:

1) the thermal activation conditions of quartz and α-C_2SH, kilchoanite or hydroxyledgrewite samples have a critical influence on the properties of created binding materials;
2) the developed conditions of hydrothermal treatment allow producing calcium silicates and/or calcium silicates hydrates from a non-stoichiometric initial mixture.

Scientific novelty of the research:

1) a new methodology for the formation of anhydrous calcium silicate – kilchoanite – under hydrothermal conditions was developed.
2) for the first time, a dibasic calcium silicate hydrate, hydroxyledgrewite ($Ca_9(SiO_4)_4(OH)_2$), was synthesized under hydrothermal conditions (CaO/SiO_2=2.25; 48 h; 200 °C), its physical and chemical properties were investigated, and this compound was used for the production of an environmentally friendly cementitious material.

Practical significance of the scientific research:

An innovative preparation technique for the production of environmentally friendly cementitious materials which combines the hydrothermal synthesis of precursors and their solid-state sintering at a low temperature is developed. The properties of the created materials correspond to the requirements of belite and special low-heat cements. The obtained environmentally friendly cementitious materials can be used as an alternative for the ordinary Portland cement. The preparation technique of the above mentioned materials requires a 600–1000 °C lower calcination temperature as well as a lower quantity of calcium carbonate, which leads to lower CO_2 emissions.

Approval and publication of the research results:

The results of the dissertation were published in 6 scientific publications included in the Clarivate Analytics Web of Science database: 4 of them were published in the *Journal of Thermal Analysis and Calorimetry*; 1 in *Scientia Iranica C* and 1 in the *Journal of the American Ceramic Society*. In addition, the results were presented in one scientific publication included in the Scopus database (*Solid State Phenomena*), and one patent was registered at the National Patent Office.

The results were presented in 7 conferences, 6 of which were international: "BaltSilica 2018" (2018, Latvia), "International Conference of Thermal Analysis and Calorimetry in Russia (RTAC-2016)" (2016, Russia), "18th international Conference-School Advanced Materials and Technologies" (2016, Lithuania), "BaltSilica 2016" (2016, Lithuania), "Particulate Solids in Science, Industry and the Environment 2015" (2015, Slovakia), "3rd Central and Eastern European Conference on Thermal Analysis and Calorimetry" (2015, Slovenia).

Structure and contents of the dissertation:

The dissertation consists of the introduction, literature overview, experimental part, results and discussion, conclusions and the list of references and publications on the dissertation topic. The list of references features 188 bibliographic sources. The main results are discussed on 110 pages and illustrated in 14 tables and 67 figures.

The contribution of the author and co-authors:

The author synthesized and described all the dibasic calcium silicate hydrates which are mentioned in the thesis, examined the peculiarities of early hydration of the obtained environmentally friendly cementitious material, determined the compressive strength of the binder material and performed thermodynamic calculations. Kęstutis Baltakys advised on the progress of the experiment and the preparation of the manuscripts. Anatolijus Eisinas consulted on the synthesis and thermodynamic calculations. Raimundas Šiaučiūnas advised on the hydrothermal synthesis of calcium silicates. Jelena Škamat and Andrius Kudžma consulted on microcalorimetry technique.

1. Literature Review

1.1 Classification of calcium silicate hydrates

Calcium silicate hydrates (C-S-H) whose formula is expressed by the molar ratio of constituent components $xCaO{\cdot}ySiO_2{\cdot}zH_2O$ (where indexes *x*, *y*, *z* stand for the number of moles) are a silicic acid salt (1, 2). Many of these compounds are found as natural minerals while others can be produced either by air curing, e.g., cement or concrete (2, 3), or hydrothermally by high pressure steam treatment in an autoclave (4). The production processes for fiber cement, calcium silicate boards and autoclaved aerated concrete cover the whole range of calcium silicate hydrates from poorly crystallized to well crystallized ones(3, 5). The hydration products of Portland cement are primary calcium silicate hydrate gels which are a mixture of poorly crystallized particles.

The ternary $CaO\text{-}SiO_2\text{-}H_2O$ system includes more than 40 calcium silicate hydrates ranging from amorphous to crystalline compounds with various compositions in a wide range of CaO/SiO_2 ratio between 0.44–3.0 (1, 6–8). They can be used as fillers, as adsorbents, as bioactive materials, as environmentally friendly cementitious materials and in other fields (9–18). It is known that the crystallization reaction and the peculiarities of C-S-H depend on many factors, such as the type of silica, CaO/SiO_2 molar ratio, the curing conditions, the surface area of materials, the amount of water and the type of lime, and the pollution of raw materials(1, 19–25). For these reasons, C-S-H is the subject of numerous scientific studies. However, the literature concerning the formation and peculiarities of C-S-H is not unequivocal. The most recognized classification of C-S-H was presented by H. F. W. Taylor and R. M. Roy which was supplemented in 1996 by W. Kraus and G. Nolze and in 2008 by I.G. Richardson (1). This classification consists of wollastonite, tobermorite, jennite, gyrolite, $\gamma\text{-}C_2S$, and other groups of C-S-H (Table 1.1).

Table 1.1. Classification of calcium silicate hydrates(1)

Name	Formula	CaO/SiO_2
Wollastonite group		
Foshagite	$Ca_4(Si_3O_9)(OH)_2$	1.33
Hillebrandite	$Ca_2(SiO_3)(OH)_2$	2.0
Nekoite	$Ca_3Si_6O_{15}\cdot 7H_2O$	0.5
Okenite	$[Ca_8(Si_6O_{16})(Si_6O_{15})\cdot 2(H_2O)_6]^{4-}[Ca_2(H_2O)_9\cdot 3H_2O]^{4+}$	0.56
Pectolite	$Ca_2NaHSi_3O_9$	1.0
Wollastonite 1A	$Ca_3Si_3O_9$	1.0
Xonotlite	$Ca_6Si_6O_{17}(OH)_2$	1.0
Tobermorite group		
Clinotobermorite	$Ca_5Si_6O_{17}\cdot 5H_2O$	0.83
Clinotobermorite 9 Å	$Ca_5Si_6O_{16}(OH)_2$	0.83
Oyelite	$Ca_{10}B_2Si_8O_{29}\cdot 12.5H_2O$	1.25
9 Å tobermorite (riversideite)	$Ca_5Si_6O_{16}(OH)_2$	0.83
Anomalous 11 Å tobermorite	$Ca_4Si_6O_{15}(OH)_2\cdot 5H_2O$	0.67
Normal 11 Å tobermorite	$Ca_{4.5}Si_6O_{16}(OH)\cdot 5H_2O$	0.75
14Å tobermorite (plombierite)	$Ca_5Si_6O_{16}(OH)_2\cdot 7H_2O$	0.83
C-S-H(I)		<1.5
Jennite group		
Jennite	$Ca_9Si_6O_{18}(OH)_6\cdot 8H_2O$	1.5
Metajennite	$Ca_9Si_6O_{18}(OH)_6\cdot 8H_2O$	1.5
C-S-H(II)		>1.5
Gyrolite Group		
Fedorite	$(Na,K)_2(Ca,Na)_7(Si,Al)_{16}O_{38}(F,OH)2\cdot 3.5H_2O$	0.56
Gyrolite	$NaCa_{16}Si_{23}AlO_{60}(OH)_8\cdot 14H_2O$	0.71
K-phase	$Ca_7Si_{16}O_{38}(OH)_2$	0.44
Reyerite	$Na_2Ca_{14}Si_{22}Al_2O_{58}(OH)_8\cdot 6H_2O$	0.67
Truscottite	$Ca_{14}Si_{24}O_{58}(OH)_8\cdot 2H_2O$	0.58
Z-phase	$Ca_9Si_{16}O_{40}(OH)_2\cdot 14H_2O$	0.56
γ-C_2S group		
Calcium chondrodite	$Ca_5(SiO_4)_2(OH)_2$	2.5
Kilchoanite	$Ca_6(SiO_4)(Si_3O_{10})$	1.5
Pavlovskyite or C_8S_5	$Ca_8(SiO_4)_2(Si_3O_{10})$	1.6
Other calcium silicate phases		
Afwillite	$Ca_3(SiO_3OH)_2\cdot 2H_2O$	1.5
α-C_2SH	$Ca_2(HSiO_4)(OH)$	2.0
Cuspidine	$Ca_4(F_{1.5}(OH)_{0.5})Si_2O_7$	2.0
Dellaite	$Ca_6(Si_2O_7)(SiO_4)(OH)_2$	2.0
Jaffeite	$Ca_6[Si_2O_7](OH)_6$	3.0
Killalaite	$Ca_{6.4}(H_{0.6}Si_2O_7)_2(OH)_2$	1.6
Poldervaartite	$Ca(Ca_{0.67}Mn_{0.33})(HSiO_4)(OH)$	2.0
Rosenhahnite	$Ca_3Si_3O_8(OH)_2$	1.0
Suolunite	$CaSiO_{2.5}(OH)\cdot 0.5H_2O$	1.0
Tilleyite	$Ca_5Si_2O_7(CO_3)_2$	2.5
Y-phase	$Ca_6(Si_2O_7)(OH)_6$	2.0
Other high temperature cement phases		
Bicchulite	$Ca_2(Al_2SiO_6)(OH)_2$	0.67
Fukalite	$Ca_4(Si_2O_6)(CO_3)(OH)_2$	2.0
Katoite Hydrogarnet	$Ca_{1.46}AlSi_{0.55}O_6H_{3.78}$	0.94
Rustumite	$Ca_{10}(Si_2O_7)_2(SiO_4)Cl_2(OH)_2$	2.0
Scawtite	$Ca_7(Si_6O_{18})(CO_3)\cdot 2H_2O$	1.17

Wollastonite group minerals arewidely used in the industry. *Xonotlite* is an ultra-light insulation material which has a number of beneficial properties: low thermal conductivity, wide application temperature range, environmental friendliness and low density (26, 27). This compound can be easily synthesized under hydrothermal conditions at 190–400 °C when the molar ratio of the primary mixture is C/S=1.0 (28, 29). Meanwhile, *wollastonite* is a white glassy silicate material formed as a deposit or as tabular crystals of metamorphosed limestone (30). It has wide application and is used in concrete, as a coating material, in porcelain, etc. Due to the special properties, such as biocompatibility, bioactivity, degradability, low shrinkage and good strength properties, wollastonite has been used widely in biomedicine (9–11, 30–32). In practice, for the synthesis of wollastonite, various raw materials and methods, such as using diatomite, SiO_2 dust from filters, slag, synthesizing at low temperature, a solid state reaction, fusion and the hydrothermal process are applied (9, 33). Recently, more and more interest has been paid to *hillebrandite* because its basis environmentally friendly cementitious materials have been created (2, 15, 34). The formation of this hydrate is related to the reactivity and homogeneity of the starting materials mixture as well as the concentration of the aqueous suspension. By the thermal dissociation of hillebrandite, at temperatures ranging from 500 °C to700 °C, β-C_2S can be obtained, which is stable at room temperature and highly reactive (35, 36).

Tobermorite group minerals. Tobermorite is a type of crystalline calcium silicate which occurs in the nature where it was formed in an alkaline environment under hydrothermal condition. Many studies have shown that tobermorite fibers exhibit several excellent characteristics, such as light weight, flame-retardant and high compressive strength, which makes it very efficient as a heat insulating and fire-resistant building material (37–41). The most important type is 11 Å tobermorite which is the major phase found in aerated autoclaved concretes (39). Tobermorite can be synthesized by hydrothermal synthesis in the $CaO–SiO_2–H_2O$ system, but other different approaches, such as microwave-assisted synthesis or mechanochemical synthesis, have also been successfully applied (37–39). However, many variable factors exert influence on the obtained amount and morphology of synthesized tobermorite. For this reason, natural tobermorite is usually more highly crystalline than synthetic tobermorite.

Jennite group minerals. Jennite is a rare natural mineral usually found in contact with 14 Å tobermorite. It can be synthesized hydrothermally in a CaO and SiO_2 mixture within the 60–100 °C temperature range (1, 23, 42, 43). Jennite is an important structural prototype of C–S–H gel that is a major component of cement hydrate. For this reason, the structure, dynamics, and the mechanical properties of jennite have been investigated by many authors (1, 23, 42, 43, 44). The crystal structure of jennite is composed of tilleyite ribbons of edge-sharing calcium octahedral, Si–O dreierketten chains running along [010], and additional calcium octahedral sitting in between the chains.

Gyrolite group minerals. The compounds of this group are commonly found in volcanic and basaltic rocks, voids or gaps; they exist only together with related minerals (24, 45, 46). Gyrolite group compounds can be synthesized under

hydrothermal conditions (150–350 °C) in CaO and SiO_2 mixtures (with the molar ratio of CaO and SiO_2 being equal to ~0.66). However, the outlined synthesis route is a very complex and time consuming process. In recent years, the interest in gyrolite has grown considerably because this mineral can be used as an adsorbent (24, 45, 46). *Gyrolite* is commonly synthesized under hydrothermal conditions from amorphous silica, but, according to the studies when crystalline quartz is used as the SiO_2 source, it is impossible to obtain this compound even after 168 h of hydrothermal treatment at 200 °C (7, 45, 47). Synthesis of gyrolite strongly depends on the SiO_2 source; due to the low quartz solubility rate, the solution contains significant excess of Ca ions (46). It is associated with forming compounds featuring a higher Ca/SiO_2 ratio (tobermorite, xonotlite) than it was expected under stoichiometric composition of the starting materials. In the case of amorphous silica, pure gyrolite can be synthesized at 175 °C after 72 h and at 200 °C after 32 h (24, 25, 45–49).

γ-C_2S group minerals. Literature data on the minerals of this group is fairly limited. *Kilchoanite* and *C_8S_5* belong to sorosilicates with $[Si_3O_{10}]^{-8}$ and $[SiO_4]^{-4}$ groups. These minerals have both isolated tetrahedra (Q0) and finite triple chains. The silicon tetrahedra are connected to 6 and 8-fold coordinated calcium atoms (44).

Other calcium silicate hydrate phases. Most of these compounds are less significant for the cement and binding materials chemistry; however, they are widely used elsewhere.

Afwillite is denoted by low density, heat-insulating and incombustible properties. It is known that afwillite is usually synthesized by the hydrothermal reaction of lime and silica under hydrothermal conditions at temperatures above 200 °C. Nevertheless, it was reported that afwillite can be obtained by mechanochemical synthesis or during the hydration of tricalcium silicate. Horgnies *et al*. (50) describe that, under mechanochemical synthesis conditions, the afwillite content in the (dry) solids exceeds 54% after 2 days, which represents about 90% of the theoretical maximum possible. Also, these authors found that afwillite during C_3S hydration can be used as a dry powder or as an accelerator, and that hydrated C_3S pastes with an afwillite additive have much lower drying shrinkages than their analogues.

Cuspidine is a rare mineral which is usually obtained as a hydrothermal or solid-state reactions product. Cuspidine is used as a mold flux which plays the decisive role in a casting mold during commercial continuous casting of steels: it controls the horizontal mold heat transfer and lubricating the solidified steel shell from the oscillating mold (51–55).

α-C_2SH is a fairly common compound formed during the hardening of autoclaved calcium silicate products; it has gained new interest because on its basis a family of new hydraulic cementitious materials has been created (56–59).

Other high temperature cement phases. These compounds are less significant for the industry, and only katoite hydrogarnet is widely used in ordinary Portland cement and aluminate cement.

The synthesis, properties and structure of the compounds with molar ratio C/S = 0.8–1.0 (11 Å tobermorite, xonotlite) have been analyzed in detail (26, 29, 60–65). Recently, the synthesis, properties and the structure of dibasic calcium

silicate hydrates have recovered major interest because, on its bases, environmentally friendly cementitious materials (EFCM) which are not only less costly energy-wise but also less harmful to the nature (13, 15, 56, 57, 66, 67) have been developed. However, the properties and the crystallization reaction of the precursors (calcium silicate hydrates)for EFCM depend on many factors, such as the type of silica, CaO/SiO_2 molar ratio, the curing conditions, the surface area of materials, the amount of water, the type of lime, and the pollution of raw materials (23–25, 59). In order to successfully use calcium silicates hydrates in the EFCM technologies, it is necessary to determine the crystallization reactions and the properties of the above mentioned compounds.

1.2 Synthesis, properties and structure of high basicity calcium silicates and calcium silicate hydrates

α-C_2SH ($Ca_2(SiO_3OH)(OH)$) is dibasic calcium silicate hydrate which does not exist in the natural environment and forms during hydrothermal synthesis (56). α-C_2S hydrate was first discovered in steam-cured Portland cement mortars by Thorvaldson and Shelton who also described its optical properties. It has since been prepared under hydrothermal conditions either from calcium oxide and silica gel or from anhydrous dicalcium silicates (68). α-C_2SH is produced primarily in the process used to form 11 Å tobermorite when a suspension of calcium hydroxide and fairly large size quartz is hydrothermally treated at about 155 °C. The thermal and spectroscopic properties of this phase have been reported in (69, 70). Whereas the reassignment of powder diffraction peaks has been reported, the crystal structure has not been refined since Heller's original study (71). Heller (71) discovered that, under the conditions studied (100–200 °C; up to 7 days), the initial product was usually calcium silicate hydrate (I). Further treatment yielded α-C_2SH and finally hillebrandite and/or afwillite. α-$C_2SH$was synthesized from mixtures of lime slurry and quartz in compositions with 1.8 to 2.4 CaO/SiO_2 molar ratios (72). However, this series of compounds, free of all contaminants, showed X-ray patterns containing many or nearly all lines of crystalline $Ca(OH)_2$. Synthesis is possible from lime and quartz (73-75) or amorphous silica (76) or silica acid (77, 78) mixtures or from dibasic calcium silicate (C_2S) polymorphs (77, 79). According to several sources (77, 78), α-C_2SH forms quite easily under hydrothermal conditions from CaO and silicic acid as the starting materials in the temperature range of 150–200 °C. Crystallization from quartz is very slow, with the best results being obtained when using C_2S polymorphs as the starting material (79, 80). As indicated by Taylor (68), seeding aids the formation of α-C_2SH under hydrothermal conditions.

Hong and Glasser (23) constructed phase relations in the lime-rich (>50% $Ca(OH)_2$) portion of the $CaO–SiO_2–H_2O$ system at saturated steam pressures (Ca/Si=0.83–3.0; 55–220 °C; 360 days). It should be underlined that α-C_2SH was always formed together with portlandite.

Kalousek *et al*. (72) studied the effects of two forms of silica, quartz and silicic acid, the methods of mixing, and autoclaving conditions on the formation of the lime-rich crystalline calcium silicate hydrates designated as alpha-, beta-, and gamma-type hydrates. α-$C_2SH$was synthesized from mixtures of lime slurry and

quartz in compositions with 1.8 to 2.4 CaO/SiO_2 molar ratios. However, this series of compounds, free of all contaminants, showed X-ray patterns containing many or nearly all lines of crystalline $Ca(OH)_2$.

Black *et al*. (40) prepared by hydrothermal treatment a number of crystalline calcium-silicate-hydrate (C-S-H) phases with calcium–silicon ratios varying from approximately 0.5 (K-phase) to 2.0 (hillebrandite and α-dicalcium silicate hydrate). They showed that X-ray photoelectron spectroscopy (XPS) can be used to obtain valuable structural information for C-S-H phases. Thus the formation of α-C_2SH from different mixtures (with molar ratio C/S=2) is a complex and long-term process because of a low solubility of CaO-containing compounds and/or reactivity of raw materials. In order to accelerate the interaction between intermediary compounds in the CaO–amorphous SiO_2–H_2O system and to avoid unreacted portlandite in the products, the molar ratio (C/S) of the initial mixture was reduced to1.75.

Hu *et al*. (81) determined that α-C_2SH is stable at low temperatures and starts to decompose at 180 °C to form Ca-rich jaffeite and finally dellaite at 350 °C for 8 days. Hillebrandite was a stable phase at lower temperatures than 350 °C, but was transformed directly to dellaite at temperatures higher than 350 °C within 1–2 days. Dellaite was reversibly transformed to hillebrandite at lower temperatures below 300 °C with the formation of a small amount of the C-S-H compounds with a C/S ratio of 1.5. Meanwhile, hillebrandite is stable only over a short range of temperature between 160 °C and 210 °C whereas at higher temperatures it decomposes to α-C_2SH and portlandite after a very long term hydrothermal treatment when the reactions of intermediary compounds formation have been completed (23).

Ishida *et al*. (77) showed that the thermal treatment of α-C_2SH (synthesized in the mixtures with CaO/SiO_2 molar ratio 2) between 390 °C and 490 °C in air leads to the formation of anhydrous phase Ca_2SiO_4. The crystallographic data of this phase, called x-C_2S, was provided by Miyazaki *et al*. (82), and the crystal structure was determined by Toraya and Yamazaki (83). Also, these authors proposed a mechanism of transformation of α-C_2SH into x-C_2S with further heating up to 920–960 °C leading to the formation of a'$_L$-C_2S, which transforms into β-C_2S upon subsequent cooling (Fig. 1.1). According to Garbev *et al*. (78), NaOH and quartz clearly reduces the transformation temperature of α-C_2SH into x-C_2S by about 50 °C compared with the alkali-free synthesized sample. Also, these authors showed that dellaite transformation into x-C_2S depends on the starting materials being at 560 °C and 620 °C for alkali-activated and alkali-free syntheses, respectively. Meanwhile, the transformation of x-C_2S to a'$_L$-C_2S also occurred at a lower temperature in the presence of alkali during synthesis. The end product after cooling down from 900 °C to room temperature was β-C_2S. Nevertheless, the transformation mechanism, the exact reaction sequence and the nature of the corresponding products in the course of dehydration remain a controversial issue (16).

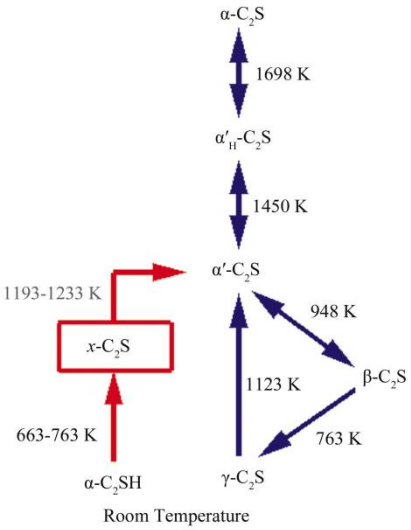

Fig. 1.1. Phase relationship of C_2S polymorph(83)

α-C_2SH with isolated silicate tetrahedrons possesses the lowest degree of polymerization, and is one of members of the neosilicates (16, 44, 78, 79, 81). The crystal structure of α-C_2SH was first described by Heller. It consists of isolated acidic $SiO_3(OH)$ tetrahedral sharing edges with $Ca(O,OH)_6$ and $Ca(O,OH)_7$ polyhedra. Of interest are strong hydrogen bonds, first believed to interconnect the $SiO_3(OH)$ tetrahedra and the Ca(O,OH)n polyhedra. Conversely, Pampuh and Swiderski suggest that hydrogen bonds interconnect the $SiO_3(OH)$ tetrahedra. The complete crystal structure was solved by Marsh(84).

α-C_2SH consists of $[HSiO_4]^{3-}$ anion groups connected with the hydrogen bond, and silicon in this structure is coordinated with three oxygen atoms and one hydroxyl group (Fig. 1.2) (16, 44). The calcium atoms are six and sevenfold coordinated. The space group of α-C_2SH is $P2_12_12_1$ with an orthorhombic lattice and the following parameters: a=0.9476 nm, b=0.9198 and c=1.0648 nm. The hydrogen atom fully occupies crystallographic sites at 0.238, 0.438, 0.110 and 0.406, 0.413, 0.339 (85).

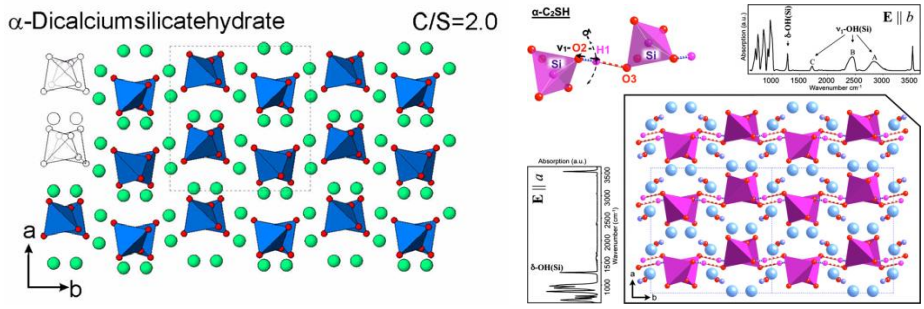

a b

Fig. 1.2. Structure of α-C_2SH presented in different literature: a – (44) b – (16). Bottom right (b): α-C_2SH structure after Marsh along {001} showing zig-zag chains of hydrogen-bonded

silicate tetrahedra parallel to *b*; the rectangles represent unit cells. The morphology of α-C_2SH crystal is visualized schematically in the respective orientation. Top right (b): Polarized IR spectrum of α-C_2SH with E||b. Bottom left (b): Polarized IR spectrum of α-C_2SH with E||a. Top left (b): Detail of the α-C_2SH structure illustrating the m1-O–H(Si) and d-O–H(Si) vibrations

Kilchoanite $Ca_6(SiO_4)(Si_3O_{10})$, (C/S=1.5), a polymorph of $Ca_3Si_2O_7$, was reported as a natural mineral by Agrell and Guy (86). This mineral is typically formed during the pyrometamorphism of siliceous limestones (87). The formation of kilchoanite at relatively low temperatures depends on the nature of the starting materials and hydrothermal conditions. Kilchoanite was first synthesized as a new phase by Roy who called it Phase-Z and considered it to have the composition $9CaO{\cdot}6SiO_2{\cdot}H_2O$ (88).

Mitsuda (89) and Taylor (90) reported that kilchoanite could be prepared from mixtures of lime and quartz at 280–600 °C temperature and 500–1000 MPa pressure. With further results, Mitsuda *et al*. (91) revealed that, by using the rapid heating method, the γ-dicalcium silicate was formed as an initial product from mixtures of lime and silica acid and was replaced by kilchoanite and a small amount of $8CaO{\cdot}5SiO_2$ at 220–250 °C temperature. Speakman *et al*. (92) reported hydrothermal reactions of γ-dicalcium silicate with or without added lime or silica at 150–600 °C and showed that kilchoanite formed readily from mixtures containing γ-dicalcium silicate at 180–220 °C. Taylor (90) found a close structural relation between kilchoanite and γ-dicalcium silicate. This suggests topotactic hydrothermal reaction between the starting material and the products. Mitsuda *et al*. (91) discovered that kilchoanite was formed in fine quartz or silicic acid and lime suspension when the molar ratio of CaO/SiO_2 was equal to 1.5.

According to Yanagisawa *et al*. (93), β-dicalcium silicate can be used as a precursor for kilchoanite synthesis. These authors also determined the metastable phase of C_8S_5 recrystallization to kilchoanite and reinhardbraunsite by long time reactions at higher temperatures than 200 °C. After 1 day at 350 °C, C_8S_5 was completely decomposed to kilchoanite and reinhardbraunsite. Having treated β-dicalcium silicate at 400 °C up to 5 days, dellaite was obtained together with kilchoanite and reinhardbraunsite. The same tendency was observed by Hu *et al*. (81), kilchoanite and reinhardbraunsite were formed by the hydrothermal treatment of β-C_2S at temperatures above 260 °C for 24 h. These compounds were stable even at higher temperatures, and, only after 5 days of hydrothermal treatment at 400 °C, traces of dellaite were formed. Thus, these authors stated that the formation of kilchoanite (C/S = 1.5) from compounds with C/S = 2.0 at lower temperatures can be explained by the increase in solubility of $Ca(OH)_2$ at lower temperatures. Furthermore, Garbev *et al*. (44) described that the set afwillite-killalaite-kilchoanite with C/S ratio of 1.5 has a direct relationship between the degree of polymerization and the temperature of formation, and a higher synthesis temperature is required reading from left to right. The synthesis, structure and chemistry of kilchoanite were also studied by other scientists, yet their opinions seem to differ (40, 85, 94, 95, 96, 97).

Kilchoanite belongs to the sorosilicates group with $[Si_3O_{10}]^{-8}$ and $[SiO_4]^{-4}$. The crystal system is orthorhombic with parameters a = 1.142 nm, b = 0.509 nm, c = 2.195 nm. Also, kilchoanite recrystallized into two space groups, each of which could be in either of two orientations; Imam or Imcm (centrosymmetric) and Ima2 or I2cm (non-centrosymmetric) (1, 44, 85, 87, 90). Kilchoanite was the first mineral found with both isolated tetrahedra (Q0) and finite triple chains (Fig. 1.3) (44, 85). The silicon tetrahedra are connected to 6 and 8-fold coordinated calcium atoms. The triple chains (also called kilchoanite chains) contain one Q2 tetrahedron and two Q1 tetrahedra. The number of chains and isolated tetrahedra is equal in kilchoanite, thus there are ¼Q0, ½Q1 and ¼Q3 tetrahedra in the structure (44). Roy *et al*. (88, 98) showed that kilchoanite made hydrothermally at 715 °C was essentially anhydrous, but Speakman *et al*. (92) obtained evidence that specimens obtained at lower temperatures contained combined water.

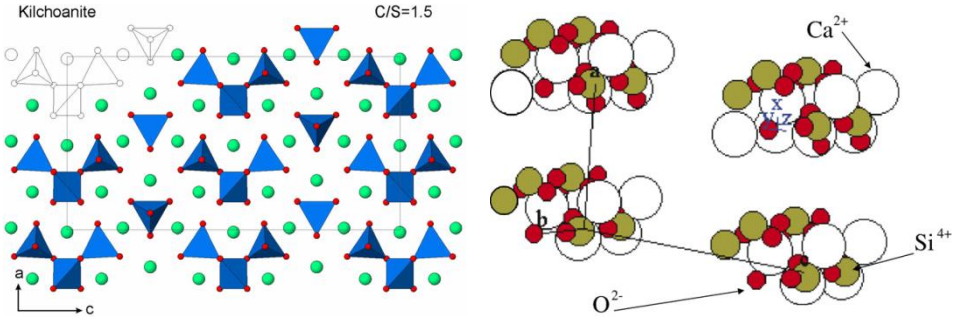

a b

Fig. 1.3. Structure of kilchoanite presented in different literature: a – (44), b – (85)

Petschnig (87) obtained single crystals of kilchoanite during the hydrothermal treatment (100 MPa and 800 °C) of rubidium calcium silicate glass and determined the crystal structure from single-crystal X-ray diffraction data. This author calculated the following unit-cell parameters: a=2.19641 nm, b=0.50841 nm, c=1.14403 nm, V=1.27751 nm^3, Z=2. It was determined that the structure belongs to the group of mixed anion silicates consisting of isolated tetrahedra ($[SiO_4]^-$) and trimers ($[Si_3O_{10}]^-$) at the ratio of 1:1, and the crystallochemical formula can be written as $Ca_6[SiO_4][Si_3O_{10}]$ (Fig. 1.4).

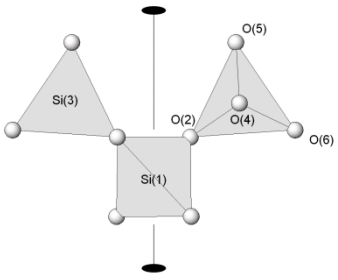

Fig. 1.4. A single 'horseshoe-like' $[Si_3O_{10}]^-$group in kilchoanite (87)

Cuspidine ($3CaO{\cdot}2SiO_2{\cdot}CaF_2$) was first described by Scacchi in the ejected blocks of metamorphosed limestone at Vesuvius, but a detailed and systematic morphological description of well-terminated crystals was given first by Rath from material at Cozzolino in Resina, Vesuvius (51–55, 99). Cuspidine is a member of the sorosilicates (Si_2O_7 group) and can contain additional O, OH, F and H_2O (55). It is a rare mineral and is usually obtained as a hydrothermal treatment product in experiments designed to substitute fluoride for hydroxyl ions in calcium aluminum silicate hydrate (55). Cuspidine is easily formed by solid-state reactions in the system CaF_2–$CaSiO_3$–Ca_2SiO_4 and is stable till 1450 °C; above 1450 °C, the decomposition and formation of CaF_2 and Ca_2SiO_4 is observed (54, 55).

Martín-Sedeño *et al*. (51) determined that minerals of the cuspidine group can be described with the general formula $A_4(Si_2O_7)X_2$, where *A* is a large divalent cation, and *X* is a monovalent or divalent anion (OH^-, F^-, O^{2-}). The authors state that the archetype compound of the cuspidine family is $Ca_4(Si_2O_7)(OH)_2$ which crystallizes in the space group $P2_1/c$. Also, it was determined that the cuspidine framework is built up from ribbons of edge sharing CaO_7/CaO_8 polyhedra running parallel to the *a*-axis with tetrahedral disilicate groups, Si_2O_7, interconnecting theses chains through vertexes. Martín-Sedeño *et al*. (51) suggested writing the structural formula of cuspidine as $Ca_4(Si_2O_7{\square}_1)(OH)_2$, where the square shows the empty site in between the disilicate group.

Cuspidine is generally used as mold flux which plays the decisive role in a casting mold during commercial continuous casting of steels: controlling the horizontal mold heat transfer and lubricating the solidified steel shell from an oscillating mold (51–55). Romo-Castañeda *et al*. (99) stated that cuspidine is one of the most important compounds crystallized in mold flux film during the thin slab casting process.

Jung *et al*. (100) noted that cuspidine is a key ingredient in the continuous casting process to improve the quality of the cast slabs. These authors determined that cuspidine precipitation occurs at ~1200 °C, and that 40–50 % of the liquid remains till 1000 °C. It is worth noting that the melting temperature of pure cuspidine is ~1400 °C.

Hydroxyledgrewite ($Ca_9(SiO_4)_4(OH)_2$) is the hydroxyl analogue of ***edgrewite*** ($Ca_9(SiO_4)_4F_2$) approved by The Commission on New Minerals, Nomenclature and Classification (CNMNC) of the International Mineralogical Association (IMA) in March 2012 and September 2011, respectively. Edgrewite was named in honor of Edward S. Grew, a well-known scientist in the areas of mineralogy and petrology (101). These minerals were discovered in one of the seven large xenoliths of carbonate silicate skarn within the Upper Chegem caldera, Northern Caucasus, Kabardino-Balkaria, Russia (101, 102). According to Galuskin *et al*. (103), the xenoliths are interpreted to be terrigenous-carbonate rocks metamorphosed to calc-silicate skarn under conditions of the sanidinite facies ($T > 900$ °C and P ~100–200 MPa). Edgrewite and hydroxyledgrewite formed at somewhat lower temperatures during retrogression following crystallization of larnite skarns (101).

Bultfonteinite, hillebrandite, jennite, and chegemite-fluorchegemite are the most widespread minerals associated with edgrewite and hydroxyledgrewite.

Galuskin *et al*. (101) also described the physical and optical properties, the chemical composition and the crystal structure of natural edgrewite and hydroxyledgrewite. The outlined minerals show combinations of pinacoids and rhombic prisms. Edgrewite and hydroxyledgrewite form a solid-solution $Ca_9(SiO_4)_4(F,OH)_2$, in which the proportion of the edgrewite end-member $Ca_9(SiO_4)4F_2$ ranges from 31% at F = 1.52 wt% to 74% at F content = 3.64 wt%.

Hydroxyledgrewite belongs to the nesosilicates or orthosilicates group; these silicates possess the lowest degree of polymerization possible, namely C-S-H phases with isolated silicon tetrahedra (Q0) (44). The humite group (104) is a subgroup of nesosilicates with the general formula $A_n(SiO_4)_m(F,OH)_2$ (*A* shows *n* moles of cation, *m* – the moles of SiO_4). Meanwhile, the given group formula for calcium members can be written as $n{\cdot}Ca_2SiO_4+Ca_3(SiO_4)(F,OH)_2$, where Ca_2SiO_4 presents the 'calcio-olivine', and $Ca_3(SiO_4)(F,OH)_2$ the hypothetical 'calcio-norbergite'. When n = 3, the formula of edgrewite $Ca_9(SiO_4)_4F_2$ and hydroxyledgrewite $Ca_9(SiO_4)_4(OH)_2$(Ca/Si=2.25:1) is obtained(101, 105).According to Galuskin *et al*. (101), the structure projection of edgrewite along {100} (Fig. 1.5, a) is similar to clinohumite. Meanwhile, hydrogen bonds of hydroxyledgrewite (Fig. 1.5, b) are related/connected with O9 and/or F9.

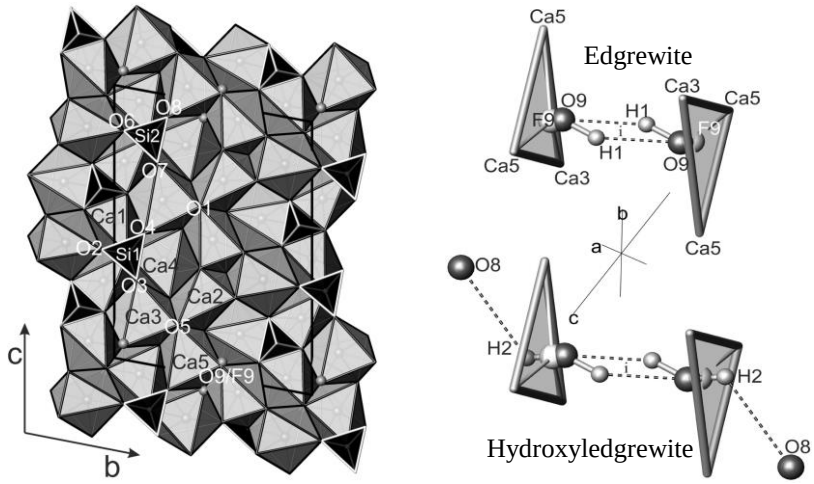

a b

Fig. 1.5.a – Polyhedral drawing of the edgrewite structure projected along a in P21/c11 setting. The small gray spheres at octahedral corners represent F9/O9 sites. SiO_4 groups are black with white rims, CaO_6 octahedra are gray with black rims. **b** – Hydrogen bonding in edgrewite and hydroxyledgrewite(101)

C_8S_5 – pavlovskyite ($Ca_8(SiO_4)_2(Si_3O_{10})$) was first synthesized by Funk and wrongly named as γ-C_2SH (103). $C_8S_5$was reported as a natural mineral by Galuskin *et al*. (103), and the mineral name pavlovskyite was approved by The Commission on New Minerals, Nomenclature and Classification (CNMNC) of the International

Mineralogical Association (IMA) (CNMNC IMA) in January 2011. Speakman *et al*. (92) determined that C_8S_5 formed from γ-C_2S under hydrothermal conditions at 150–600 °C and 15–350 bars. These authors summarized the formation and recrystallization process of C_8S_5:

$$9Ca_2SiO_4 + 2H_2O \rightarrow Ca_8Si_5O_{18} + 2Ca_5(SiO_4)_2(OH)_2 \quad \text{(Eq. 1.1)}$$
$$4Ca_8Si_5O_{18} + H_2O \rightarrow 4.5Ca_6(SiO_4)(Si_3O_{10}) + Ca_5(SiO_4)_2(OH)_2 \quad \text{(Eq. 1.2)}$$
$$1.5Ca_6(SiO_4)(Si_3O_{10}) + 3Ca_5(SiO_4)_2(OH)_2 \rightarrow 4Ca_6(Si_2O_7)(SiO_4)(OH)_2 \quad \text{(Eq. 1.3)}$$

Reaction 1.1 was complete after 72 h at 180 °C (2MPa); during this reaction, C_8S_5 (analog of the mineral pavlovskyite) and calcium chondrodite (analog of the mineral reinhardbraunsite) were formed. It should be underlined that the above mentioned compounds are related to the olivine structure. Reaction 1.2 was complete after 168 h at 250 °C (4 MPa); C_8S_5 becomes metastable and recrystallized to kilchoanite and calcium chondrodite. Finally, after 72 h at 600 °C (20 MPa), dellaite was formed (Reaction 1.3). It is worth mentioning that Speakman *et al*. (92) concluded that C_8S_5 is not a stable compound at any condition, and that the structure of C_8S_5 composed of alternate layers of kilchoanite and γ-Ca_2SiO_4.

Meller *et al*. (24, 37) described the hydrothermal reactions of the $CaO–Al_2O_3–SiO_2–H_2O$ system at temperatures from 200 °C to 350 °C. Meller *et al*. (24) found that C_8S_5 formed when 11% to 33% of silica flour was added in oil well cement. These authors noted that it is also absent from the Taylor's diagram and assumed that C_8S_5 is a metastable phase in the $CaO–Al_2O_3–SiO_2–H_2O$ system either because of the short curing period or because the impurities in the cement alter the phase boundaries of the pure system.

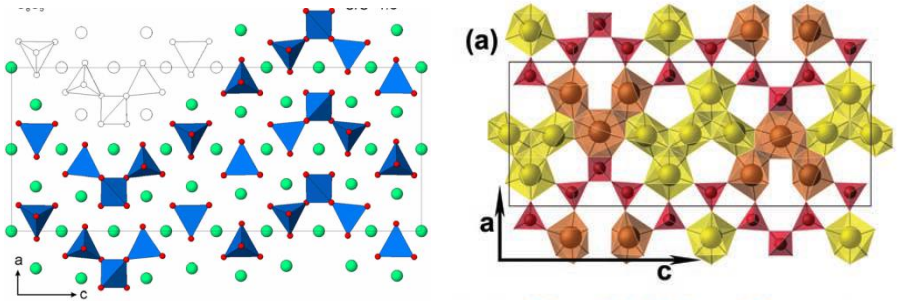

a b

Fig. 1.6. The structure of synthetic (44) (a) and natural (103) C_8S_5. Modules of Ca_2SiO_4 (calcio-olivine) and $Ca_4Si_3O_{10}$ are in yellow and in brown, respectively.

The structure of C_8S_5 is poorly documented in the literature, and no crystal structure refinement currently exists (24). According to Garbev *et al*. (44), the structure of C_8S_5, (C/S=1.6) is similar to that of kilchoanite. The number of isolated tetrahedra is twice that of the triple chains, thus there are 2/5 Q0, 2/5 Q1 and 1/5 Q3 silicon tetrahedra in the structure (Fig. 1.6, a). Galuskin *et al*. (103) refined the structure of C_8S_5(Fig. 1.6, b) and obtained that its structure consists of kilchoanite and calcium olivine (γ-Ca_2SiO_4) modules. These authors determined that the

projection along c calcium polyhedra is connected by SiO_4 and Si_3O_{10} (Fig. 1.6, b), while the projection along b mentioned polyhedral and Si tetrahedra build up layers parallel to {010} (103).

1.3 The application of calcium silicates and calcium silicate hydrates on environmentally friendly cementitious materials

According to Olivier *et al*. (106-108), in 2016, the global greenhouse gas emission reached about 49 Gt, and it continues to grow, while the largest part (~65 %) of greenhouse gas emitted through human activities is carbon dioxide. In fact, the cement industry accounts for approximately 5–7 % of global CO_2 emissions (66, 106, 107, 109–113). The presently mentioned gas is released during limestone calcination and fuel combustion (15, 109, 114–118): every tone of ordinary Portland cement (OPC) emits 0.89 to 1.1 tonne of carbon dioxide. Also, while manufacturing cement, a considerable quantity of energy (4.7–6.3 GJ/t) is used (119–124). According to literature (66, 106, 107, 109, 111-113), the cement industry has to reduce CO_2 emissions by more than 60% in order to help limit global temperature rise to 2–3 °C by 2050. However, over the same period, cement production is expected to grow some 43% to 73% (109, 112, 125–129). Hence, the current industry strategies which include the use of energy-efficient process technologies, alternative fuels and the development of environmentally friendly cementitious materials may help reduce greenhouse gas emission [124, 129].

Nowadays, intensive research and development is being carried out on the environmentally friendly and economically attractive synthesis technology of higher basicity calcium silicates, because, on its basis, environmentally friendly cementitious materials have been created (Celitement, Solidia, β-C_2S rich cement, etc.) (2, 15, 17, 56–58, 66, 67, 78, 129–132). The commonly used synthesis technologies of the outlined compounds are expensive and complex because solid-state sintering requires a high reaction temperature (1100–1450 °C) while the sol–gel method involves not only calcination at elevated temperatures (1000–1250 °C), but also very pure starting materials(131, 133–139). Another more promising approach is the production in a three-step process: 1) hydrothermal synthesis of higher basicity calcium silicates or calcium silicate hydrates (CaO/SiO_2 ratio from 1.25 till 2.0); 2) mechanochemical or thermal treatment of the hydrothermal products together with siliceous raw materials like sand, blast-furnace slag, glass, etc., or silica (usually 1:1); 3) cement curing in the water or CO_2 atmosphere. The main feature of this technology is that the energy consumption and the CO_2 emissions associated with cement production can be reduced up to 30–70%(13, 15, 56, 66, 67, 130, 140).

‘Celitement’ is mostly developed environmentally friendly cementitious material based on hydraulic calcium silicates, while ‘Solidia cement’ is based on non-hydraulic calcium silicates (15, 56, 57, 66, 67, 109, 130, 140). According to literature, ‘Celitement’ can be produced while using dibasic calcium silicate hydrates obtained by hydrothermal synthesis (α-C_2SH, hillebrandite) (15, 56, 57, 67, 130), meanwhile, ‘Solidia cement’ can be produced by using non-hydraulic calcium

silicate with CaO/SiO_2 at a molar ratio from 1 till 1.5 (kilchoanite, rankinite, wollastonite) (15, 66, 109, 130).

According to Garbev *et al*. (141), in order to transform α-C_2SH and other calcium silicates hydrates in a hydraulic state, the hydrogen bonds must be destroyed. The activation can be done by mechanical (milling) and thermal treatment. These authors state that, depending on the primary mixtures, carbon dioxide emitted during the production of environmentally friendly cementitious material can be reduced up to 47 % (16, 56, 141).

Link *et al*. (142) synthesized α-C_2SH (purity ~90 %) under hydrothermal conditions at 200 °C temperature for 16 h. Later on, the obtained products were calcined in the 400–800 °C temperature range. The authors determined that the calcination of the main synthesis product leads to a multiphase of dicalcium silicates consisting of an amorphous material, x-C_2S, γ-$C_2S$and β-C_2S. These authors also stated that the most reactive phase is of amorphous content, while x-C_2S is the most reactive crystalline phase (142). It was determined that α-C_2SH calcined at 400–450 °C temperature is hydraulic active, and, after 3 days of reaction with water, the degree of hydration was approximately equal to 89 %.

The technology for producing environmentally friendly cementitious materials based on dibasic calcium silicates hydrates was investigated by other authors (18, 58, 77, 132, 143–147). Siauciunas *et al*. (58, 132, 144–146) determined that by milling synthetic α-C_2SH with quartz sand, α-C_2SH partially decomposed while quartz partially amorphized. Also, the authors found out that, during alternative binder material hydration, the induction and acceleration periods lasted 45–48 min and 4–4.5 h, respectively. Also these authors determined the mechanical properties of obtained binder material: the bending and compressive strength after 28 days of hydration were equal to 5.22 and 20.45 MPa, respectively.

****

According to literature, ordinary Portland cement will be produced for at least the next 100 years, however, in order to reduce CO_2 emissions and energy consumption, it is necessary to developed new cementitious materials as well as touse renewable energy and carbon capture technologies. Environmentally friendly cementitious materials (‘Celtement’, ‘Solidia cement’) with low carbon emission can be produced in a three-step process: 1) synthesis of higher basicity calcium silicate hydrates or calcium silicates (CaO/SiO_2 ratio from 1.25 till 2.0); 2) tribochemical activation of the hydrothermal products (‘Celitement’); 3) cement curing in the water or CO_2 atmosphere. As it was mentioned above, the first step of the referenced EFCM technologies is the synthesis of calcium silicates or calcium silicate hydrates. However, the crystallization reaction of these materials depends on many factors, such as the type of silica, CaO/SiO_2 molar ratio, curing conditions, the surface area of materials, the amount of water, the type of lime, and the purity of raw materials. Also, there is little data about the influence of precursors on the properties of EFCM. Thus the synthesis, structure and chemistry of these compounds were studied by many scientists, yet their opinions seem to differ.

α-C_2SH is commonly used for the synthesis of EFCM which is based on reactive dibasic calcium silicate forms (x-C_2S, β-C_2S). Calcium silicate hydrate can be synthesized under hydrothermal conditions from the mixtures of lime slurry and quartz/amorphous silica/silica acid in which CaO/SiO_2 molar ratios vary from 1.8 to 2.4. Meanwhile, kilchoanite forms from mixtures of lime and silica source at 200–600 °C under hydrothermal conditions. This compound is non-hydraulic, however, it interacts with carbon dioxide and can be used for manufacturing of carbonation-hardening cements.

Thus, there is little data (and it is not comprehensive) in the references about the synthesis and properties of α-C_2SH, kilchoanite and hydroxyledgrewite as well as on its application for the manufacturing of EFCM.

2. Materials and Methods

The following reagents were used:

1) calcium oxide which was produced by burning $Ca(OH)_2$ (*Reaktiv*, Russia) at 550 °C temperature for 1 h, ground for 30 s in a vibrating cup mill *Pulverisette 9* (speed: 600 rpm).S_a = 2071 m^2/kg (by CILAS LD 1090 granulometer), CaO = 98.7 %.

2) $SiO_2 \cdot nH_2O$ (*Reaktiv*, Russia) was ground for 2.5 min in a vibrating cup mill (speed: 850 rpm), S_a = 1291 m^2/kg, purity – 94.81 %.

3) γ-Al_2O_3 (*Sigma-Aldrich*, Germany) was produced by burning aluminum hydroxide at 475 °C for 5 hours (S_a = 1130 m^2/kg,purity 99 %).

4) quartz sand (*Anykščių kvarcas*) (SiO_2>95 %, S_a = 28.7 m^2/kg) was sieved through a sieve with a mesh width of 400 μm.

Hydrothermal synthesis

The synthesis of calcium silicate hydrates and calcium silicates was based on the hydrothermal method. Due to the higher basicity of calcium silicates and calcium silicates hydrates formation peculiarities (1, 23, 24, 89, 91, 142), the primary mixtures whose compositions correspond to the molar ratios $CaO/(SiO_2+Al_2O_3)$ = 1.5; 1.75 or 2.25 and $Al_2O_3/(SiO_2+Al_2O_3)$ = 0; 0.025 or 0.05 were prepared (Table 2.1). Later on, the primary mixtures were mixed with water to reach the water/solid ratio of the suspension equal to 10.0. The hydrothermal synthesis was carried out in unstirred suspensions in 25 ml volume PTFE cells which were placed in a stainless steel autoclave (*Parr Instruments*, Germany), under saturated steam pressure in a 175-220 °C temperature range for 4; 8; 16; 24; 48; 72 hours by applying extra argon gas (1 MPa). Temperature was reached within 2 h. After hydrothermal treatments, the autoclave was quenched to room temperature. Having performed the synthesis, the suspensions were filtered, products rinsed with acetone to prevent carbonization of materials, dried at ~50 °C temperature for 24 h, and sieved through a sieve with an 80 μm mesh.

Table 2.1 The composition of primary mixtures

Molar ratio $CaO/(SiO_2+Al_2O_3)$	1.5			1.75		2.25
Molar ratio $Al_2O_3/(SiO_2+Al_2O_3)$	0	0.025	0.05	0	0.025	0
The quantity of CaO, %	57.35	56.95	56.58	61.07	59.74	66.86
The quantity of SiO_2, %	42.65	41.33	40.00	38.93	37.16	33.14
The quantity of Al_2O_3, %	0	1.72	3.42	0	3.09	0

Manufacture of binder material

The binder material (BM) was prepared by mixing synthesis products and quartz sand or granite cutting waste (1:1 by mass) in a homogeniser (*Turbula*) at 34 rpm for 30 min. Later on, a BM sample was ground in a vibrating cup mill (*Pulverisette* 9) at 950 rpm for 4–5 min and burned at 100–1000 °C for 0.5–1 h (56–59, 141–143).

The X-ray diffraction analysis was performed on:

1) D8 Advance diffractometer (*Bruker AXS*, Germany) operating at the tube voltage of 40 kV and tube current of 40 mA. The X-ray beam was filtered with Ni 0.02 mm filter to select the CuKα wavelength. Diffraction patterns were recorded in a *Bragg-Brentano* geometry by using a fast counting detector *Bruker LynxEye* based on the silicon strip technology. The samples were scanned over the range 2θ = 3–70° at a scanning speed of 6°/min using a coupled two theta/theta scan type.

2) *DRON–6* diffractometer (*Bourevestnik*, Russia) operating at the tube voltage of 30 kV and tube current of 20 mA was used. The X-ray beam was filtered with Ni 0.02 mm filter to select the CuKα wavelength. Diffraction patterns were recorded in a *Bragg-Brentano* geometry using a graphite monochromator. The samples were scanned over the range 2θ = 3–70° in steps of 2θ = 0.02°.

Calculation of crystallinity and crystallite size

XRD software *Diffrac.Topas 4.2* was used for the calculation of crystallinity and the crystallite size. The full width half maximum (FWHM) values were measured by fitting a SPV function to the peaks using *Diffrac.Topas* software. The percentage of crystallinity was determined by Eq. (2.1):

$$X_C = \frac{A_C}{A_C + A_A}, \quad \text{(Eq. 2.1)}$$

where A_C is the area under the curve for the crystalline peak and A_A is the area of the amorphous material.

The mean crystallite size was determined following the Scherrer equation (Eq. 2.2) (148, 149, 150):

$$D_{hkl} = \frac{k_{hkl} \cdot \lambda}{\beta_{hkl} \cdot cos\theta}, \quad \text{(Eq. 2.2)}$$

where λ is the wavelength of the Cu Kα radiation, θ is Bragg's diffraction angle, β_{hkl} is the full width at half maximum intensity, and k is a shape factor (the value used in this study was 0.94)(148, 150).

Quantitative XRD analysis

The amount of unreacted portlandite was calculated by quantitative XRD analysis (QXRD). For this reason, a calibration curve was plotted by using portlandite and quartz mixture. The amount of portlandite in the mixture varied from 0 % to 30 % by mass. The porlandite quantity was calculated from the intensity change of the basic reflection (0.262 nm) (Fig. 2.1). Each calculation was done five times, and it was determined that their data declined no more than 3 % from the mean. The calculated values were taken as a function of the amount of portlandite in the mixture (Fig. 2.2). The straight line correlation coefficient R^2 was equal to 0.9978; thus the calibration curve was reliable.

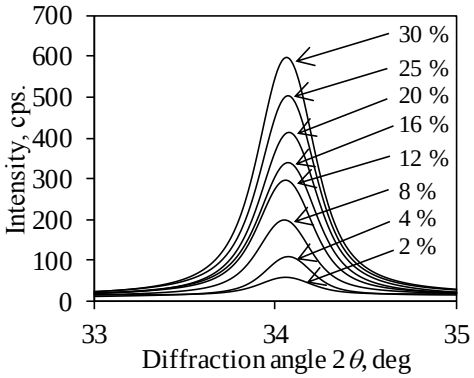

Fig. 2.1. The change of the main diffraction peak intensity of portlandite (*d*-spacing — 0.262 nm) in mixtures with quartz

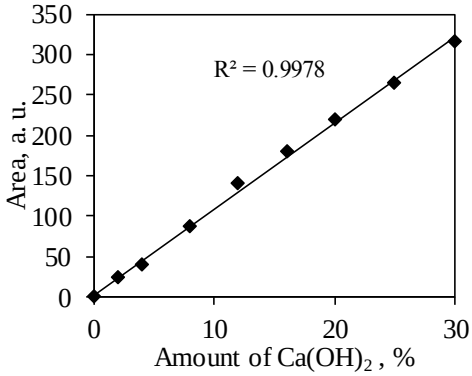

Fig. 2.2. Relationship between the diffraction peak (*d*-spacing — 0.262 nm) area and the quantity of portlandite in mixtures with quartz

The measurements of the thermal stability and phase transformation were prepared with:

1) *Linseis PT1000* instrument (*Linseis*, Germany): a heating rate of 15 °C/min, the temperature range from 30 °C up to 1000 °C, nitrogen atmosphere and the sample mass was equal to ~13 mg. Ceramic sample handlers and crucibles of Pt were used.

2) *Netzsch* instrument *STA 409 PC Luxx* (*Netzsch*, Germany): a heating rate of 15 °C/min, the temperature range from 30 °C up to 1000 °C, nitrogen atmosphere and the sample mass was equal to ~13 mg. Ceramic sample handlers and crucibles of Pt-Rh were used.

3) *Netzcsh Polyma DSC 214* instrument (*Netzsch*, Germany): a heating rate of 10 °C/min, the temperature ranged from 30 °C up to 600 °C under nitrogen atmosphere. Ceramic sample handlers and aluminum crucibles were used.

4) In-situ XRD analysis was made with a high-temperature camera *MTC-hightemp* (*Bruker AXS*, Germany). The measurements were carried out with a step

width of 0.02 2θ and 0.6 s/step at a heating rate of 50 °C/min after equilibration for 5 min at the desired temperature.

Determination of specific heat capacity

Differential scanning calorimetry was applied for measuring the specific heat capacity (C_P) of samples at a heating rate of 10 °C/min, the temperature ranged between 25 – 600 °C under air atmosphere. The measurement was carried out on a *Netzcsh Polyma DSC 214* instrument by using ceramic sample handlers and aluminum crucibles. C_P values at different temperatures were calculated according to the following equation (Eq. 2.3):

$$C_P = \frac{m_{standard}}{m_{sample}} \cdot \frac{DSC_{sample} - DSC_{bas}}{DSC_{standard} - DSC_{bas}} \cdot Cp_{standard} \qquad \text{(Eq. 2.3)}$$

where $C_{Pstandard}$ is the value of the specific heat of the standard, J/(g·K); $m_{standard}$ is the mass of the standard, mg; m_{sample} is the mass of the sample, mg; DSC_{sample} is the value of the DSC signal at the temperature from the sample curve, mW; $DSC_{standard}$ – value of DSC signal at temperature from the standard curve, mW; DSC_{bas} is the value of the DSC signal at the temperature from the baseline, mW.

Fourier Transform Infrared Spectroscopy was carried out with the help of a *Perkin Elmer FT–IR Spectrum X* system (*PerkinElmer*, USA). Specimens were prepared by mixing 1 mg of the sample with 200 mg of KBr. The spectral analysis was performed in the range of 4000–400 cm^{-1} with a spectral resolution of 1 cm^{-1}.

Scanning electron microscopy was performed by using *JEOL JSM-7600F* (*JEOL*, Japan) instrument at an accelerating voltage of 10 kV, and a working distance of 8.6 mm.

Transmission electron microscope was performed by using *Tecnai G2 F20 X-TWIN* instrument (*FEI*, Netherlands) with a Schottky type field emission electron source. The accelerating voltage was 200 kV. In order to take TEM images, a high angle annular dark field detector (HAADFD) were used.

Isothermal calorimetry

An eight channel *TAM Air III* isothermal calorimeter (*TA Instruments*, UK) was used to investigate the heat evolution rate of the binder materials samples. Glass ampoules (20 ml) each containing 3 g dry cementitious material were placed in the calorimeter and the injection units for each ampoule filled with amounts of water equivalent to a w/s ratio of 0.5. After a steady temperature of 25 °C had been reached, the water was injected into the ampoules and mixed inside the calorimeter with the dry material for 20 s (frequency 2-3 s^{-1}). The heat evolution rate was then measured over a period of 72 h. Repetition of the measurements showed deviations in total heat below 3 % for samples of a similar type. Apart from the first minutes of water additive and mixing, the heat evolution rates were essentially identical.

The compressive strength test of the samples was performed with automatic cement compression machine *EL39-1501/01 Autotest250* (*ELE International*, USA). Samples (20×20×20 mm) were formed of the BM when the ratio of water to BM was equal to 0.35. During the first day, the samples were kept in molds at 20 ± 1°C and 100 % humidity. After 24 h of formation, the samples were transferred into distilled water and stored there for 2, 6, 13 and 27 days at 20±1 °C. The data of the compressive strength test was calculated as the arithmetic mean of the six individual

results. The samples (for instrumental analysis) were crushed to powder, dried at a temperature of 50±5 °C and sieved through a sieve with a mesh width of 80 μm.

The surface area and particle size distribution were measured by using:

1) *CILAS 1090 LD* grain-size analyzer (*CILAS*, France), which featured a sensitivity range from 0.04 to 500 μm. The particles were dispersed by ultrasound for 2 min while the obscuration of particles in water reached 14%. The ultrasound duration during the measurement was 70 s. The standard operating procedure in use was the Fraunhöfer method.

2) A BET surface area analyzer *KELVIN 1042 Sorptometer* (*Costech Instruments*, USA) was employed. The specific surface area was calculated by the BET equation using the data of the lower part of N_2 adsorption isotherm ($0.05 < p/p_0 < 0.35$):

$$\frac{1}{X\left(\frac{p_0}{p}-1\right)} = \frac{C-1}{X_m \cdot C} \cdot \frac{p}{p_0} + \frac{1}{X_m \cdot C} \qquad (2.4)$$

where X is the mass of adsorbate adsorbed on the sample at relative pressure p/p_0 (p is the partial pressure of adsorbate and p_0 is the saturated vapor pressure of adsorbate); X_m is the mass of adsorbate adsorbed at a coverage of one monolayer; C is a constant which is a function of the heat of the adsorbate condensation and the heat of adsorption (C_{BET}).

The BET equation yields a straight line when $\frac{1}{X\left(\frac{p_0}{p}-1\right)}$ is plotted versus $\frac{p}{p_0}$. The slope of $\frac{C-1}{X_m \cdot C}$ and the intercept of $\frac{1}{X_m \cdot C}$ was used to determine X_m and C: $S = slope = \frac{C-1}{X_m \cdot C}$ and $I = intercept = \frac{1}{X_m \cdot C}$. Solving for X_m yields $X_m = \frac{1}{S+I}$. The BET plot is usually found to be linear in the range p/p_0 = 0.05–0.35. The total surface area of the sample S_t was determined by the equation $S_t = \frac{X_m \cdot N \cdot A_{cs}}{M}$, where M is the molecular mass of the adsorbate, N is Avogadro constant, A_{cs} is the cross-sectional area occupied by each nitrogen molecule ($16.2 \cdot 10^{-20}$ m^2). The specific surface area was obtained by the equation $S_{BET} = \frac{S_t}{m}$, where m is the mass of the synthesis product sample.

The total pore volume and the pore size distribution were calculated according to the corrected Kelvin equation and Orr *et al*. scheme (157) using the entire N_2 desorption isotherm at 77 K. The Kelvin equation relates the adsorbate vapor pressure depression to the radius of a capillary which was filled with adsorbate:

$$ln\frac{p}{p_0} = -2\frac{\gamma \cdot V_m \cdot \cos\theta}{R \cdot T \cdot r_k}, \qquad (2.5)$$

where p is the saturated vapor pressure in equilibrium with the adsorbate condensed in a capillary or pore, p_0 the normal adsorbate saturated vapor pressure, γ is the surface tension of nitrogen at its boiling point (γ = 8.85 ergs/cm^2 at (-195.8 °C)), V_m is the molar volume of liquid nitrogen (V_m = 34.7 cm^3), θ is the wetting angle (usually taken 0° and cos θ = 1), R the gas constant is ($R = 8.134 \cdot 10^7$ ergs deg^{-1} mol^{-1}), T the absolute temperature is (T = 77 K) and r_K is the Kelvin radius of pore.

Thermodynamic calculations

For the thermodynamic calculations of the hypothetical reaction parameters, the values of enthalpy $\left(\Delta_r H_{298}^{0,f}\right)$, entropy $\left(\Delta_r S_{298}^{0,f}\right)$ and molar specific heat capacities (C_p) of the formed compounds are applied and given in Table 2.2. For the estimations, a method of absolute entropies was used; according to this method, the change of reaction standard free Gibbs energy $\Delta_r G_T^0$ was calculated with the equation:

$$\Delta_r G_T^0 = \Delta_r H_T^0 - T \cdot \Delta_r S_T^0, \quad \text{(Eq. 2.6)}$$

where $\Delta_r H_T^0$ and $\Delta_r S_T^0$ are the changes of reaction enthalpy and entropy in temperature. Enthalpy and entropy for the reaction can be calculated from the equations:

$$\Delta_r H_T^0 = \Delta_r H_{298}^0 + \Delta_r C_P\left(T_r - 298\right) \quad \text{(Eq. 2.7)}$$

$$\Delta_r S_T^0 = \Delta_r S_{298}^0 + \Delta_r C_P \left(\frac{T_r}{298}\right) \quad \text{(Eq. 2.8)}$$

where $\Delta_r H_{298}^0$ is the standard enthalpy change of the reactions, J/mol; $\Delta_r S_{298}^0$ is the standard entropy change of the reactions, J/mol. The standard molar thermodynamic properties values at 25 °C and 1 bar (Table 2.2) were taken from the literature (151–154).

Table 2.2 Standard molar thermodynamic properties at 25 °C and 1 bar (151–154)

Material	$\Delta H_{298}^{0,f}$, kJ/mol	$\Delta S_{298}^{0,f}$, J/(mol·K)	$\Delta G_{298}^{0,f}$, kJ/mol	ΔC_P, J/(mol·K)
$H_2O_{(g)}$	-241.8	188.7	-228.6	33.2
SiO_2	-903.0	41.0	-915.2	44.4
CaO	-635.1	38.1	-603.5	43.1
$Ca(OH)_2$	-985.1	83.4	-897.5	87.4
γ-Al_2O_3	-1662.0	51.0	-1568.3	118.3
α-C_2SH	-2634.9	122.4	-2430.9	111.9
C_2S	-2308.0	128.0	-2193.2	162.1
C_2SH	-2662.5	179.7	-2482.0	177.5
C_3S_2	-3973.0	192.2	-3790.3	205.0
$C_3S_2H_3$	-4682.9	312.3	-4305.3	328.5
C-S-H(I)	-1916.0	80.0	-1744.4	-
C-S-H(II)	-2723.0	140.0	-2480.8	-
AS_2H_2	-4119.8	205.0	-3799.8	146.1
$C_2AH_{7.5}$	-5277.6	450.0	-4695.5	-
C_2AH_8	-5433.0	440.0	-4812.8	558.4
C_3AH_6	-5537.3	422.0	-5008.2	446.0
C_4AH_{13}	-8302.0	700.0	-7326.56	930.3
C_4AH_{19}	-10018.0	1120.0	-8749.9	1382.0
CAH_{10}	-5288.2	610.0	-4623.0	-
$C_2A_2S_2H$	-6239.6	263.6	-5855.1	323.4
C_2AS_3H	-6193.6	292.8	-5816.66	331.1
C_2ASH_8	-6360.0	546	-5705.12	602.1
$C_3AS_{0.8}H_{4.4}$	-5855.0	369.0	-5368.0	423.4
$C_3AS_{0.41}H_{2.59}$	-5699.1	399.0	5192.9	430.0
$C_3AS_{0.84}H_{4.32}$	-5847.5	375.0	-5365.2	413.0
C_4ASH_{12}	-8750.0	821.0	-7778.5	942.1

3. Results and Discussion

3.1. Formation of α-C_2SH in 1.5CaO–(1-x)SiO_2·nH_2O–xAl_2O_3–H_2O suspensions at 175 °C and application as a precursor for binder material

3.1.1. Hydrothermal synthesis of α-C_2SH and α-C_2SH–Al

It was determined that in unstirred CaO–SiO_2·nH_2O–H_2O suspensions when the molar ratio (CaO/SiO_2) of the primary mixture was equal to 1.5, within 4 hours of isothermal curing at 175 °C dicalcium silicate hydrates – α-C_2SH (PDF 04-009-6343; *d*-spacing–0.422; 0.326; 0.266; 0.241 nm) and semi-crystalline calcium silicate hydrates C-S-H were formed (PDF 00-033-0306; *d*-spacing – 0.304; 0.279; 0.182 nm and PDF 00-034-0002; *d*-spacing – 0.307; 0.280; 0.183 nm) (Fig. 3.1, curve 1). Also, a broad basal reflection typical to amorphous structure compounds was identified in the interval of 26–37° diffraction angles. It should be noted that under these synthesis conditions, the basic reflections (PDF 04-012-0489; *d*-spacing–0.493; 0,262; 0.193 nm) of partially unreacted portlandite was observed in X-ray diffraction patterns. Meanwhile, the synthesis products were carbonated because the diffraction peaks characteristic to calcium carbonate (PDF 04-012-0489; *d*-spacing – 0.304; 0.228; 0.191 nm) were detected in the XRD patterns.

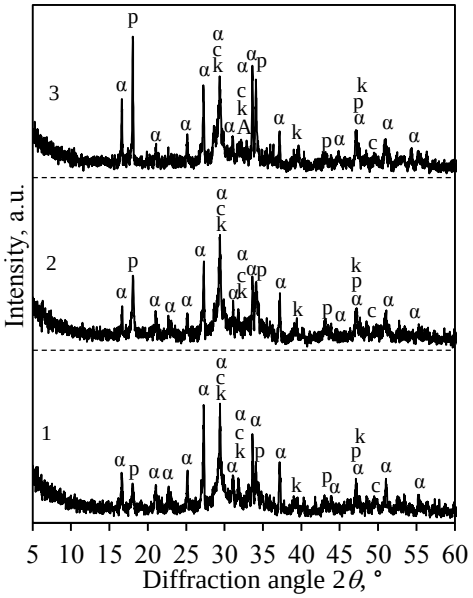

Fig. 3.1.XRD patterns of synthesis products when the duration of hydrothermal synthesis at 175 °C temperature is 4 h. The molar ratios of primary mixtures were equal to: CaO/(SiO_2+Al_2O_3)=1.5 and Al_2O_3/(SiO_2+Al_2O_3)=0 (curve 1), 0.025 (curve 2) or 0.05 (curve 3). Indexes: c – C-S-H; α – α-C_2SH; p – $Ca(OH)_2$; A – hydrogrossular; k – $CaCO_3$

STA analysis data confirmed XRD results: in DSC curve, the first endothermic effect can be assigned to the removal of crystallization water in calcium silicate hydrates. Meanwhile, an endothermic effect at ~459 °C temperature can be attributed to the dehydration of α-C_2SH as well as to the decomposition of

portlandite (Fig. 3.2, a, curve 2). However, due to the small amount of portlandite, the above mentioned thermal effects cannot be distinguished in the STA curves and their derivatives. Above 800 °C temperature, two exothermic effects reflecting to C-S-H(I) (~849 °C) and C-S-H(II) (~879 °C) recrystallization to wollastonite (Fig. 3.2, a, curve 2) were detected. Furthermore, an endothermic effect at ~723 °C temperature can be assigned to the decomposition of calcium carbonate (Fig. 3.2, curve 2).

It was determined that, in the mixtures with $CaO/(SiO_2+Al_2O_3)$ = 1.5 and $Al_2O_3/(SiO_2+Al_2O_3)$ = 0.025 or 0.05 molar ratio, Al_2O_3 additive changes not only the sequence of the formed compounds but also their stability during the synthesis. It was obtained that portlandite reacted slower because, after 4 h of isothermal curing, more intensive diffraction maximums (*d*-spacing – 0.493 and 0.262 nm) characteristic to the latter compound were identified in the XRD patterns (Fig. 3.1, curves 2 and 3). On the other hand, under these synthesis conditions, Al_2O_3 additive negatively results in the formation of α-C_2SH: a decrement of integral intensity of an individual Bragg peak (*d*-spacing–0.326 nm) from 342 cps ($Al_2O_3/(SiO_2+Al_2O_3)$ = 0) to 270 cps ($Al_2O_3/(SiO_2+Al_2O_3)$ = 0.05) was observed (Fig. 3.1, curves 1 and 3). This fact was confirmed by thermal analysis: due to a higher quantity of unreacted portlandite, the endothermic effect characteristic to mentioned compound at 420 °C temperature can be distinguished from dehydration of α-C_2SH (469°C) (Fig. 3.2, c, curves 2 and 3). It is worth mentioning that due to α-C_2SH crystals orientation, the diffraction peaks whose *d*-spacing is 0.533 nm from planes {002} and 0.266 nm from planes {004} are more intensive comparing with etalon PDF 04-009-6343. The same result was obtained in other authors' works (58, 132, 143).

It should be noted that in the mixtures with Al_2O_3additive, it is probable that part of Al^{3+} ions incorporated into the calcium silicate hydrates structure whereas another part reacted with calcium oxide and/or silica dioxide. Thus the small amount of calcium aluminum silicate hydrates or calcium aluminum hydrates ($Ca_3Al_2(SiO_4)_{3-x}(OH)_{4x}$) can be formed in the synthesis products. However, the formed compounds cannot be clearly distinguished because the peaks of diffraction maximums of the mentioned compounds are small and interplanar distances *d* (*d*-spacing – 0.508; 0.438; 0.330; 0.277; 0.226; 0.202 nm) overlapped (Table 3.1; Fig. 3.1, curves 2 and 3). For this reason, these compounds were named in generally hydrogarnets, where the number of SiO_2 moles varied from 0 to 3.

Table 3.1. The interlayer distances of calcium aluminum silicate hydrates

Interlayer distances d, nm	The interlayer distances of hydrogrossular from PDF-4 database						
	$Ca_4Al_4Si_2O_{12}(OH)_4$ PDF No. 04-013-1605	$Ca_3Al_{2.8}O_{12.075}(OH)_{4.8}$ PDF No. 01-076-2505	$Ca_3Al_2(OH)_{12}$ PDF No. 00-024-0217	$Ca_3Al_2SiO_4(OH)_8$ PDF No. 00-038-0368	$Al_3Si_2O_7(OH)_3$ PDF No. 00-049-0096	$Ca_3Al_2Si_{0.64}O_{2.56}(OH)_{9.44}$ PDF No. 04-017-1482	$Ca_3Al_{2.85}O_{2.55}(OH)_{9.45}$ PDF No. 04-017-1504
0.51		0.509	0.513	0.505		0.505	0.509
0.44					0.436		0.441
0.36	0.360						
0.34			0.336				
0.33					0.328	0.331	0.333
0.31		0.312		0.309		0.310	0.311
0.28	0.279	0.279	0.281	0.276	0.278	0.277	0.279
0.25	0.255				0.246		0.244
0.23		0.228	0.230	0.226		0.226	0.228
0.21	0.208						
0.20		0.202	0.204	0.200	0.197	0.200	0.202
0.17			0.168				
0.16	0.156						

The formation of hydrogarnets was confirmed by STA analysis: in the DSC curve, an endothermic effect at ~356 °C temperature can be attributed to the dehydration of mentioned compound (in DDSC~311 °C) (Fig. 3.2, b, curves 2 and 3). In addition, a larger amount of Al_2O_3 additive in the initial mixture (the molar ratio of $Al_2O_3/(SiO_2+Al_2O_3)$ = 0.05) stimulates the formation of calcium aluminum silicate hydrates. The STA analysis data showed that, after 4 h, the heat flow of the endothermic effect at 352 °C increased (Fig. 3.2, c, curves 2 and 3).

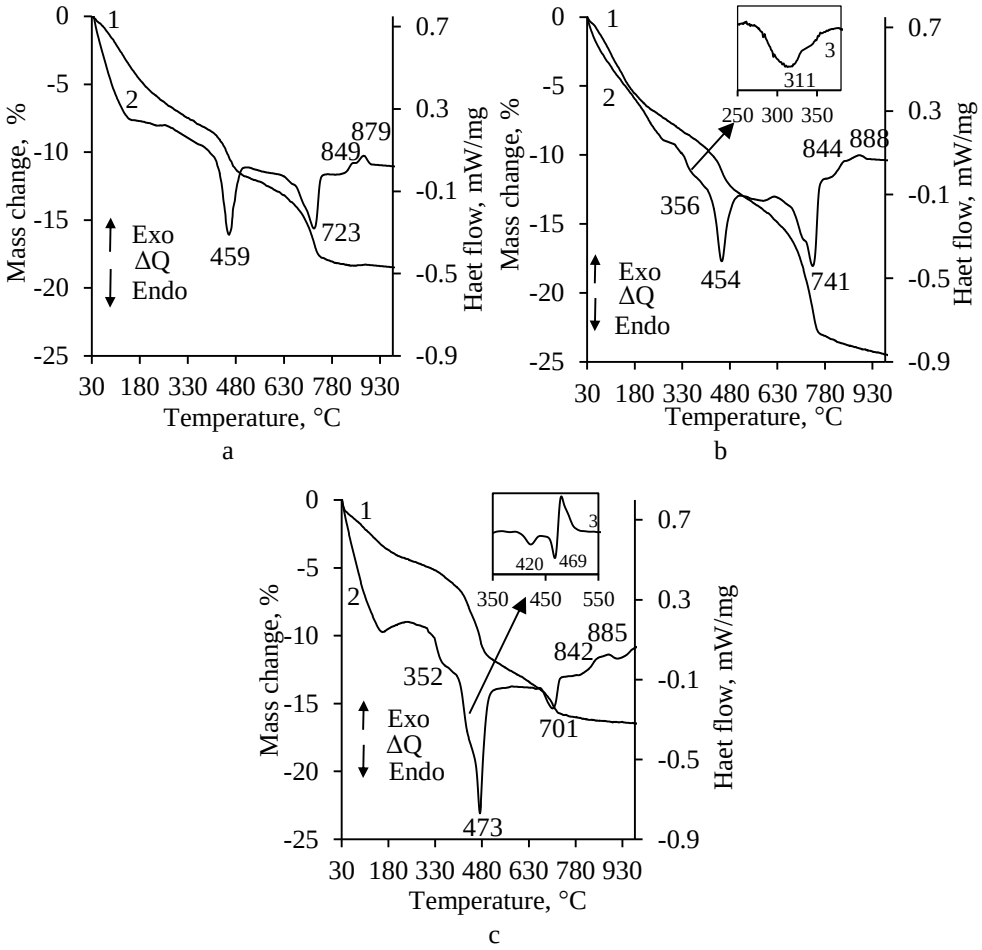

Fig. 3.2. STA curves of the synthesis products formed in the mixtures with the molar ratios of $CaO/(SiO_2+Al_2O_3)$=1.5 and $Al_2O_3/(SiO_2+Al_2O_3)$=0 (a), 0.025 (b) or 0.05 (c), when the duration of hydrothermal synthesis at 175 °C temperature is 4 h.
1 – TGA; 2 – DSC; 3 – DDSC

The interaction degree between raw materials is greater in a pure mixture when the duration of isothermal treatment is prolonged to 8 h: the initial formed compound – portlandite – has fully reacted, thus typical diffraction peaks for this compound are not detected on the XRD pattern. It should be noted that a significant increase in the intensity of α-C_2SH diffraction maximums is observed; while a broad basal reflection without peaks in 26–37° diffraction angles range disappeared. Also, STA analysis data showed that, at ~470 °C, the amount of the adsorbed heat attributed to dehydration of α-C_2SH was increased to 62.13 J/g (Table 3.2).

It was observed that in the mixtures with an Al_2O_3 additive, the formation of synthesis products is quite complicated. For this reason, even after 16 h of isothermal curing, quite intensive diffraction peaks of unreacted portlandite were observed in X-ray diffraction patterns. When hydrothermal synthesis is extended to

24 hours, $Ca(OH)_2$ reacts, and dibasic calcium silicate hydrates dominate in the products. Besides, the amount of adsorbed heat attributed to the dehydration of α-C_2SH was increased to 98.97 J/g (Table 3.2). It should be underlined that after 24 h of isothermal curing, in all the investigated samples, semi-crystalline C-S-H(II) becomes metastable because an exothermic effect at ~885 °C was not observed.

Table 3.2. The thermal characteristics of α-C_2SH formed at different duration of hydrothermal synthesis in the mixtures with the molar ratios of $Al_2O_3/(SiO_2+Al_2O_3)$=0, 0.025 or 0.05

The heat of thermal effect in a 400–500 °C temperature range, J/g			
The molar ratio **(**$Al_2O_3/(SiO_2+Al_2O_3)$) of primary mixtures	0	0.025	0.05
Hydrothermal synthesis duration, h	Heat of thermal effect, J/g	Heat of thermal effect, J/g	Heat of thermal effect, J/g
4	50.12	47.43	112.4
8	62.13	108.20	95.20
16	79.55	74.84	69.14
24	85.55	104.40	98.97
48	64.71	75.63	72.01
72	68.25	67.40	62.24

It was determined that by prolonging the duration of hydrothermal synthesis to 72 h, α-C_2SH still remains stable in both pure and with Al_2O_3 additive mixtures because no visible changes in the intensity of the basic reflections typical to the mentioned compound are detected (Fig. 3.3); meanwhile the heat flow of dehydration is decreased to 68.25 and 62.24 J/g, respectively (Fig. 3.4, Table 3.2). It is worth mentioning that due to the increased amount or crystallinity of hydrogrossular few diffraction peaks corresponding to this compound were clearly distinguished in the XRD pattern (Fig. 3.3).

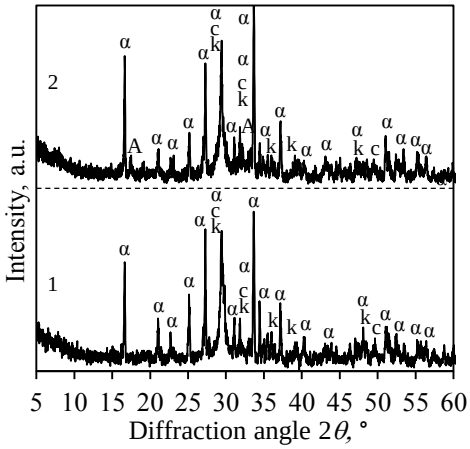

Fig. 3.3. X-ray diffraction patterns of synthesis products when the duration of hydrothermal synthesis at 175 °C temperature is 72 h. The molar ratios of primary mixtures were equal to: $CaO/(SiO_2+Al_2O_3)$=1.5 and $Al_2O_3/(SiO_2+Al_2O_3)$=0 (curve 1) or 0.05 (curve 2). Indexes: c – C-S-H; α – α-C_2SH; k – $CaCO_3$; A – hydrogrossular

Moreover, the thermal effect intensity of C-S-H(I) recrystallization to wollastonite at ~849 °C increased (Fig. 3.4). In the mixtures with Al_2O_3 additive, an endothermic effect at ~353 °C temperature typical to the dehydration of hydrogrossular was observed (Fig. 3.4, b).

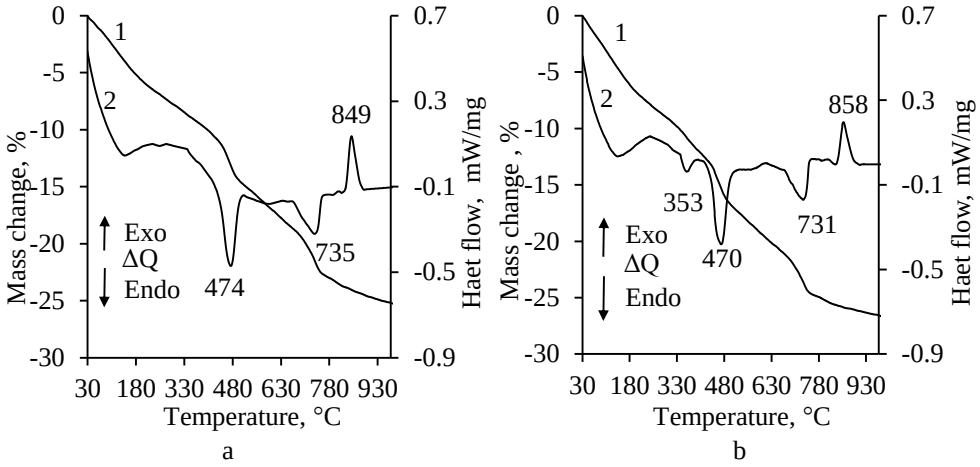

Fig. 3.4. STA curves of the synthesis products formed in the mixtures with the molar ratios of $CaO/(SiO_2+Al_2O_3)$=1.5 and $Al_2O_3/(SiO_2+Al_2O_3)$=0 (a) or 0.05 (b) when the duration of hydrothermal synthesis at 175 °C temperature is 72 h. 1 – TGA; 2 – DSC

Thus, after 72 h of synthesis, the intensities of diffraction peaks and the values of α-C_2SH dehydration heat were close, suggesting that Al_2O_3 additive as well as hydrothermal treatment duration have no influence on the quantity of formed α-C_2SH (Fig. 3.4, curve 2; Table 3.2).

3.1.2. Thermal stability of α-C_2SH and α-C_2SH–Al

The literature concerning thermal stability and other parameters of synthetic α-C_2SH with Al_2O_3 additive is scarce. For this reason, the influence of calcination temperature on the thermal stability of α-C_2SH and α-C_2SH–Al ($Al_2O_3/(SiO_2+Al_2O_3)$ = 0.05) samples synthesized after 24 h (Fig. 3.5.) was investigated.

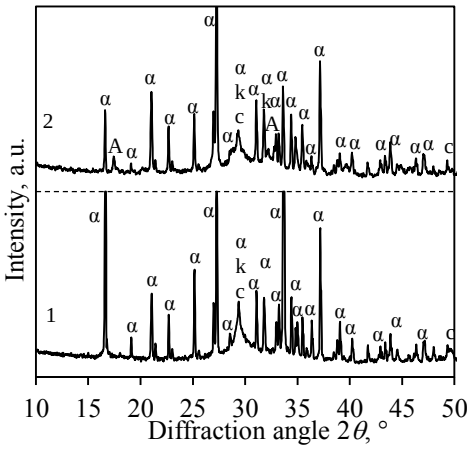

Fig. 3.5. XRD patterns of the synthesis products formed in the mixtures with the molar ratios of $CaO/(SiO_2+Al_2O_3)$ = 1.5 and $Al_2O_3/(SiO_2+Al_2O_3)$ = 0 (1 curve) or 0.05 (2 curve), when the duration of hydrothermal treatment at 175 °C temperature is 24 h. Indexes: α – α-C_2SH; k – calcite; c – C-S-H; A – hydrogrossular

It was estimated that in the pure system, α-C_2SH is stable in a 25–400 °C temperature range although the intensity of diffraction peaks characteristic to this compound slightly decreased (Fig. 3.5, curve 1, Fig. 3.6, a). It should be noted that under these calcination conditions, the dehydration of semicrystalline C-S-H type compounds proceeded, thus a broad basal reflection in 26–37° diffraction angles range was increased and can be assigned to amorphous structure compounds (Fig. 3.5, curve 1, Fig. 3.6, a). It was calculated that the quantity of the crystallinity phase decreased 1.78 times from 83.95 % to 47.13 % (Fig. 3.7). Meanwhile, in the higher temperature of calcination (450 °C), α-C_2SH fully recrystallized to anhydrous C_2S phases: x-C_2S (PDF 00-055-0591; *d*-spacing – 0.345; 0.326; 0.303; 0.293 nm) and calcium olivine (PDF 04-006-8894; *d*-spacing – 0.301; 0.275; 0.273; 0.191 nm) (Fig. 3.6, a). It should be underlined that amorphous phases dominated in the products because the quantity of crystallinity phase decreased to 29.75 % (Fig. 3.7). Furthermore, when the temperature of calcination increased to 750 °C, x-C_2S becomes metastable and recrystallized into two new C_2S modification: α'-C_2S (PDF 00-036-0642; d-spacing – 0.276; 0.275; 0.269; 0.220 nm) and β-C_2S (PDF 00-033-0302; *d*-spacing – 0.279; 0.278; 0.275; 0.219 nm) (Fig. 3.6, a). The difference between these results and those of literature(77, 78) which observed that x-C_2S are stable up to 800 °C and α'-C_2S formed up to 900–1000 °C could be due to the differences in the synthesis method, especially the molar ratio of primary mixtures. It is worth mentioning that the crystallinity of calcination products at 750 °C increased more than two times: from 29.75 to 68.07 % (Fig. 3.7). At 900 °C,

diffraction peaks characteristic to calcium olivine disappeared, meanwhile, the intensity of diffraction peaks characteristic to β-C_2S increased (Fig. 3.6, a). Also, C-S-H(I), which is represented in the sample (Fig. 3.5), becomes metastable, consequently reflections of wollastonite (PDF 04-010-2581; *d*-spacing – 0.352; 0.332; 0.309; 0.298 nm) are visible. Unexpected results were obtained after calcination at 1000 °C temperature because in the product traces of kilchoanite (PDF 00-029-0370, *d*-spacing 0.355; 0.305; 0.288; 0.267 nm) and C_8S_5 (PDF 00-029-0368; *d*-spacing 0.361; 0.305; 0.284; 0.269 nm) were formed. It should be mentioned that these data values are in good agreement with the calculations of the quantity of crystallinity phases which increased to 91.43 % (Fig. 3.7).

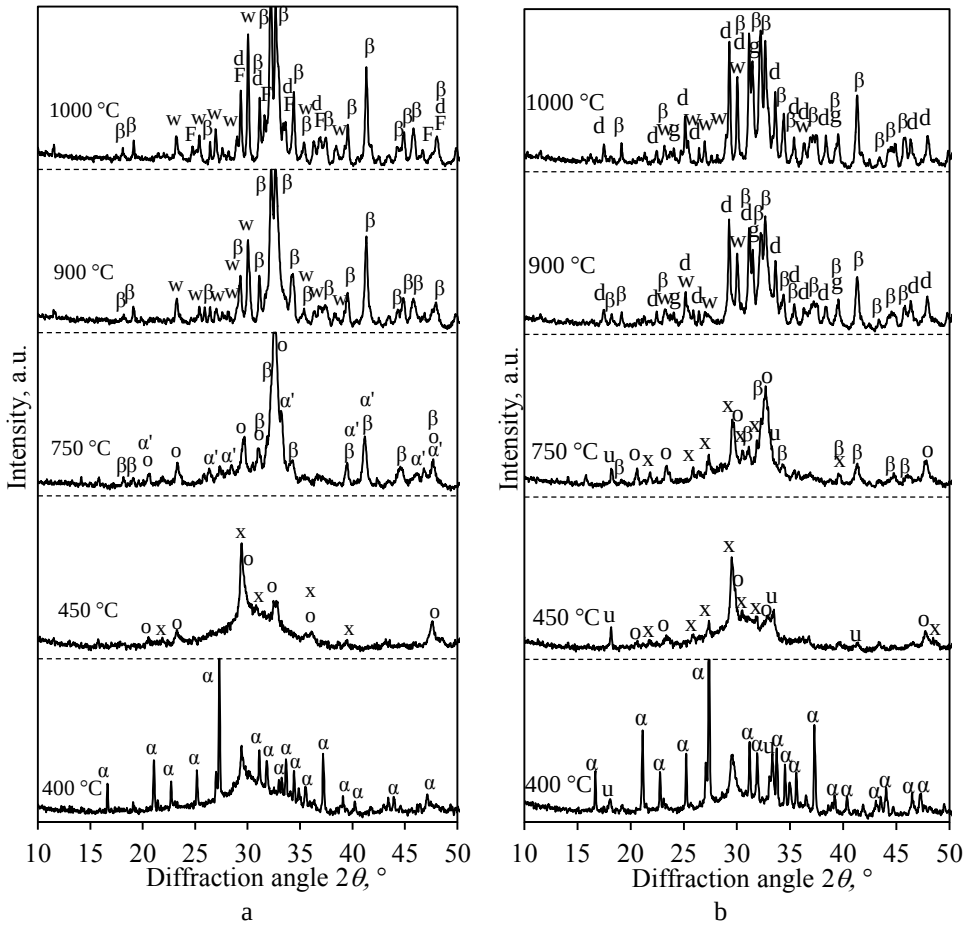

Fig. 3.6. XRD patterns of calcined α-C_2SH (a) and α-C_2SH-Al samples (b). Indexes: α – α-C_2SH; x – x-C_2S; o – calcium olivine; u – CA/CAS; α' – α'-C_2S; β – β-C_2S; g – gehlenite; w – wollastonite; d – kilchoanite; F – C_8S_5

It was determined that γ-Al_2O_3 additive changes not only the sequence of the formed compounds but also their stability during the calcination. XRD analysis data showed that, after calcination at 400 °C, the crystallinity of α-C_2SH-Al sample is 1.45 times higher than that of the pure samples (Fig. 3.7). Therefore, based on the

current observation, it is hypothesized that α-C_2SH formed in the mixtures with Al_2O_3 additive is more stable. On the other hand, under these calcination conditions, hydrogrossular samples are metastable and recrystallized to calcium aluminate (CA) (PDF 01-078-2975; *d*-spacing – 0.490; 0.268; 0.245; 0.219 nm) and/or calcium aluminate silicate (CAS) (PDF 00-055-0709; d-spacing – 0.489; 0.299; 0.67; 0.244 nm) (Fig. 3.6, b). The present results are consistent with literature data (155, 156, 157). Meanwhile, after calcination at 450 °C there are no significant changes on the products of calcination comparing with the pure sample (Fig. 3.6), although the crystallinity of α-C_2SH–Al sample is 1.37 times higher (Fig. 3.7). Significant differences between α-C_2SH and α-C_2SH–Al samples were observed after calcination at 750 °C. It was estimated that in α-C_2SH–Al sample, x-C_2S and calcium olivine remained stable, however, small intensity diffraction peaks of β-C_2S were observed. It should be noted that under these calcination conditions, in the pure system, x-C_2S was recrystallized into intermediary compounds and α'-C_2S was formed (Fig. 3.6, a). After increasing the temperature (900 °C), β-C_2S dominated in the products. Meanwhile, CA or/and CAS was fully recrystallized to gehlenite (PDF 01-089-6887; *d*-spacing – 0.371; 0.306; 0.284; 0.175 nm). It is worth mentioning that, in the products, high intensity diffraction peaks of kilchoanite and wollastonite were identified. Meanwhile, in the pure samples, traces of kilchoanite were identified only after calcination at 1000 °C. It was estimated that, after calcination at 1000 °C, products remain unchanged, although the crystallinity increased to 95.71% (Fig. 3.7).

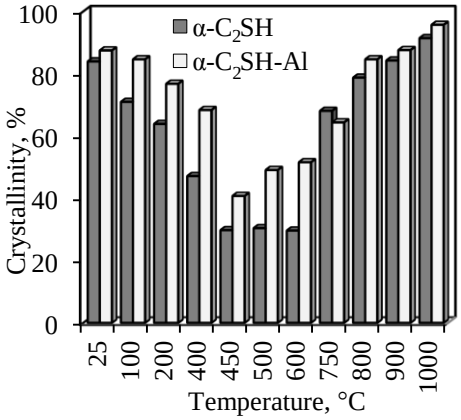

Fig. 3.7. Changes of crystallinity at 25-1000 °C temperature

3.1.3. Hydration properties of BM based on α-C_2SH or α-C_2SH–Al

It is known that the product of hydrothermal synthesis does not exhibit hydraulic activity because it is stabilized by hydrogen bonds in which silanol groups are involved. In order to achieve hydraulic activity, the mixture of this product must be activated by milling with or without another inert component containing SiO_2, such as quartz, and subsequently thermally treated. In this case, the hydrogen bonds are destroyed, and the reactive fragments are deposited in a disordered state on the

silicate surfaces (8, 13). For these reasons, in order to create a hydraulically active BM sample, α-C_2SH and α-C_2SH-Al (A/(S+A) = 0.05) samples were milled in a vibrating cup mill at 950 rpm for 5 min and thermally treated at 100–750 °C for 1 h. The reactivity of the prepared α-C_2SH samples was evaluated through the microcalorimetric analysis, and the results are presented in Fig. 3.8 and Fig. 3.9. The hydration curves of α-C_2SH samples prepared with the use of prior milling with subsequent thermal treatment at 400, 450 and 500 °C temperatures exhibit two distinctive peaks (Fig. 3.8), where the first one is associated with the initial wetting and dissolution of components after the first contact with water (the first exothermic effect), and then, after the initial reaction, the period of slow reaction (induction period) starts followed by a speed-up reaction (acceleration period), mainly controlled by nucleation and growth of hydrates (second exothermic effect) (6, 158–163). The curves of the above mentioned samples (Fig. 3.8) are characterized by similar initial peaks with the heat flow slight above 0.02 W/g, indicating a weak influence of the applied activation temperature (400–500 °C) on the initial reaction. The earliest (after 2.2 h) maximum of the heat release related to a speed-up reaction was obtained with α-C_2SH samples treated at 400 °C temperatures (Fig. 3.8). The peak heat flow was ~3.25 mW/g, which is comparable to the heat release of ordinary cement; the quantity of heat released after 70 h of hydration was 139.02 J/g (Fig. 3.9). The raised activation temperature (up to 450 °C) resulted in a more intensive exothermic effect with the maximum (~4.25 mW/g) which appeared after ~4.5 h (Fig. 3.8), and increased the cumulative heat (188.92 J/g) (Fig. 3.9, curve 2). The α-C_2SH samples reactivity was reduced when the treatment temperature was increased up to 500 °C, however, the maximum heat flow still reached ~2.8 mW/g (Fig. 3.8) and only a slight reduction of the total amount of heat was observed (178.73 J/g) (Fig. 3.9) as compared to that of α-C_2SH samples treated at 450 °C, which indicated that the hydration process was extended. After milling and treating at 750 °C temperature, the α-C_2SH sample showed poor reactivity at the initial stage; the induction period was prolonged up to ~15 h (Fig. 3.8) and followed by a very slow increase in the heat rate with a further very slow reaction resulting in the total heat of 88.45 J/g after 70 h (Fig. 3.9), which likely may be associated with the delayed dissolution and very slow reaction rate of β-C_2S (35, 93, 158). The comparison of the results discussed and the crystallinity of the investigated α-C_2SH samples (Fig. 3.7 and Fig. 3.8) show strong direct dependence of α-C_2SH samples reactivity on the level of its amorphisation. Such observation is consistent with the research of Link *et al*. (142), where it was also shown that the amorphous phase is the most reactive constituent. Under the 450 °C temperature, the most amorphisized material was obtained (crystallinity – 29.75 %). On the sample, thermally treated at 450 °C temperature without prior milling (Fig. 3.8), the most intensive initial exothermic effect was determined. Despite the fact that at this stage its heat flow (~0.9 W/g) exceeded that of the other samples more than three times, no evidence of hydration was observed in the further heat flow evolution (Fig. 3.8), which indicated the key role of the milling for the BM activation.

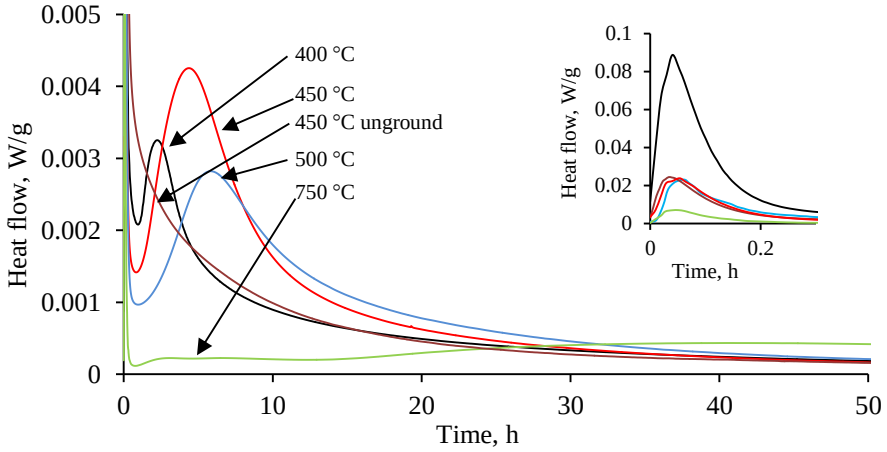

Fig. 3.8. Heat evolution rate of unground and ground α-C_2SH samples at different temperatures of calcination

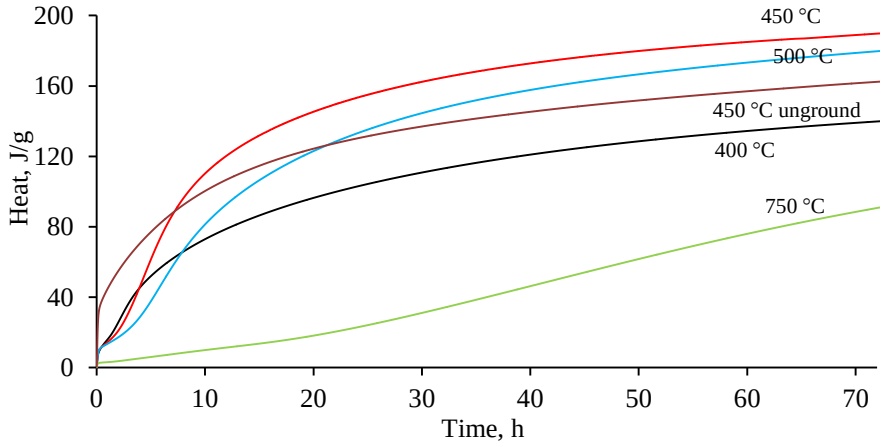

Fig. 3.9. Cumulative heat of unground and ground α-C_2SH samples at different temperatures of calcination

The addition of Al_2O_3 during synthesis did not influence significantly the initial hydration stage of α-C_2SH–Al samples treated at 450 °C temperature with prior milling (Fig. 3.10, a). The first exothermic peak was found to be analogous to that of the pure system (Fig. 3.8) with a slightly decreased maximum heat flow close to 0.02 W/g. However, in the further heat flow evolution, the two-step hydration process was observed clearly indicated by two distinctive exothermic effects. The first weak peak (~1.0 W/g) appeared after ~4 h of hydration and was followed by the second acceleration of reaction rate after ~5.5 h (Fig. 3.10, a). Probably, the second exothermic reaction occurs due to the hydration of calcium aluminate and/or calcium aluminate silicate, while the third one due to calcium silicates hydration. It was obtained that the cumulative heat after 5 h of hydration was 30.36 J/g (Fig. 3.10, b), which is two times lower as compared to a pure system within the same duration (61.44 J/g) (Fig. 3.9). The following main exothermic effect in α-C_2SH–Al samples

was accompanied by a more intensive peak (~2.5 mW/g); it appeared after ~11.5 h (Fig. 3.10, a). After 30 h of hydration, the total amount of the released heat was 162.34 J/g for the α-C_2SH sample and 148.14 J/g for the α-C_2SH–Al sample; after 70 h of hydration the total heat was found to be fairly similar: 188.92 J/g and 186.52 J/g, respectively (Fig. 3.10, b and Fig. 3.9).

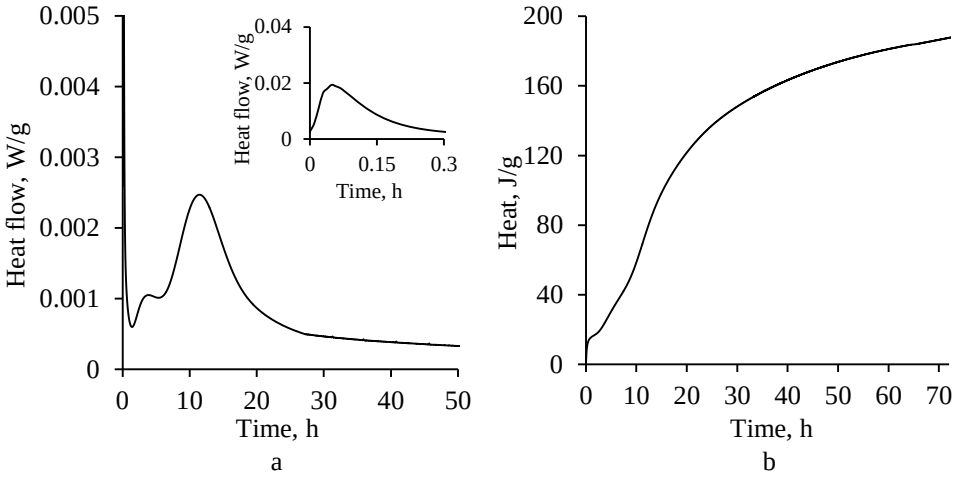

Fig. 3.10. Heat evolution rate (a) and cumulative heat (b) of α-C_2SH–Al samples

When summarizing the above outlined results, it can be stated that α-C_2SH sample reactivity strongly depends on the level of its amorphisation. The best results were obtained after calcination at 450 °C: an intensive exothermic effect with the maximum (~4.25 mW/g), appeared after ~4.5 h, and cumulative heat after 70 h – 188.92 J/g.

It is known, that in order to produce products (bricks, beam), cementitious materials are always mixed with filler such as sand. Thus in the next stage of the experiments, binder material was prepared by milling synthesis products and quartz sand.

3.1.4. Hydration properties of BM based on α-C_2SH or α-C_2SH–Al and quartz sand

In this part of the work, the binder material was prepared by milling synthetic α-C_2SH or α-C_2SH-Al (24 h, 175 °C, A/(S+A) = 0 or 0.05) and quartz sand (the ratio of components was equal to 1:1 by mass) and thermally treated at 450 °C for 1 h. After milling, the mean diameter of the particles of BM-α-Q and BM-α-Al-Q samples was equal to 10.11 and 10.21 μm, respectively. It was determined that, after the outlined process, the sample is significantly amorphized because the intensity of the diffraction peaks characteristic to α-C_2SH (*d*-spacing – 0.327; 0.242; 0.288; 0.422 nm) significantly decreased (Fig. 3.11. curve 2). It should be noted that milling also results in the destruction of quartz: a decrement of integral intensity of quartz individual Bragg peak (*d*-spacing–0.335 nm) was observed from 695 cps to 548 cps. Thus the structure of the hydrothermal synthesis products is partially destroyed during the milling but a large quantity of crystallization water remains in

the milled product preventing more active reaction during the hydration. For that, the mixture was thermally treated at 450 °C for 1 h. As expected, after calcination, x-C_2S and calcium olivine were formed in the products (Fig. 3.11). However, the low intensity diffraction peak (*d*-spacing 0.327 nm) of α-C_2SH was still presented in the samples. Also it was observed that the intensity of quartz main peak (*d*-spacing0.335 nm) decreased from 548 to 461 cps (Fig. 3.11. curves 2–3), presumably during calcination part of quartz reacted with calcium ions. As a result, CaO/SiO_2 ratio decreases and the formation of semicrystalline calcium silicate hydrate C-S-H is possible. The effectiveness of the discussed method was tested by microcalorimetry analysis.

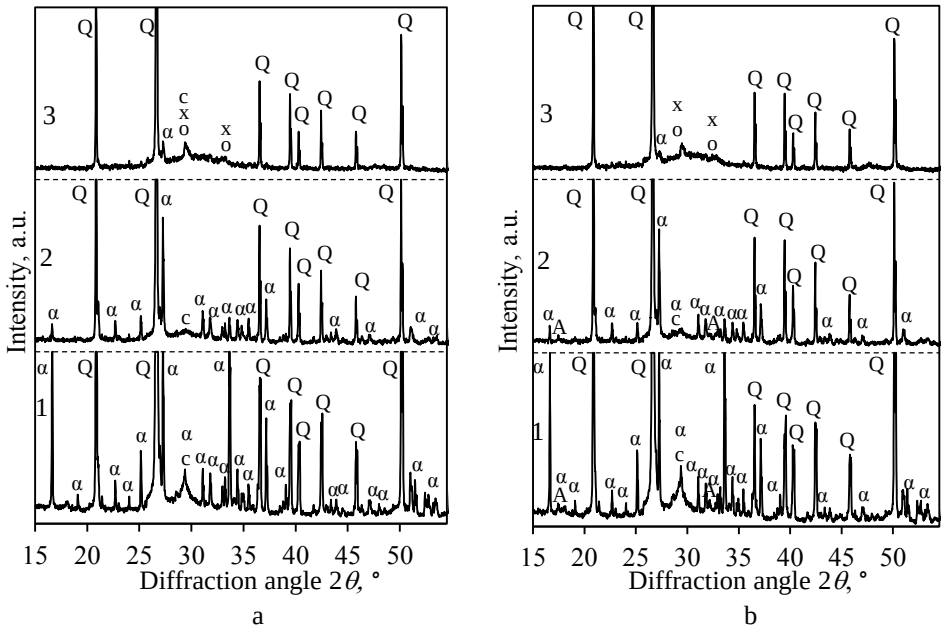

Fig. 3.11. XRD patterns of prepared BM samples based on: a – α-C_2SH; b – α-C_2SH-Al, before milling (curve 1) after milling (curve 2) and burning (curve 3). Indexes: α – α-C_2SH; Q – quartz; c – C-S-H; x – x-C_2S; o – calcium olivine; A – hydrogrossular

Data on the rates of heat evolution (W/g) of BM samples is presented in Figure 3.12. As in the previous case (Fig. 3.8 and Fig. 3.10, a), the heat release curves obtained during the hydration of BM-α-Q and BM-α-Al-Q samples show two and three distinctive peaks, respectively (Fig. 3.12). According to literature (6, 159–163), the first exothermic reaction is caused by the dissolution of the sample constituents, which results in the development of surface hydrates on the sample particles. It was determined that the BM-α-Al-Q sample shows a slightly higher maximum heat release rate (0.0106 W/g) compared with the BM-α-Q sample (0.0095 W/g). Thus the results shown in Figure 3.12 indicate that there is no significant effect from type of α-C_2SH component at this stage. Therefore, based on the current observation, it is hypothesized that the α-C_2SH component does not noticeably contribute to or influence chemically the initial reactions.

The further hydration showed a period of slow reaction (the induction period) followed by a speed-up reaction (the acceleration period). The above mentioned stage of hydration is widely thought to be nucleation and growth controlled (6, 159–163).It was determined that the γ-Al_2O_3 additive changed both the heat flow and the total quantity of the heat released during hydration. It was determined that the induction period in the BM-α-Q sample lasts ~1.5 h while in the BM-α-Al-Q sample it was shortened to 40–50 min (Fig. 3.12, a).It was observed that the second exothermic reaction in the BM-α-Q sample proceeded from 2 to 9 h (Fig. 3.12, a, curve 1), and, during this process, the total amount of heat was increased to 51.92 J/g (Fig. 3.12, b, curve 1). Meanwhile, in the BM-α-Al-Q sample, the quantity of the heat released within the same duration of hydration was two times lower and equal to 25.47 J/g (Fig. 3.12, b, curve 2). The prime reason is that, during the same period, only the second exothermic reaction which can be related with calcium aluminate and/or calcium aluminate silicate hydration, proceeded. It is worth mentioning that the main hydration reaction (the 3rd exothermic reaction) ended only after 18 h; during this process, the released amount of heat was equal to 56.81 J/g.

At the later stages of hydration, the calorimetric curve of BM showed the slower continued reaction because the rate of heat evolution decreased. It can be seen in Figure 3.12, b, that the total heat (90.53 J/g) for the BM-α-Q sample after 60 hours is not significantly different to that of the BM-α-Al-Q sample (96.27 J/g). This is consistent with the nucleation hypothesis whereby no chemical reaction (exothermic or not) occurs, so that the total heat release after 60 hours should be fairly similar for all BM samples.

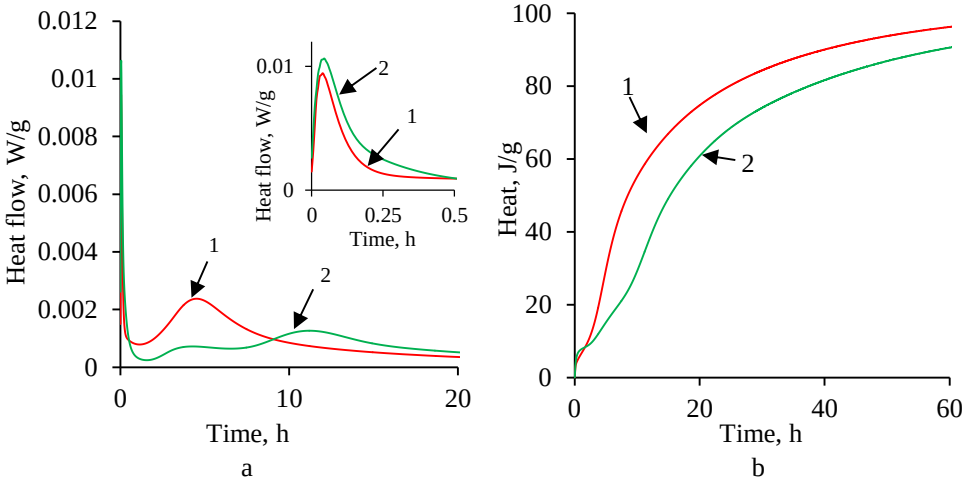

Fig. 3.12. Heat evolution rate (a) and cumulative heat (b) of BM samples based on: 1 – α-C_2SH; 2 – α-C_2SH-Al

The reactivity of the primary mixture components is one of the most important factors which predetermine the mineral composition of the products. In order to evaluate the quantity of the reacted quartz and the heat of the formed compounds (calcium silicate hydrate) during the hydration of BM samples, the experiments performed in the framework of microcalorimetric analysis were repeated under

laboratory conditions in a thermostat at a temperature of 25 °C, when the reactions were repeated at different time periods: 0, 2, 4.5, 9, 11.5, 18 h and halted by using acetone. Later on, the samples were crushed to powder, dried at a temperature of 50 ± 5 °C and put through a sieve with an 80 μm mesh. The selected durations of the halted reactions coincide with the duration interval of the second exothermic reaction, when different compositions of BM samples were used.

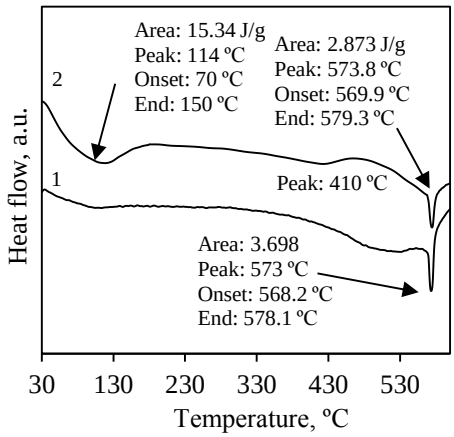

Fig. 3.13. DSC curves of the BM-α-Al-Q sample when the duration of hydration, h is: 1 – 0; 2 – 18

Firstly, the quantity of unreacted quartz was determined by QDSC (Fig. 3.13. and Fig. 3.14, a). The quantity of quartz was calculated from the heat change of the endothermic effect at 573 °C. The quantity of quartz in the BM samples (before hydration) was equal to 100 % (Fig. 3.14, a, curve 1–2). As it stems from the data shown in Figure 3.14, only 5 % of quartz reacts during the first 4 hours of hydration in both BM samples, and the further reduction of its quantity depends on the duration of process. In the BM-α-Q sample, quartz reacts considerably quicker, and about 28–30 % of it is bound during 11.5–18 hours of hydration (Fig. 3.14, a). Meanwhile, in the BM-α-Al-Q sample, within 11.5 h of hydration, quartz reacted 2.5 times less, and within 18 h by 1.4 times less.

The quantity of the dehydration heat (due to the loss of water from C-S-H) depends on the duration of hydration. It was observed that, in the BM-α-Q sample, the largest difference between the absorbed heat (10.66 J/g) of dehydration reactions within the temperature range of 50–150 °C after 4.5 h of hydration is due to the loss of water from the formed C-S-H compounds. It was determined that the heat of the dehydration process slightly increased when the experiment was prolonged to 18 h. Meanwhile, in the BM-α-Al-Q sample, the same amount of heat (10.66 J/g) was absorbed within 11.5 h of hydration (Fig. 3.14, b). This data agrees with the results of the heat evolution rate and confirms that the quantity of calcium silicate hydrates compounds increases during the hydration of BM samples.

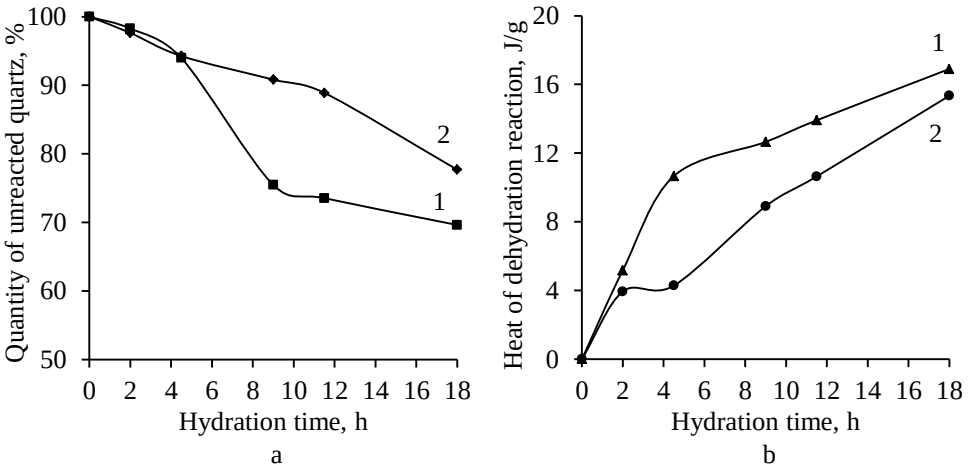

Fig. 3.14. The quantity of unreacted quartz (a) and the heat of dehydration reactions due to the loss of water from C-S-H (endothermic peak at 50–150 °C) (b) during the hydration of BM-α-Q (curve 1) and BM-α-Al-Q (curve 2) samples

As expected, when the duration of hydration was extended, the amount of the formed products (variable composition and structure calcium silicate hydrates) was increased. It is clearly seen in XRD patterns (Fig. 3.15): the prolongation of the duration from 2 to 18 h led to the increase in diffraction peak area (*d*-spacing – 0.303 nm) from 45.65 to 164.46 a. u. Moreover, it was observed that, in the BM-α-Al-Q sample after 2 h of hydration, the latter diffraction maximum area was larger than in the pure system (55.08 a. u.). However, after 18 h of reaction, the area was smaller comparing to the BM-α-Q sample and equal to 140.12 a. u. The results of XRD analysis were in a good agreement with the DSC data (Fig 3.14 and Fig.3.15).

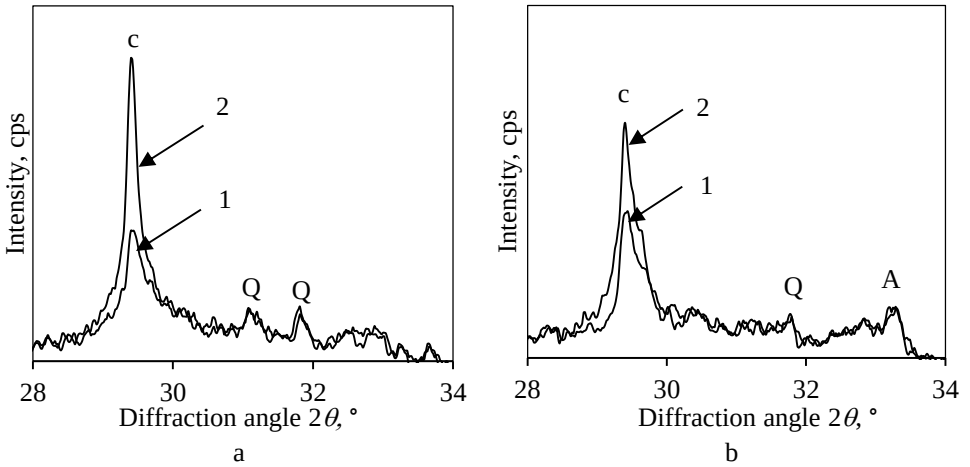

Fig. 3.15. The change of the main diffraction peak of C-S-H (*d*-spacing–0.303 nm) in BM-α-Q (a) and BM-α-Al-Q (b) samples after hydration, h:1 – 2; 2 – 18. Indexes: A –hydrogrossular; Q – quartz; c – C-S-H

Interestingly, during the hydration of the BM-α-Al-Q sample, calcium aluminates and/or calcium aluminate silicates react with water, and hydrogrossular family compounds form in the products (*d*-spacing – 0.269 nm) (Fig. 3.15, b). This data agrees with the DSC results because the small endothermic effect at ~410 °C temperature which can be assigned to the decomposition of the hydrogrossular substance was identified (Fig. 3.13). Moreover, this data agrees with the results of the microcalorimetric analysis data and confirms that the formed compounds with Al^{3+} ions during hydrothermal synthesis have a crucial effect on the hydration mechanism of BM.

It is known that the formation of calcium silicate hydrates depends not only on the used additives, but also on the calcium oxide and silicon dioxide molar ratio (1, 23–25, 56–59, 88–92, 142). Thus, in order to examine the influence of C/S molar ratios on the crystallization reaction of α-C_2SH under hydrothermal conditions, in the next stage of the experiment, the synthesis of the above mentioned compound in $1.75CaO–(1-x)SiO_2 \cdot nH_2O–xAl_2O_3–H_2O$ suspensions at 175 °C was performed.

Acknowledgements:

Reprinted/Adapted by permission from Springer Nature: Springer Nature; Journal of Thermal Analysis and Calorimetry / The influence of aluminum additive on the α-C_2S hydrate formation process / K. Baltakys, A. Eisinas, T. Dambrauskas, 121:75-84. 2015 https://doi.org/10.1007/s10973-015-4591-3; License No. 4505290941002

Reprinted/Adapted by permission from Springer Nature: Springer Nature; Journal of Thermal Analysis and Calorimetry / Hydration peculiarities of high basicity calcium silicate hydrate samples / T. Dambrauskas, K. Baltakys, J. Škamat A. Kudžma, 131:491-499. 2018 https://doi.org/10.1007/s10973-017-6320-6; License No. 4505290855836

3.2. Formation of α-C_2SH in 1.75CaO–(1-x)SiO_2·nH_2O–xAl_2O_3–H_2O suspensions at 175 °C

It was determined that in 1.75CaO–SiO_2·nH_2O–H_2O suspensions, within 4 hours of isothermal curing at 175 °C α-C_2SH and semicrystalline calcium silicate hydrates were formed (Fig. 3.16, a, curve 1). It is worth mentioning that the intensity of diffraction peaks of unreacted portlandite was~4 times higher compared to the 1.5CaO–SiO_2·nH_2O–H_2O system (Fig. 3.1, curve 1).

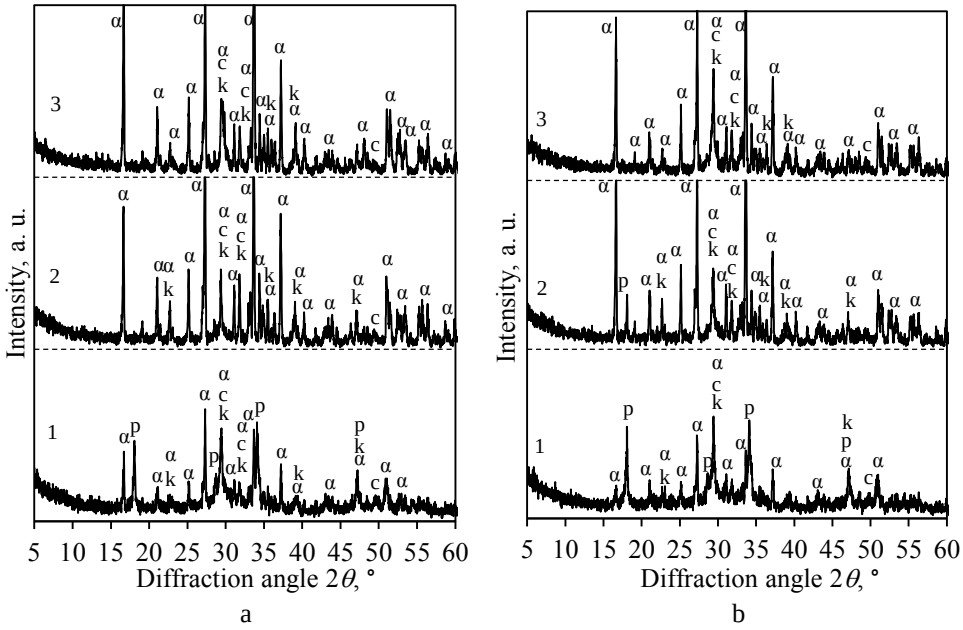

Fig 3.16.XRD patterns of the synthesis products when the molar ratio of the primary mixtureswere equal to CaO/(SiO_2+Al_2O_3)=1.75 and Al_2O_3/(SiO_2+Al_2O_3)=0 (a) or 0.025 (b). Duration of hydrothermal synthesis at 175 °C temperature, h: 1 – 4; 2 – 24; 3 – 72. Indexes: c – C-S-H; α – α-C_2SH;p – $Ca(OH)_2$; k – $CaCO_3$

The previous results were confirmed by STA analysis data. As expected, the dehydration of α-C_2SH as well as the decomposition of portlandite overlaps each other within the 400–500 °C temperature range (Fig. 3,17, a). More information was obtained from a derivative of the TGA curve (DTGA): the decomposition of portlandite was observed within the 410–435°C temperature range while the dehydration of α-C_2SH took place at higher temperatures (435–486 °C) (Fig. 3.17, a, curve 3). Moreover, it was estimated that, during the decomposition of portlandite, the synthesis products lose ~2.23 % of mass, which is equivalent to 7.19 % of portlandite (Fig. 3.17, a, curves 1, 3; Table 3.3). Meanwhile, within the 435–486 °C temperature range, the mass loss is equal to 1.43 %, resulting in 15.09 % of the formed α-C_2SH. It should be underlined that the mentioned data is in good agreement with QXRD results (Table 3.3). It is worth mentioning that in the mixture with a lower CaO/SiO_2 molar ratio (1.5), due to the small quantity of portlandite, it was not possible to distinguish the thermal effect of the latter compound from

α-C_2SH (Fig. 3.2). Also, two very small exothermic effects at ~834 °C and ~869 °C characteristic to recrystallization of C-S-H(I) and C-S-H(II), respectively, were identified (Fig. 3.17, a, curve 2). In addition, the decomposition of calcium carbonate was observed at ~719 °C (Fig. 3.17, a, curve 2), while TGA analysis data showed that 14.59 % of the latter compound is present in the synthesis products (Fig. 3.17, a, curve 1).

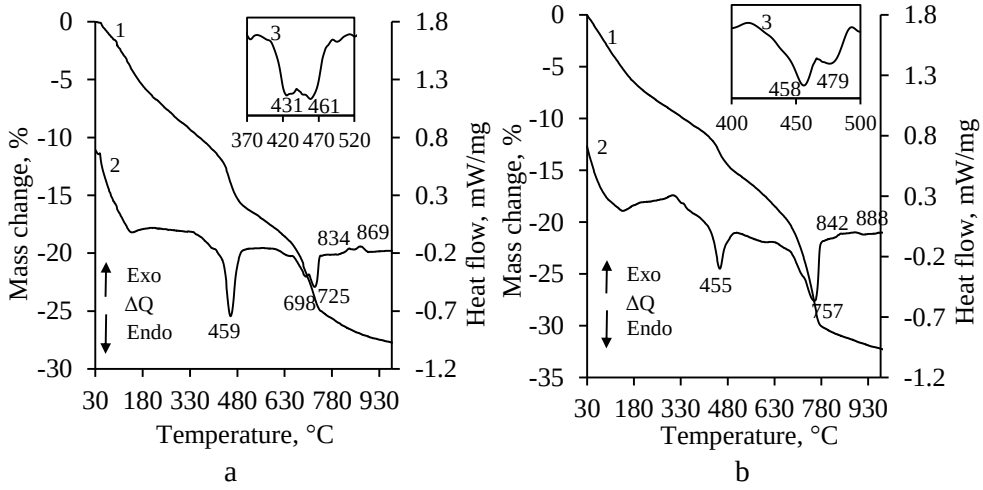

Fig 3.17. STA curves of the synthesis products when the molar ratio of the primary mixtures was equal to $CaO/(SiO_2+Al_2O_3)$=1.75 and $Al_2O_3/(SiO_2+Al_2O_3)$=0 (a) or 0.025 (b). Duration of hydrothermal synthesis at 175 °C temperature is 4 h.
1 – TGA; 2 – DSC; 3 – DTGA

Table 3.3. The quantity of α-C_2SH, $Ca(OH)_2$ and $CaCO_3$ (%) in the products

The molar ratio of $Al_2O_3/(SiO_2+Al_2O_3)$ in the primary mixtures	Compound	Quantity according to the TGA method, %					
		Synthesis duration, h					
		4	8	16	24	48	72
0	α-C_2SH	15.09	-	49.35	63.44	62.91	59.32
	$Ca(OH)_2$	7.19	-	1.42	0	0	0
	$CaCO_3$	14.59	-	9.55	2.96	3.11	3.32
0.025	α-C_2SH	8.97	30.93	38.32	45.74	62.91	65.66
	$Ca(OH)_2$	10.89	5.97	3.51	1.62	0	0
	$CaCO_3$	25.07	16.36	8.45	7.11	5.77	4.58
		Quantity according to the QXRD method, %					
0	$Ca(OH)_2$	7.54	3.56	1.12	0	0	0
0.025	$Ca(OH)_2$	11.04	6.37	3.75	1.29	0	0

As expected, in the mixtures with $CaO/(SiO_2+Al_2O_3)$ = 1.75 and $Al_2O_3/(SiO_2+Al_2O_3)$ = 0.025 molar ratio, Al_2O_3 additive changes the stability of the formed compounds. XRD analysis data showed that portlandite reacted slower, because, after 4 h of isothermal curing, more unreacted portlandite was observed in the synthesis products (Table 3.3). For this reason, lower intensity diffraction peaks of α-C_2SH were obtained in the system (Fig. 3.16, b, curve 1). It should be noted

that only 1.7 % of Al_2O_3 was added to the initial mixture, therefore, the diffraction peaks characteristic to hydrogrossular were not identified in the XRD curve (Fig. 3.16, b, curve 1).

The previous data was additionally confirmed by STA and DSC analysis. It was estimated that, after 4 h of synthesis, about 11 % of portlandite is present in the products, and only 9 % of α-C_2SH is formed (Table 3.3). It should be noted that under all experimental conditions, in the mixtures with the Al_2O_3 additive, an endothermic effect at ~300–400 °C temperature range typical of the dehydration of hydrogrossular was not observed (Fig. 3.17 and Fig. 3.19). In order to confirm the obtained data, the samples were characterized by DSC analysis with E thermocouple which is more sensitive. As expected, DSC analysis data confirmed the above mentioned results that all Al^{3+} ions were incorporated in the structure of the synthesis products (Fig. 3.18). Moreover, at higher temperatures, C-S-H(I) (~842 °C) and C-S-H(II) (~888 °C) recrystallization processes are observed (Fig. 4, b, curve 2). It was determined that the quantity of the formed calcium carbonate in the mixtures with $CaO/(SiO_2+Al_2O_3)$ = 1.75 and $Al_2O_3/(SiO_2+Al_2O_3)$ = 0.025 was ~1.7 times higher than in the pure system (Table 3.3). Probably, the difference stemmed from a higher quantity of unreacted portlandite which has a lower resistance to carbonization (41, 60, 164–166).

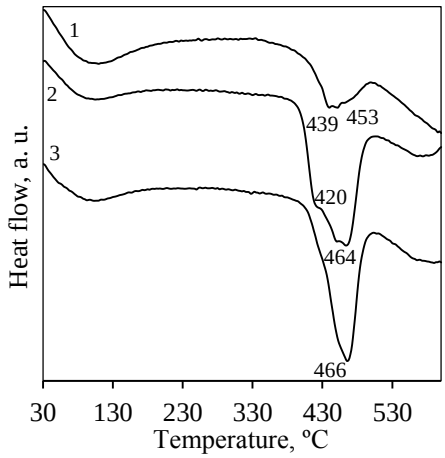

Fig 3.18. DSC curves of the synthesis products when the molar ratio of the primary mixture was equal to $CaO/(SiO_2+Al_2O_3)$=1.75 and $Al_2O_3/(SiO_2+Al_2O_3)$=0.025. Duration of hydrothermal synthesis at 175 °C temperature is, h: 1 – 4; 2 – 24; 3 – 72

By continuing the synthesis (24 h), in a pure system, the intensity of the diffraction maximums characteristic to α-C_2SH were increased, meanwhile, $Ca(OH)_2$ fully reacts (Fig. 3.16, a, curve 2). According to the TGA data (Table 3.3), it was calculated that the quantity of formed α-C_2SH was equal to 63.44 %, meanwhile in the mixtures with CaO/SiO_2 = 1.5, the quantity of the above mentioned compound was 1ower (~51 %). It should be underlined that, under these synthesis conditions, C-S-H(II) became metastable because the exothermic effect at ~885 °C was not observed (Fig. 3.19, a). As expected, the heat flow of C-S-H(I)

recrystallization to wollastonite was increased up to 13.42 J/g (Fig. 3.19, a). Meanwhile in the mixtures with Al_2O_3 additive, quite intensive diffraction peaks of unreacted portlandite as well as thermal effect of its decomposition at 443 °C were observed (Fig. 3.16, b, curve 2 and Fig. 3.19, b).

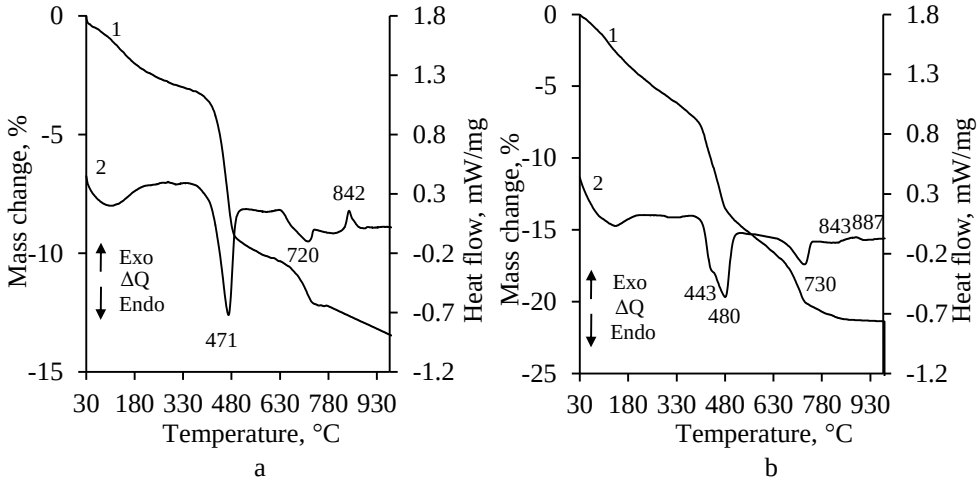

Fig 3.19. STA (1 – TGA; 2 – DSC) curves of synthesis products when the molar ratio of the primary mixtures were equal to $CaO/(SiO_2+Al_2O_3)=1.75$ and $Al_2O_3/(SiO_2+Al_2O_3)=0$ (a) or 0.025 (b). The duration of hydrothermal synthesis at 175 °C temperature was 24 h.

Thus, after 48–72 h of synthesis, the intensities of the diffraction peaks and the quantity of α-C_2SH were close, suggesting that the Al_2O_3 additive has no influence on the quantity of the formed α-C_2SH (Fig. 3.16, Table 3.3).

It is thus possible to assume that, when curing the mixture of CaO and amorphous SiO_2 at 175 °C temperature under the saturated steam pressure, the reactions of the new compounds formation occurred in the following sequence:

$$1.75CaO+SiO_2\cdot nH_2O+H_2O \xrightarrow{4\text{-}16h} \begin{matrix}\text{portlandite}\\ \text{C-S-H(I)}\\ \text{C-S-H(II)}\\ \alpha\text{-}C_2SH\end{matrix} \xrightarrow{24\text{-}72h} \begin{matrix}\text{C-S-H(I)}\\ \alpha\text{-}C_2SH\end{matrix}$$

It was determined that the additive of Al_2O_3 changes the stability duration intervals of the primary and intermediates compounds:

$$1.75CaO+SiO_2\cdot nH_2O+H_2O+0.025Al_2O_3 \xrightarrow{4\text{-}24h} \begin{matrix}\text{portlandite}\\ \text{C-S-H(I)}\\ \text{C-S-H(II)}\\ \alpha\text{-}C_2SH\end{matrix} \xrightarrow{48h} \begin{matrix}\text{C-S-H(I)}\\ \text{C-S-H(II)}\\ \alpha\text{-}C_2SH\end{matrix} \xrightarrow{72h} \begin{matrix}\text{C-S-H(I)}\\ \alpha\text{-}C_2SH\end{matrix}$$

By summarizing the results discussed in Sections 3.1 and 3.2, it can be stated that the optimal synthesis duration for α-C_2SH is 24 h because portlandite fully

reacts, and the amount of α-C_2SH is the highest. Also, it is recommended to use mixtures with a lower molar ratio (C/S=1.5) because it requires a lower amount of CaO; consequently, the emission of CO_2 is reduced up to ~16 %.

In order to increase the reaction rate and avoid the formation of intermediate compounds, in the next stage of the experiment, hydrothermal synthesis was carried out in 1.5CaO–(1-x)$SiO_2 \cdot nH_2O$–xAl_2O_3–H_2O suspensions at 200 °C temperature.

Acknowledgements:

Reprinted/Adapted by permission from Trans Tech Publications: Trans Tech Publications; Solid state phenomena / The Synthesis of α-C_2S Hydrate Substituted with Al^{3+} Ions in Mixture with CaO/SiO_2=1.75/ K. Baltakys, T. Dambrauskas, A. Eisinas, 244: 26–33. 2016 https://doi.org/10.4028/www.scientific.net/SSP.244.26; License No. 4462520983212

3.3. Formation of α-C_2SH in 1.5CaO–(1-x)$SiO_2 \cdot nH_2O$–xAl_2O_3–H_2O suspensions at 200°C and application as a precursor for binder material

3.3.1. Hydrothermal synthesis of α-C_2SH in a pure system

It was determined that in 1.5CaO–$SiO_2 \cdot nH_2O$–H_2O suspensions at 200 °C temperature, the calcium containing compound – portlandite – reacted heavily because after 4 h of isothermal curing, quite intensive characteristics of the latter compound diffraction maximums (*d-spacing* – 0.493 and 0.262 nm) were identified in the XRD curve (Fig. 3.20, curve 1). For this reason, only a fair amount of α-C_2SH and semicrystalline C-S-H were formed in the products. It should be underlined that the intensities of the diffraction peaks characteristic to portlandite were 3 times higher, whereas those of α-C_2SH were 20 times lower in comparison with the results obtained after synthesis in a pure system at 175 °C temperature (Fig. 3.1). Also, a broad basal reflection common in amorphous structure compounds was identified in the interval of 26–37° diffraction angles.

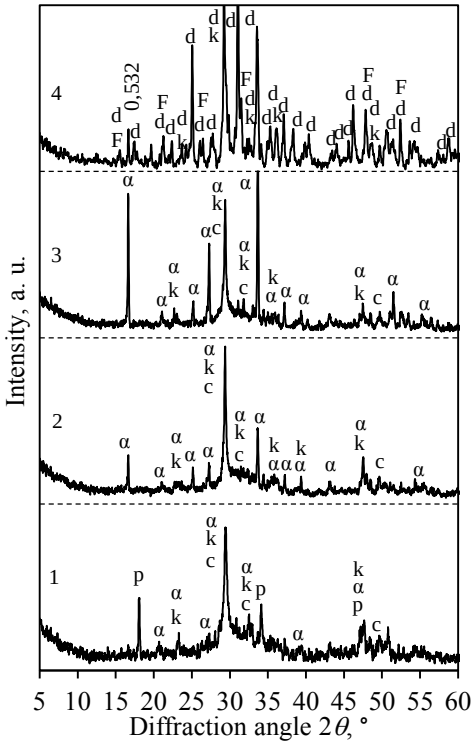

Fig. 3.20. XRD patterns of the synthesis products when the molar ratio of the primary mixture was equal to CaO/SiO_2=1.5. Duration of hydrothermal treatment at 200 °C temperature, h: 1 – 4; 2 – 8; 3 – 16; 4 – 72. Indexes: c – C-S-H; α – α-C_2SH; p – $Ca(OH)_2$; d – kilchoanite; k – $CaCO_3$; F – C_8S_5

STA analysis data is in good agreement with XRD results (Fig. 3.21). In the DSC curve, the first endothermic effect (30–210 °C) can be assigned to the dehydration of crystallization water in calcium silicate hydrates. The second endothermic effect at ~ 459 °C temperature can be attributed to the dehydration of α-C_2SH as well as to the decomposition of portlandite (Fig. 3.21, curves 2 and 3). Moreover, during these reactions, the estimated amount of the heat flow (22.54 J/g, Table 3.4) confirmed that only a small quantity of dibasic calcium silicate hydrate was formed in the synthesis products (Fig. 3.21, curve 2). Meanwhile, above the 800 °C temperature, two exothermic effects were identified: at ~842 °C and ~877 °C temperatures characteristic to C-S-H(I) and C-S-H(II), respectively, reflecting their recrystallization to wollastonite (Fig. 3.21, curves 2 and 3). It was calculated that, during the process, the quantity of the heat flow is equal to: 1.53 J/g for C-S-H(I) and 5.61 J/g for C-S-H(II) (Table 3.4). Furthermore, an endothermic effect at ~714 °C temperature can be assigned to the decomposition of calcium carbonate (Fig. 3.21, curve 2). According to the TGA analysis data, it was calculated that 8 % of the latter compound is present in the synthesis products.

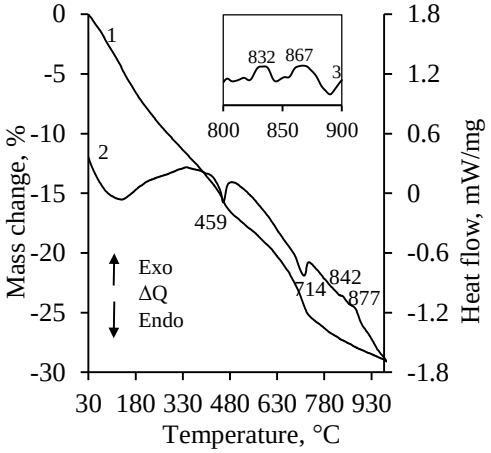

Fig 3.21. STA (1 – TGA; 2 – DSC; 3 – DDSC) curves of synthesis products when the molar ratio of the primary mixture was equal to CaO/SiO_2=1.5. Duration of hydrothermal synthesis at 200 °C temperature was 4 h.

Table 3.4. Dependence of pH value of medium and the heat of thermal effects typical of α-C_2SH, C-S-H(I) and C-S-H(II) on the duration of synthesis

Synthesis duration, h	pH value of liquid medium	Heat of thermal effect, J/g		
		Temperature range, °C		
		400-500	830-850	850-880
		α-C_2SH	C-S-H(I)	C-S-H(II)
4	12.39	-	1.53	5.61
8	12.37	58.55	0.11	7.32
16	12.25	94.03	0.8	6.72
24	12.15	16.97	6.39	0
72	11.90	0	3.59	0

The FT-IR spectrum of the synthesis products obtained after 4 h of treatment is presented in Figure 3.22. In the bending vibrations range, intensive triplet at ~454, ~514 and ~559 cm^{-1}, which can be assigned to δ(Si-O-Si) and δ(O-Si-O) signals, were observed. Also, a broad absorption band at 965 cm^{-1} can be attributed to symmetrical ν_s(O-SiO-) stretching vibrations. Meanwhile, the bending δ(OH(Si)) signals were observed at 1281 cm^{-1} (Fig. 3.22). The identification of dibasic calcium silicate hydrates absorption bands of $\nu(OH^-)$ and $\nu(H_2O)$ stretching vibrations is complicated. The bands at 3642 and 3538 cm^{-1} prove that clearly distinguished OH^- positions exist in the structure of samples which are connected only with Ca atoms and are not influenced by hydrogen bridge links. It should be noted that the absorption band at 3642 cm^{-1} confirms that the initial compound – portlandite – remains unreacted. $\nu(OH^-)$ and $\nu(H_2O)$ vibrations within a low frequency range (from 1700 to 3300 cm^{-1}) indicates that molecular water forms strong hydrogen bridge links in the interlayers. It was determined that small amounts of water of absorption and crystallization exist in the structure of the synthesis products regarding the observed absorption bands at 1638 cm^{-1} (bending $\delta(H_2O)$ vibrations) and 3466 cm^{-1} (stretching $\nu(OH^-)$ vibrations). In addition, the absorption signals at

752 and 667 cm^{-1}can be attributed to $\nu(OH^-)$ vibrations (78). It should be noted that under these experimental conditions $\nu(C\text{-}O_3^{2-})$, vibrations at 874 and 1424 cm^{-1} are clearly visible in the FT-IR spectrum due to the apparent carbonation when the products were dried in an air-conditioned chamber.

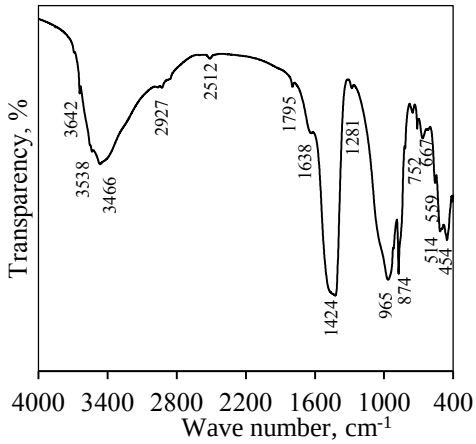

Fig. 3.22. FT-IR spectrum of the synthesis products when the molar ratio of the primary mixture was equal to CaO/SiO_2=1.5, and the duration of hydrothermal treatment at 200 °C temperature was 4 h

Within 8 h of hydrothermal synthesis, $Ca(OH)_2$ fully reacts because there was no evidence of diffraction peaks characteristic to this compound in the XRD patterns (Fig. 3.20, curve 2). This fact was confirmed by FT-IR data because the absorption band at 3642 cm^{-1} disappeared. It was determined that the intensity of α-C_2SH diffraction peaks increased several times as well as heat flow of its dehydration (from 22.54 J/g to 58.55 J/g) (Fig.3.21, curve 2; Figure 3.23, curve 2, Table 3.4). Meanwhile, the heat flow of C-S-H(I) and C-S-H(II) recrystallization to wollastonite does not appear to change.

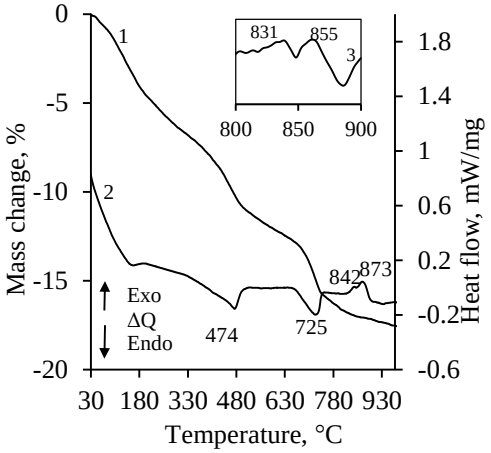

Fig. 3.23. STA (1 – TGA; 2 – DSC; 3 – DDSC) curves of the synthesis products when the molar ratio of the primary mixture was equal to CaO/SiO_2=1.5. The duration of hydrothermal synthesis at 200 °C temperature was 8 h

It was calculated that, after 8 h of isothermal treatment, the mass loss during α-C_2SH decomposition was equal to 4.45 wt. %, resulting in 48.95 % of the formed above mentioned compound (Table 3.5). It should be underlined that this value is in good agreement with the data obtained by Ishida *et al*. (77).

Table 3.5. The quantity of α-C_2SH and $CaCO_3$ in the products

Synthesis duration, h	Data according to the TGA method			
	Mass losses at 400-500°C, %	Quantity, %	Mass losses at 650-750°C, %	Quantity, %
	α-C_2SH		$CaCO_3$	
4	-	-	3.23	7.34
8	4.45	48.95	3.01	6.84
16	4.37	48.07	3.73	8.48
24	1.96	21.56	1.27	2.89
72	0	0	2.01	4.57

It was determined that by prolonging the duration of hydrothermal synthesis to 16 h, the intensity of diffraction maximums characteristic to α-C_2SH increased (Fig. 3.20, curve 3). DSC data confirmed that a larger amount of the main synthesis product – α-C_2SH – is formed due to the observed increase in the dehydration heat flow (1.6 times). It was estimated that, after 8–16 h of synthesis, about 49 % of α-C_2SH is formed (Table 3.5).

Unexpected results were obtained after 24 h of hydrothermal treatment: recrystallization of α-C_2SH to kilchoanite (PDF 04-009-7055, *d-spacing* – 0.355; 0.304; 0.288; 0.267), which does not contain water ($Ca_6(SiO_4)(Si_3O_{10})$), was observed. The XRD data was supported by STA analysis results. In the DSC curve, an endothermic effect reflecting the removal of crystallization water was not observed in the 70–150 °C temperature interval (Fig. 3.24, curve 1). Meanwhile, the heat flow of α-C_2SH dehydration decreased from 94.03 J/g to 16.97 J/g (Table 3.4),

although the latter compound was not identified in the XRD patterns. It should be underlined that, in the synthesis products, the amount of calcium carbonate decreased (2.9 wt. %) as well. This fact can be explained by the kilchoanite resistance to carbonization. Moreover, an exothermic effect typical of C-S-H(II) recrystallization to other compounds was not identified.

The present results are in good agreement with the data obtained by Black *et al*. (40). The authors determined that, during hydrothermal synthesis of α-C_2SH at 200 °C, kilchoanite also formed in the products. In this case, α-C_2SH was prepared from β-C_2S which was treated mechanochemically in an agate ball mill for 24 h and followed by hydrothermal treatment. The same tendency was observed in N. Meller *et al*.'s work (24), in which the hydrothermal reactions of an oil well cement with added silica and alumina during hydration (200 to 350 °C) was examined, and it was estimated that kilchoanite is formed in the samples at 200 °C.

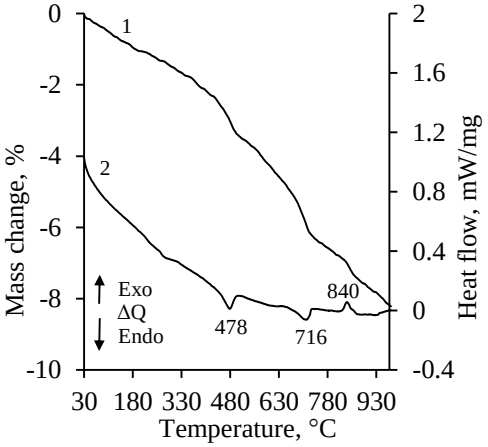

Fig. 3.24. STA (1 – TGA; 2 – DSC) curves of the synthesis products when the molar ratio of the primary mixture was equal to CaO/SiO_2=1.5. The duration of hydrothermal synthesis at 200 °C temperature was 24 h.

Furthermore, after extending the duration of isothermal curing to 48 and 72 h, α-C_2SH is fully recrystallized to kilchoanite and C_8S_5 (PDF 00-029-0368; *d*-spacing – 0.360; 0.305; 0.284; 0.269 nm) due to undetected diffraction maximums characteristic to α-C_2SH in XRD patterns (Fig. 3.20, curve 4).

It is possible to assume that, when curing the mixture of CaO and amorphous SiO_2 at 200 °C temperature under the saturated steam pressure (~27 atm), the reactions of new compounds formation occur in the following sequence:

$$1.5CaO+SiO_2\cdot nH_2O+H_2O \xrightarrow{4h} \begin{matrix}\text{portlandite}\\ \text{C-S-H(I)}\\ \text{C-S-H(II)}\\ \alpha\text{-}C_2SH\end{matrix} \xrightarrow{8h} \begin{matrix}\text{C-S-H(I)}\\ \text{C-S-H(II)}\\ \alpha\text{-}C_2SH\end{matrix} \xrightarrow{24h} \begin{matrix}\text{C-S-H(I)}\\ \alpha\text{-}C_2SH\\ \text{kilchoanite}\end{matrix} \xrightarrow{48\text{-}72h} \begin{matrix}\text{C-S-H(I)}\\ C_8S_5\\ \text{kilchoanite}\end{matrix}$$

The results of Section 3.1 showed that the addition of γ-Al_2O_3 has influence on the reactivity of primary compounds at 175 °C temperature. Thus, in the next stage

of the experiments, the influence of the presently mentioned additive on the formation of calcium silicates hydrates in $1.5CaO–xSiO_2 \cdot nH_2O–(1-x)Al_2O_3–H_2O$ system at 200 °C temperature was investigated.

3.3.2. The influence of γ-Al_2O_3 on dibasic calcium silicates hydrates crystallization at 200 °C

It was determined that in the mixtures with $CaO/(SiO_2+Al_2O_3)$ = 1.5 and $Al_2O_3/(SiO_2+Al_2O_3)$ = 0.025 molar ratio, the primary compounds reacted heavily because, after 4 h of isothermal curing, α-C_2SH did not form, and only a modest amount of semi-crystalline calcium silicate hydrates was identified (Fig. 3.25, curve 1). It should be noted that, under these experimental conditions, dibasic calcium silicate (C_2S) (PDF No. 00-049-1672; *d*-spacing – 0.301; 0.275; 0.273 nm) was formed. The present results are in good agreement with the data obtained by Mitsuda *et al*. (89, 91). Also, alongside the presently mentioned maximums, a broad basal reflection in 26–37° 2θ range was noticed and can be assigned to compounds of amorphous structure.

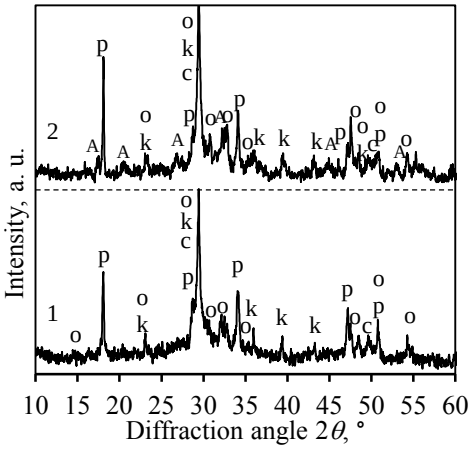

Fig. 3.25. XRD patterns of the synthesis products when the duration of hydrothermal treatment at 200 °C temperature was 4 h. The molar ratios of the primary mixtures were equal to: $CaO/(SiO_2+Al_2O_3)$=1.5 and $Al_2O_3/(SiO_2+Al_2O_3)$=0.025 (curve 1) or 0.05 (curve 2). Indexes: c – C-S-H; p – $Ca(OH)_2$; k – $CaCO_3$; o – $2CaO \cdot SiO_2$; A – hydrogrossular

XRD analysis data was additionally confirmed by STA analysis: in the DSC curve, the first endothermic effect (30–200 °C) reflects the removal of crystallization water in C-S-H; the second endothermic effect at 442 °C can be attributed to the decomposition of portlandite (Fig. 3.26, a, curve 2). Moreover, it was computed that, during the decomposition of portlandite, the synthesis products lost ~3.19 % of mass, which is equivalent to 13.11 % of portlandite (Fig. 3.26, a, curve 1). Meanwhile, two exothermic effects at ~842 °C and ~862 °C characteristic to C-S-H(I) and C-S-H(II), respectively, reflecting their recrystallization to wollastonite, were observed (Fig. 3.26, a, curve 2). Furthermore, an endothermic effect at ~723 °C can be assigned to the decomposition of calcium carbonate. According to TG analysis data, it was calculated that 9.07 % of the latter compound

is present in the synthesis products. In addition to this, STA analysis data confirmed that Al^{3+} ions were incorporated in the structure of the synthesis products because the endothermic effect within the 300–400 °C temperature range typical of the dehydration of hydrogrossular was not observed (Fig. 3.26, a).

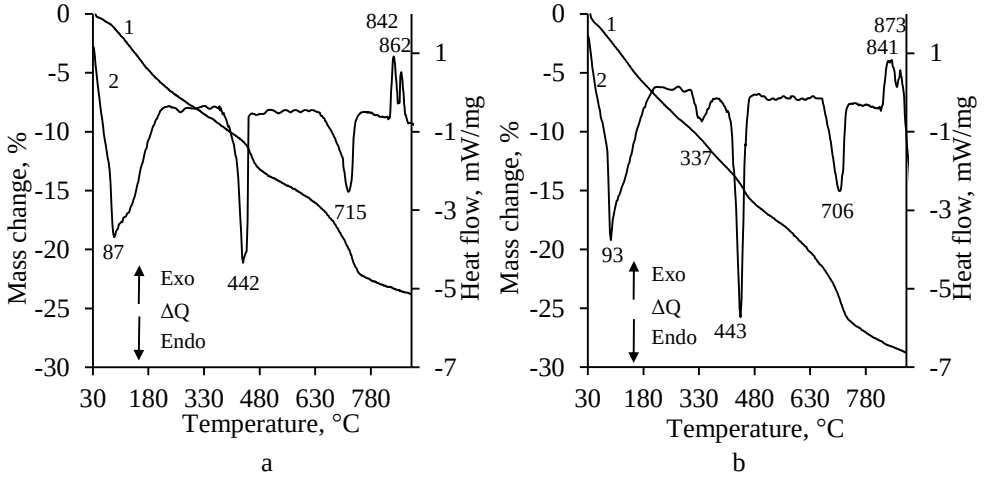

Fig. 3.26. STA curves (1 – TG; 2 – DSC) of the synthesis products when the duration of hydrothermal treatment at 200 °C temperature was 4 h. The molar ratios of primary mixtures were equal to: $CaO/(SiO_2+Al_2O_3)$=1.5 and $Al_2O_3/(SiO_2+Al_2O_3)$=0.025 (a) or 0.05 (b)

It was observed that, in the initial mixtures with a larger amount of Al_2O_3 additive (the molar ratio of $Al_2O_3/(SiO_2+Al_2O_3)$ = 0.05), more intensive diffraction maximums characteristic to C_2S and portlandite were observed (Fig. 3.25, curve 2). Moreover, TG analysis data showed that 14.6 % of portlandite did not react (Fig. 3.26, b, curve 1). It should be noted that a larger amount of Al_2O_3 additive stimulates the formation of hydrogrossular. As in the previous case, the basic reflection intensities of the mentioned compounds in the X-ray diffraction patterns are rather small as 3.4 % of Al_2O_3 was added to the initial mixture, and that is why it is very difficult to assign products to particular compounds (Fig. 3.25, curve 2). It is worth noting that STA analysis confirmed the formation of hydrogrossular because an endothermic effect characteristic to its dehydration at 337 °C temperature was identified (Fig. 3.26, b, curve 2).

While continuing the synthesis (8 h), it was observed that the formation of calcium silicate hydrates proceeds quite complicatedly. For this reason, quite intensive diffraction peaks of unreacted portlandite were observed in XRD patterns (Fig. 3.27). Moreover, C_2S and hydrogrossular remained stable. It is worth highlighting that in a pure system ($1.5CaO–SiO_2 \cdot nH_2O–H_2O$), after 4 hours of isothermal curing at 200 °C, dicalcium silicate hydrates – α-C_2SH, C-S-H(II) and a low basic semi-crystalline C-S-H(I) were formed (Fig. 3.20). It should be underlined that in the presently mentioned system, α-C_2SH without impurities of portlandite is formed after 8 h; it remained stable till 24 h of hydrothermal treatment.

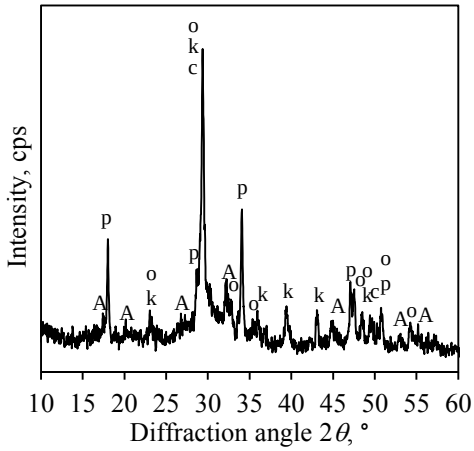

Fig. 3.27. XRD patterns of the synthesis products when the duration of hydrothermal treatment at 200 °C temperature was 8 h. The molar ratios of the primary mixtures were equal to: $CaO/(SiO_2+Al_2O_3)=1.5$ and $Al_2O_3/(SiO_2+Al_2O_3)=0.05$. Indexes: c – C-S-H; p – $Ca(OH)_2$; k – $CaCO_3$; o – $2CaO{\cdot}SiO_2$; A – hydrogrossular

The FT-IR spectrum of the synthesized product after 8 h of isothermal curing is presented in Figure 3.28. The silicate vibration regions of C-S-H spectra resemble those of C_2S, and all of them contain a characteristic set of bands in the bending vibrations range at ~453 and ~514 cm^{-1} (δ(Si-O-Si) and δ(O-Si-O)) and in the symmetrical stretching vibration range at ~969 cm^{-1} (νs(O-SiO-)) (167, 168, 169). However, the absorption band at 666 cm^{-1} can be attributed to symmetrical δ(Si-O-Si) stretching vibrations in the semi-crystalline C-S-H structure (170). Meanwhile, a duplet at ~875 and 857 cm^{-1}, which can be attributed to symmetrical ν_s(O-SiO-) stretching signals in the C_2S structure, was observed(167, 168). Also, the identified absorption band at 3654 cm^{-1} belonging to HO^- groups supports the STA and XRD analysis data which indicates that portlandite does not fully react. It was observed that, under these experimental conditions, ν(CO_3^{-2}) vibrations at 1428 cm^{-1} are clearly visible in the FT-IR spectrum.

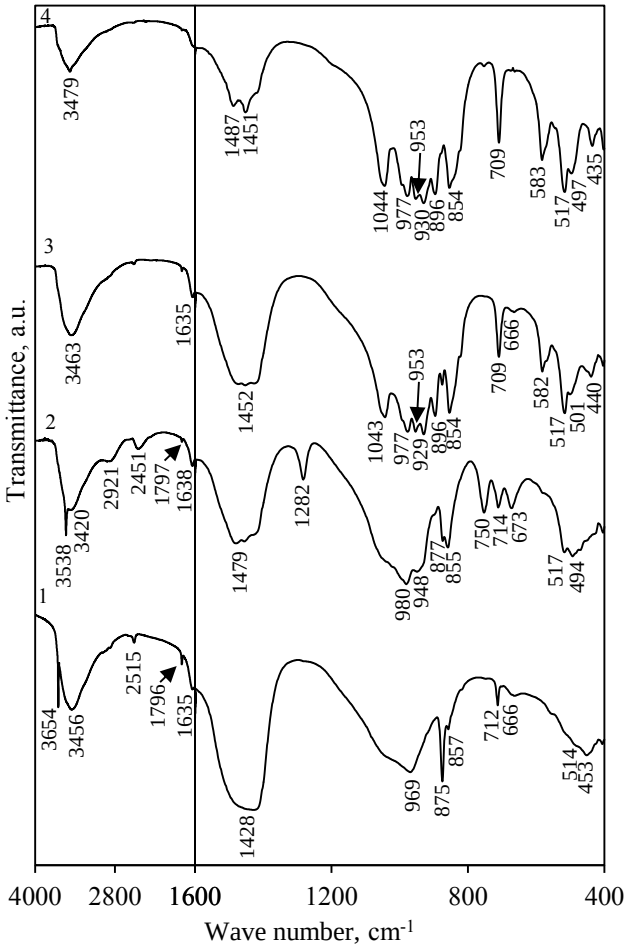

Fig. 3.28. FT-IR spectra of the synthesis products; duration of hydrothermal treatment at 200 °C temperature was, h: 1 – 8; 2 – 16; 3 – 24; 4 – 72. The molar ratios of the primary mixtures were equal to: $CaO/(SiO_2+Al_2O_3)$=1.5 and $Al_2O_3/(SiO_2+Al_2O_3)$=0.05

When hydrothermal synthesis is extended to 16 hours, portlandite reacts fully, therefore, the typical diffraction peaks, the exothermal effect and the absorption band at 3630–3660 cm^{-1}characteristic to this compound are not detected (Fig. 3.28 curve 2, Fig. 3.29). On the other hand, dicalcium silicate hydrate – α-C_2SH – was identified in the synthesis products. Also, the diffraction peaks whose *d*-spacing is 0.532 nm from planes (002) and 0.266 nm from planes (004) are more intensive and can be associated with the crystals of the α-C_2SH orientation. The decomposition of α-C_2SH is observed in the 400–500 °C temperature interval (58, 78); during the decomposition of α-C_2SH, the synthesis products lost ~2.68 % of mass, which is equivalent to 28.29 % of α-C_2SH (Fig. 3.29, b, curve 2). Also, the exothermic effect at ~851 °C and the shoulder at 859 °C characteristic to the recrystallization of semi-crystalline C-S-H(I) and C-S-H(II) type compounds to wollastonite were identified

(Fig. 3.29, b, curve 2). Furthermore, TG analysis data showed that ~2.2 % of calcium carbonate is present in the synthesis products (Fig. 3.29, b, curve 1). While continuing, the FT-IR spectrum significantly changes concerning Si-O vibrations (Fig. 3.28, curve 1–2). In the interval of 600–800 cm^{-1}, the absorption maximums are assigned to symmetrical ν_s(O-SiO-) stretching vibrations; in this particular region, a triplet at ~673, ~714 and ~750 cm^{-1} is detected. Also, a strong band at 1282 cm^{-1} typical of an OH^- bending vibration of a hydroxyl bonded to SiO_4δ(OH(Si)) can be attributed to the vibrations in the α-C_2SH structure(78). Moreover, the intensity of the absorption band at ~1479 cm^{-1}, which is assigned to $\nu(CO_3^{-2})$, decreases 2 to 3 times.

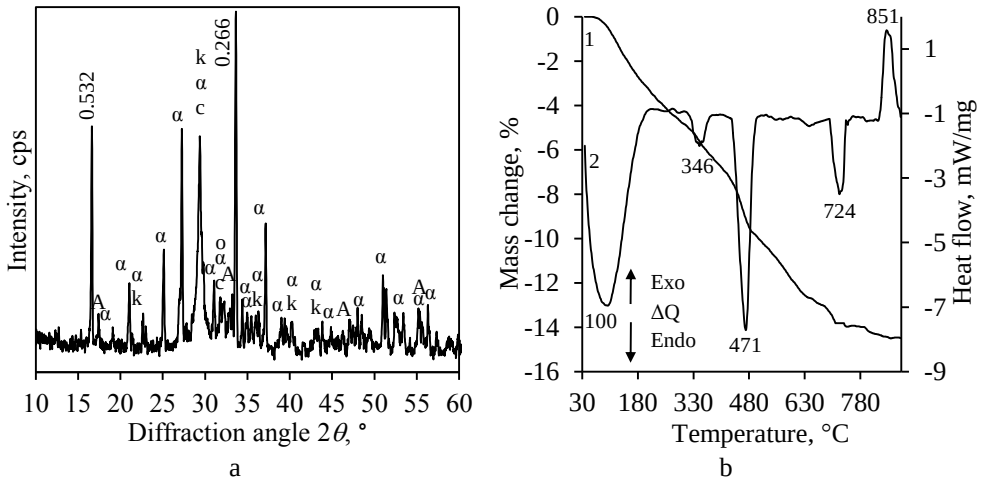

Fig. 3.29. XRD patterns (a) and STA curves (b) (1 – TG; 2 – DSC) of the synthesis products when the duration of hydrothermal treatment at 200 °C temperature was 16 h. The molar ratios of the primary mixtures were equal to: $CaO/(SiO_2+Al_2O_3)$=1.5; $Al_2O_3/(SiO_2+Al_2O_3)$=0.05. Indexes: c – C-S-H; α – α-C_2SH; k – $CaCO_3$; o – $2CaO \cdot SiO_2$; A – hydrogrossular

Furthermore, after 24 h of hydrothermal treatment in both mixtures ($Al_2O_3/(SiO_2+Al_2O_3)$ = 0.025 or 0.05), α-C_2SH is fully recrystallized to kilchoanite and C_8S_5(Fig. 3.30, a). The present results are in good agreement with the literature data (24, 40). Also, it was observed that in the mixtures with a larger amount of Al_2O_3 additive, hydrogrossular remained stable, but the amount of the adsorbed heat attributed to the dehydration of hydrogrossular slightly changed (from 11.66 to 10.36 J/g). Remarkable changes were noticed in the FT-IR spectrum of the synthesis products (Fig. 3.28, curves 2–3). The significant decrease in the intensity of the absorption bands attributed to OH^- and H_2O vibrations is observed. Meantime, the complex group of bands in the range of 800–1000 cm^{-1}, corresponding to the asymmetric and symmetric stretching vibrations of Si–O bonds, was observed. The presently mentioned bands can be attributed to vibrations in kilchoanite and the C_8S_5 structure (167, 168, 169). Besides, an absorption band assigned to asymmetrical ν_{as}(Si-O-Si) stretching vibrations was identified at ~1043 cm^{-1}; the latter one shows

that $[SiO_4]^{4-}$ tetrahedron forms triple chains in the structure of the synthesis products.

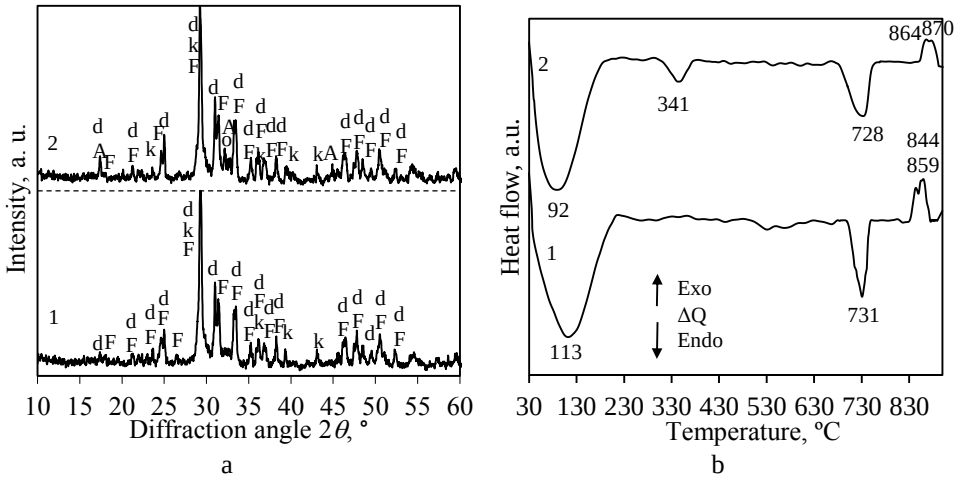

Fig. 3.30. XRD patterns (a) and DSC curves (b) of the synthesis products; the duration of hydrothermal treatment at 200 °C temperature was 24 h. The molar ratios of the primary mixtures were equal to: $CaO/(SiO_2+Al_2O_3)$=1.5 and $Al_2O_3/(SiO_2+Al_2O_3)$=0.025 (curve 1) or 0.05 (curve 2). Indexes: k – $CaCO_3$; o – $2CaO{\cdot}SiO_2$; A – hydrogrossular; F – C_8S_5; d – kilchoanite

It was determined that by prolonging the duration of hydrothermal synthesis to 48-72 h, kilchoanite and C_8S_5 remain stable in both mixtures because the intensities of the basic reflections typical of the presently mentioned compound increased (Fig. 3.31). However, in the synthesis products, small intensity diffraction peaks of scawtite (PDF No. 04-011-9710; *d*-spacing – 0.320; 0.302; 0.299 nm) were identified. The XRD data was supported by STA analysis results: in the mixtures with $Al_2O_3/(SiO_2+Al_2O_3)$ = 0.025, in the DSC curve, the first endothermic effect (30–200 °C) reflects the removal of crystallization water in C-S-H. The second endothermic effect at 715 °C can be attributed to the decomposition of scawtite and calcium carbonate (Fig. 3.32, a, curve 2). Meanwhile, in the mixtures with $Al_2O_3/(SiO_2+Al_2O_3)$ = 0.05, the endothermic effect at 342 °C temperature can be attributed to the dehydration of hydrogrossular (Fig. 3.32, b, curve 2). Moreover, it was estimated that the synthesis products within the 30 – 900 °C temperature interval lost ~12.28 % of its mass, and it is about 1.8 times more than in the mixtures containing $Al_2O_3/(SiO_2+Al_2O_3)$ = 0.025. The FT-IR spectrum showed no significant changes, only the multiplicity of absorption maximums is shifted, and the absorption band at 1400-1500 cm^{-1} attributed to $\nu(CO_3^{-2})$ vibration decreases 2 to 3 times (Fig. 3.28, curves 3–4).

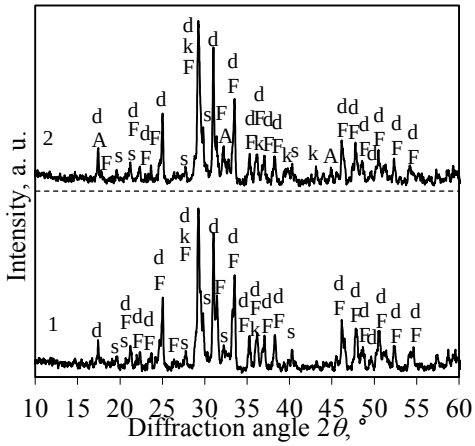

Fig. 3.31. XRD patterns of the synthesis products when the duration of hydrothermal treatment at 200 °C temperature was 48 h. The molar ratios of the primary mixtures were equal to: $CaO/(SiO_2+Al_2O_3)=1.5$ and $Al_2O_3/(SiO_2+Al_2O_3)=0.025$ (curve 1) or 0.05 (curve 2). Indexes: k – $CaCO_3$; A – hydrogrossular; F – C_8S_5; d – kilchoanite; s – scawtite

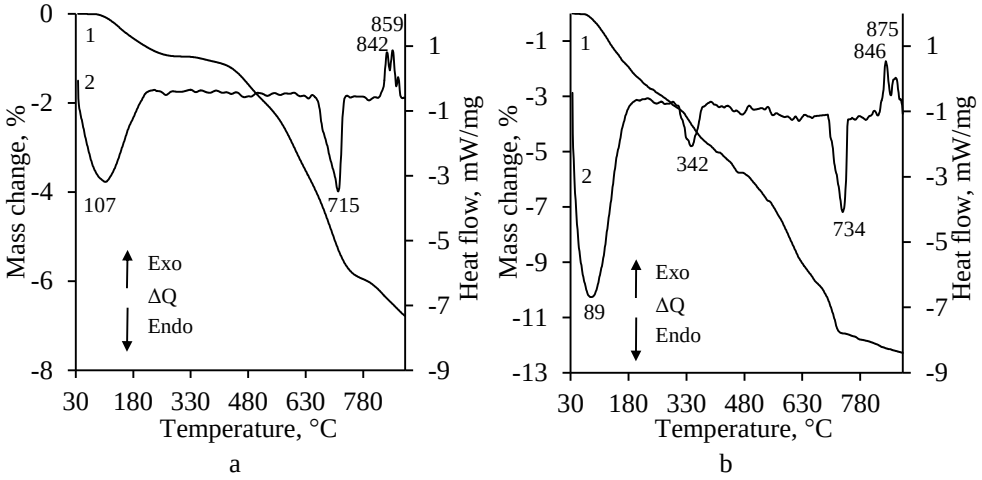

Fig. 3.32. STA curves (1 – TG; 2 – DSC) of the synthesis products when the duration of hydrothermal treatment at 200 °C was 48 h. The molar ratios of the primary mixtures were equal to: $CaO/(SiO_2+Al_2O_3)=1.5$ and $Al_2O_3/(SiO_2+Al_2O_3)=0.025$ (a) or 0.05 (b)

It is reasonable to assume that, when curing the mixture of CaO, amorphous SiO_2 and 3.4 % Al_2O_3 additive at 200 °C under saturated steam pressure, the formation of new compounds occurs in the following sequence:

$$1.5CaO+SiO_2\cdot nH_2O+0.05Al_2O_3+H_2O \xrightarrow{4\text{-}8h} \begin{matrix}2CaO\cdot SiO_2\\ \text{C-S-H(I)}\\ \text{C-S-H(II)}\\ \text{hydrogrossular}\end{matrix} \xrightarrow{16h} \begin{matrix}\text{C-S-H(I)}\\ \text{C-S-H(II)}\\ \alpha\text{-}C_2SH\\ 2CaO\cdot SiO_2\\ \text{hydrogrossular}\end{matrix} \xrightarrow{24\text{-}72h} \begin{matrix}\text{kilchoanite}\\ C_8S_5\\ 2CaO\cdot SiO_2\\ \text{CASH}\\ \text{C-S-H(I)}\\ \text{C-S-H(II)}\end{matrix}$$

The experimental data and the theoretical hypothesis were also supported by thermodynamic calculations. Crystallization reactions of C-S-H in the mixtures with $CaO/(SiO_2+Al_2O_3)$ = 1.5 and $Al_2O_3/(SiO_2+Al_2O_3)$ = 0.025 molar ratio that are possible during the hydrothermal synthesis at 200 °C are given below:

$1.5CaO + 0.975SiO_2 + 10H_2O + 0.025Al_2O_3 \rightarrow 0.975(0.83CaO{\cdot}SiO_2{\cdot}1.3H_2O\text{-}Al) + 0.69Ca(OH)_2 + 8.04H_2O$ (Eq. 3.1)

$1.5CaO + 0.975SiO_2 + 10H_2O + 0.025Al_2O_3 \rightarrow 0.90(1.67CaO{\cdot}SiO_2{\cdot}2.1H_2O\text{-}Al) + 0.05SiO_2 + 8.11H_2O$ (Eq. 3.2)

$1.5CaO + 0.975SiO_2 + 10H_2O + 0.025Al_2O_3 \rightarrow 0.75(2CaO{\cdot}SiO_2\text{-}Al) + 0.2SiO_2 + 10H_2O$ (Eq. 3.3)

$1.5CaO + 0.975SiO_2 + 10H_2O + 0.025Al_2O_3 \rightarrow 0.75(2CaO{\cdot}SiO_2{\cdot}H_2O\text{-}Al) + 0.2SiO_2 + 9.25H_2O$ (Eq. 3.4)

Note: the water/solid ratio of the suspension was equal to 10.0; the molar number of the specific compound was rounded to two decimal places.

Crystallization reactions of CASH in the mixtures with $CaO/(SiO_2+Al_2O_3)$ = 1.5 and $Al_2O_3/(SiO_2+Al_2O_3)$ = 0.025 molar ratio are given below:

$1.5CaO+ 0.95SiO_2 + 10H_2O + 0.05Al_2O_3 \rightarrow 0.05(Al_2O_3{\cdot}2SiO_2{\cdot}2H_2O) + 1.5CaO+ 0.85SiO_2 + 9.9H_2O$ (Eq. 3.5)

$1.5CaO+ 0.95SiO_2 + 10H_2O + 0.05Al_2O_3 \rightarrow 0.05(2CaO{\cdot}Al_2O_3{\cdot}4H_2O) + 1.4CaO+ 0.95SiO_2 + 9.8H_2O$ (Eq. 3.6)

$1.5CaO+ 0.95SiO_2 + 10H_2O + 0.05Al_2O_3 \rightarrow 0.05(2CaO{\cdot}Al_2O_3{\cdot}3.75H_2O) + 1.4CaO+ 0.95SiO_2 + 9.81H_2O$ (Eq. 3.7)

$1.5CaO+ 0.95SiO_2 + 10H_2O + 0.05Al_2O_3 \rightarrow 0.05(3CaO{\cdot}Al_2O_3{\cdot}3H_2O) + 1.35CaO+ 0.95SiO_2 + 9.85H_2O$ (Eq. 3.8)

$1.5CaO+ 0.95SiO_2 + 10H_2O + 0.05Al_2O_3 \rightarrow 0.05(4CaO{\cdot}Al_2O_3{\cdot}6.5H_2O) + 1.3CaO+ 0.95SiO_2 + 9.68H_2O$ (Eq. 3.9)

$1.5CaO+ 0.95SiO_2 + 10H_2O + 0.05Al_2O_3 \rightarrow 0.05(4CaO{\cdot}Al_2O_3{\cdot}9.5H_2O) + 1.3CaO+ 0.95SiO_2 + 9.525H_2O$ (Eq. 3.10)

$1.5CaO+ 0.95SiO_2 + 10H_2O + 0.05Al_2O_3 \rightarrow 0.05(CaO{\cdot}Al_2O_3{\cdot}5H_2O) + 1.45CaO+ 0.95SiO_2 + 9.75H_2O$ (Eq. 3.11)

$1.5CaO+ 0.95SiO_2 + 10H_2O + 0.05Al_2O_3 \rightarrow 0.025(CaO{\cdot}2Al_2O_3{\cdot}2SiO_2{\cdot}H_2O) + 1.48CaO+ 0.9SiO_2 + 9.98H_2O$ (Eq. 3.12)

$1.5CaO+ 0.95SiO_2 + 10H_2O + 0.05Al_2O_3 \rightarrow 0.05(2CaO{\cdot}Al_2O_3{\cdot}3SiO_2{\cdot}H_2O) + 1.4CaO+ 0.8SiO_2 + 9.95H_2O$ (Eq. 3.13)

$1.5CaO+ 0.95SiO_2 + 10H_2O + 0.05Al_2O_3 \rightarrow 0.05(2CaO{\cdot}Al_2O_3{\cdot}SiO_2{\cdot}4H_2O) + 1.4CaO+ 0.9SiO_2 + 9.8H_2O$ (Eq. 3.14)

$1.5CaO+ 0.95SiO_2 + 10H_2O + 0.05Al_2O_3 \rightarrow 0.05(3CaO{\cdot}Al_2O_3{\cdot}0.8SiO_2{\cdot}2.2H_2O) + 1.35CaO+ 0.93SiO_2 + 9.89H_2O$ (Eq. 3.15)

$1.5CaO+ 0.95SiO_2 + 10H_2O + 0.05Al_2O_3 \rightarrow 0.05(3CaO{\cdot}Al_2O_3{\cdot}0.41SiO_2{\cdot}2.59H_2O) + 1.35CaO+ 0.93SiO_2 + 9.87H_2O$ (Eq. 3.16)

$1.5CaO + 0.95SiO_2 + 10H_2O + 0.05Al_2O_3 \rightarrow 0.05(3CaO \cdot Al_2O_3 \cdot 0.84SiO_2 \cdot 2.16H_2O) + 1.35CaO + 0.91SiO_2 + 9.89H_2O$ (Eq. 3.17)

$1.5CaO + 0.95SiO_2 + 10H_2O + 0.05Al_2O_3 \rightarrow 0.05(4CaO \cdot Al_2O_3 \cdot SiO_2 \cdot 6H_2O) + 1.3CaO + 0.9SiO_2 + 9.7H_2O$ (Eq. 3.18)

It should be noted that crystallization reactions of C-S-H and CASH in the mixtures with $CaO/(SiO_2+Al_2O_3)$ = 1.5 and $Al_2O_3/(SiO_2+Al_2O_3)$ = 0.025 or 0.05 proceeded in a similar way, thus equations 3.1–3.18 are presented only with one molar ratio. Calculations were done for both mixtures, and the results of the calculations of the thermodynamic properties of C-S-H and CASH formation reactions are presented in $\Delta_r G_T^0 = f(T)$ plot (Fig. 3.33).

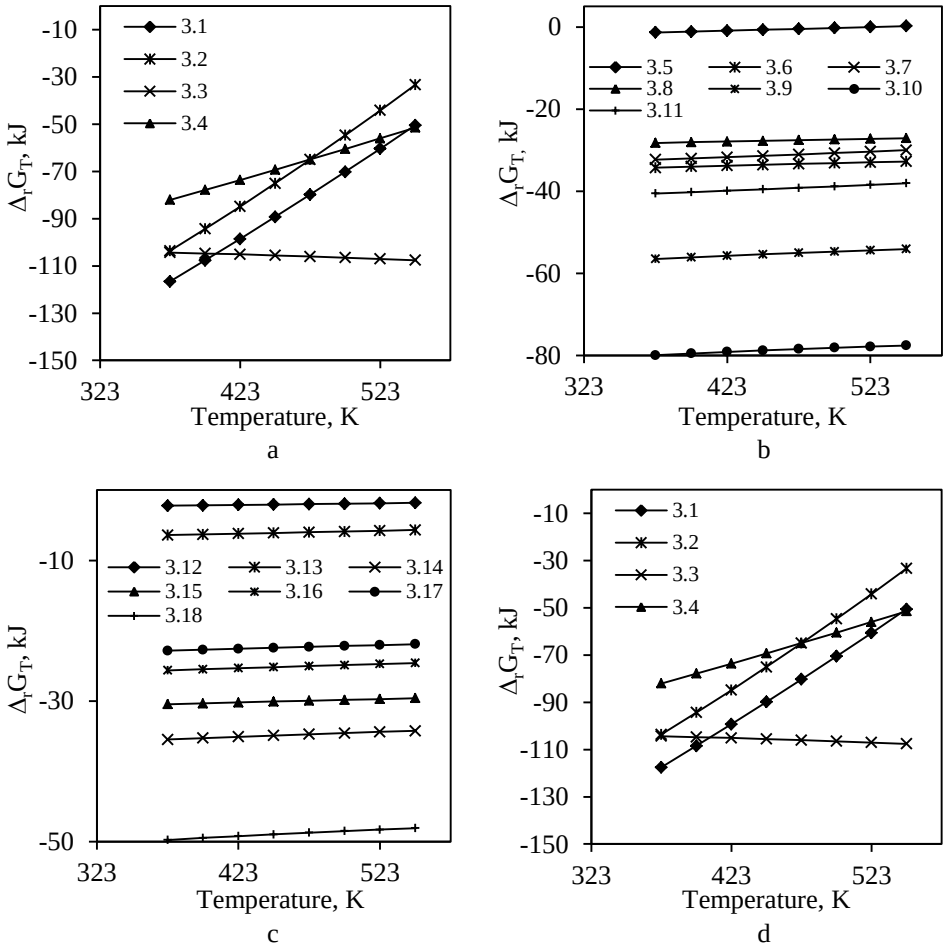

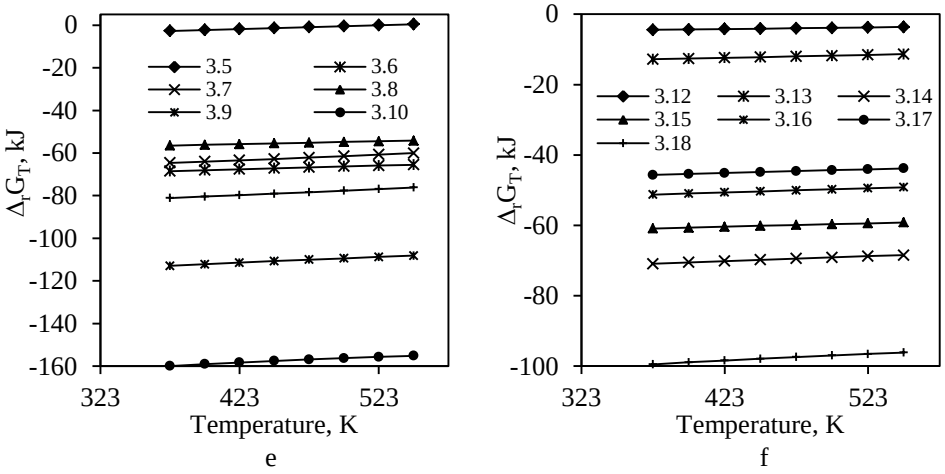

Fig. 3.33. $\Delta_r G_T$ dependence on temperature for reactions 3.1–3.18 at 373–573 K. The molar ratios of primary mixtures were equal to: $CaO/(SiO_2+Al_2O_3)$=1.5 and $Al_2O_3/(SiO_2+Al_2O_3)$=0.025 (a-c) or 0.05 (d-f).

Thermodynamic calculations showed that during the reaction in the mixtures with $CaO/(SiO_2+Al_2O_3)$ = 1.5 and $Al_2O_3/(SiO_2+Al_2O_3)$ = 0.025 molar ratio at 200 °C, the greatest possibility that C-S-H(I) and C_2S will crystallize because the changes of Gibbs free energy of reactions 3.1 and 3.3 are the lowest ($\Delta_r G_T$=-80.3 kJ and $\Delta_r G_T$=-104.5 kJ) (Fig. 3.33, a–c). On the other hand, the possibility of CASH formation is less probable (Fig. 3.33, a–c), so Al^{3+} ions will be incorporated in the structure of calcium silicate hydrates. Meanwhile, in the mixtures with a larger amount of aluminum, there is a greater possibility that $4CaO \cdot Al_2O_3 \cdot 9.5H_2O$ and $4CaO \cdot Al_2O_3 \cdot 6.5H_2O$ will be formed (Eq. 3.9 and Eq. 3.10) because the values of the above mentioned reactions $\Delta_r G_T$ are much more negative than those of other reactions (Fig. 3.33, d–e). It should be noted that, during hydrothermal synthesis, when the thermodynamically most probable reactions (Eq. 3.9 and Eq. 3.10) proceed, a large amount of unreacted calcium oxide and amorphous silica dioxide will remain in the system. For this reason C-S-H(I) and C_2S will crystallize in the products (Fig. 3.33, d).

The changes of Gibbs free energy dependence on the molar ratios of primary mixtures $Al_2O_3/(SiO_2+Al_2O_3)$ are presented in Figure 3.34. The calculations show that $4CaO \cdot Al_2O_3 \cdot 9.5H_2O$ and $4CaO \cdot Al_2O_3 \cdot 6.5H_2O$ will be formed in the products (Eq. 3.9 and Eq. 3.10) when the molar ratio of primary mixtures $Al_2O_3/(SiO_2+Al_2O_3)$ increases to more than 0.025 and 0.05, respectively (Fig. 3.34). Otherwise, Al^{3+} ions will be incorporated in the structure of calcium silicate hydrates.

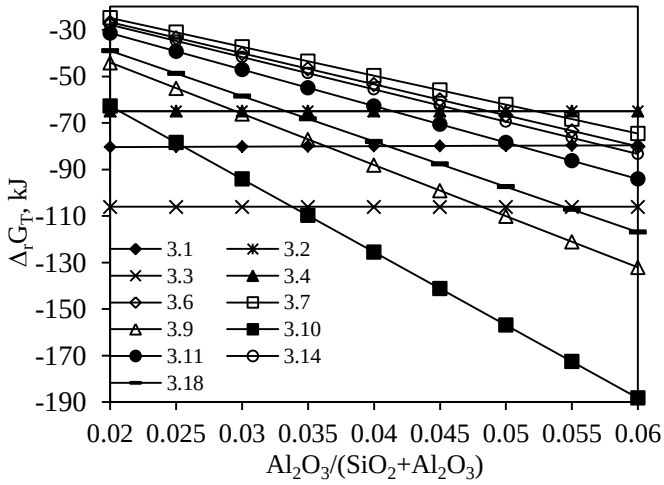

Fig. 3.34. $\Delta_r G_T$ dependence on the molar ratios of primary mixtures $Al_2O_3/(SiO_2+Al_2O_3)$ at 473 K

It should be underlined that these thermodynamic calculations are in good agreement with the experimental data because in the mixtures with $Al_2O_3/(SiO_2+Al_2O_3)$ = 0.025 molar ratio, after 4-72 h of isothermal curing Al^{3+} ions were incorporated in the synthesis products. Meantime, in the mixtures with $Al_2O_3/(SiO_2+Al_2O_3)$ = 0.05 molar ratio, after 4 h of synthesis, hydrogrossular was formed and remained stable under all experimental conditions.

3.3.3. Hydration peculiarities of α-C_2SH and quartz sample

In order to determine the possibility to use α-C_2SH synthesized at 200 °C in the production of the binder material, samples were prepared by grinding α-C_2SH (16 h) and quartz sand (Fig. 3.25, a). As expected, after grinding, the BM-α-Q sample is significantly amorphized because the intensity of diffraction maximums characteristic to α-C_2SH and quartz (Fig. 3.35, a, curve 2) as well as the area of the endothermic effect at 480 °C temperature decreased (Fig. 3.35, b). Later on, the sample was thermally treated at 450 °C for 60 min under air atmosphere. After calcination, the complete destruction of α-C_2SH took place.

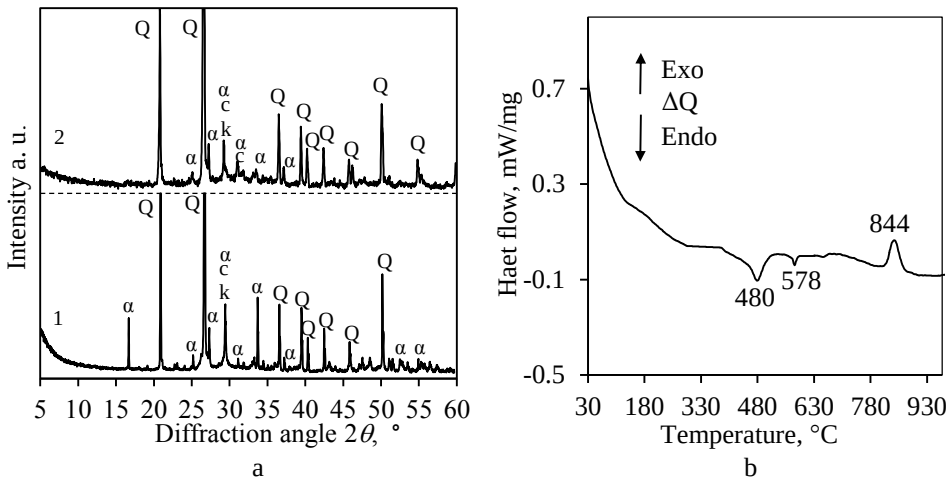

Fig. 3.35. XRD patterns (a) of the mixed (curve 1) and ground (curve 2) samples. DSC (b) curve of ground sample. Indexes: c – C-S-H; α – α-C_2SH; Q – quartz

The heat evolution curves showed two exothermic reactions (Fig. 3.36). The initial reaction – wetting and hydrolysis (first exothermic reaction) – proceeds within the first 1–2 min, and the heat flow was equal to 0.0036 W/g. Meanwhile, the next reaction, which proceeds from 0.2 h till 0.5 h, is primarily associated with the heat released due to hydration reactions (Eq. 3.19) (Fig. 3.36, a, 2). It was measured that the total heat released during the presently mentioned process was equal to 2.85 J/g (Fig.3.36, b). The maximum cumulative heat (39.75 J/g) was released by the third exothermic reaction which occurs between 3 h and 18 h (Fig. 3.36, a). Later on, the calorimetric curve of BM-α-Q showed the slow continued reaction because the rate of heat evolution decreases. Meanwhile, the amount of the total cumulative heat grows with the increasing hydration time, and, after 72 h of hydration, it was equal to 75.44 J/g (Fig.3.36, b).

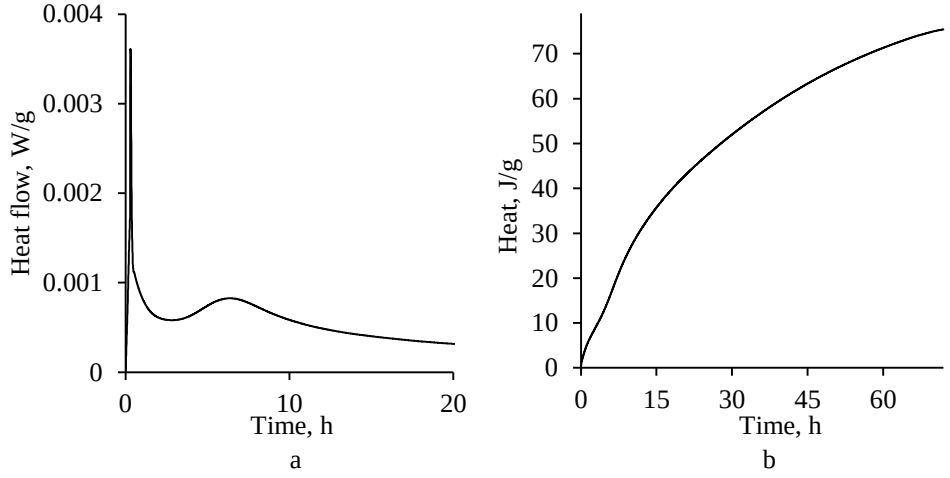

Fig. 3.36. Heat evolution rate (a) and cumulative heat (b) of BM-α-Q sample

By summarizing the hydration data (Fig. 3.35, Fig. 3.36 and Section 3.1.4), the fundamental process of chemical hydraulic reactions between BM-α-Q and water can be described by this hypothetical reaction:

$$C_{1.5}S_1 + xQ + H_2O \rightarrow C_{1.5}S_{(1+y)}H + (x-y)Q + \Delta H \quad \text{(Eq. 3.19)}$$

where: $C_{1.5}S_1$ – the products of synthesis after grinding and burning; Q – quartz; $C_{1.5}S_{(1+y)}H$ – the products of hydration; ΔH – heat; x – the molar content of quartz in the binding material; y – the molar content of the reacted quartz in hydrated cement.

In order to evaluate the mechanical properties of the BM-α-Q samples, the compressive strength properties were determined (Fig. 3.37). After three days of hydration, the compressive strength of BM was equal to 6.7 MPa. As expected, the tendency of the strength increment was observed after 7–28 days of hardening: the compressive strength increased to 15.5 MPa and 24.0 MPa, respectively (Fig. 3.37). It is worth mentioning that the obtained values are close to those of the most popular environmentally friendly brands of cement *Celitement* and *Solidia Cement* and match requirements of the belite and special low-heat cements (BS EN 1971-1:2000 and BS EN 14216-1:2004(171, 172)).

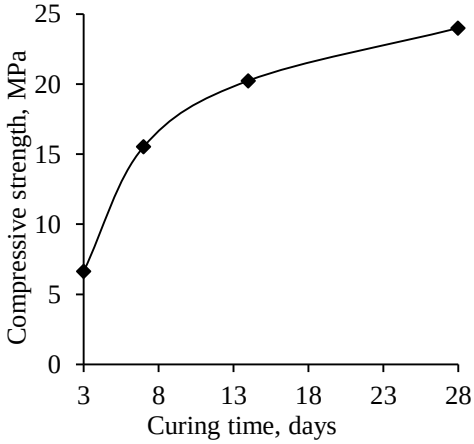

Fig. 3.37. Compressive strength of BM-α-Q samples

In order to explain the nature of the strength properties of the samples, XRD and STA analyses of the hydrated products were carried out. In the XRD analysis curve, after 28 days of hydration, peaks of calcium silicate hydrates (*d*-spacing: 0.303; 0.280; 0.184 nm) was observed (Figure 3.38, a). It should be noted that the intensity of the diffraction peaks (*d*-spacing: 0.426; 0.335; 0.182; 0.154 nm) characteristic to quartz were identified.

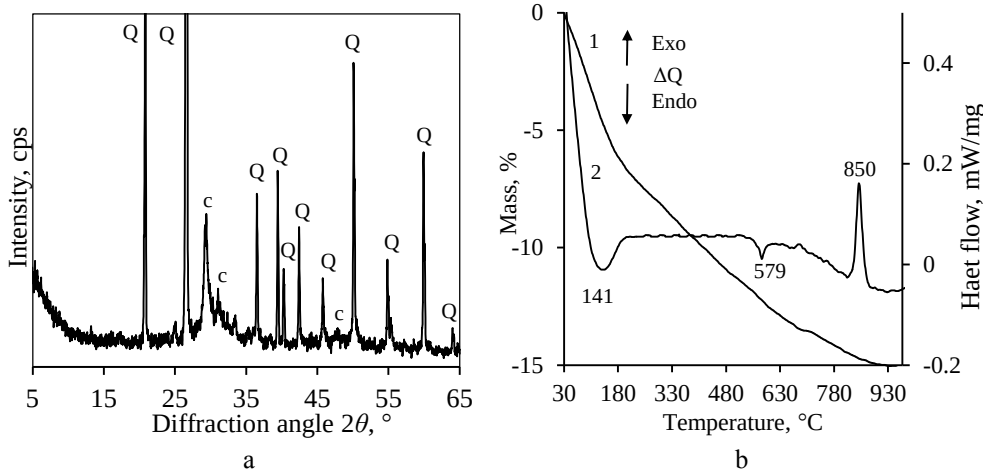

Fig. 3.38. XRD pattern and STA ((1 – TGA; 2 – DSC) curves of BM-α-Q sample at 20 °C for 28 days. Indexes: c – C-S-H; Q – quartz

The XRD results were confirmed by the DSC data. The first endothermic peak at 50–150 °C is the result of dehydration reactions due to the loss of water from the C-S-H structure. The endothermic peak at 579 °C shows the α-β transition of quartz. The exothermic peak (850 °C) is associated with the recrystallization of C-S-H into wollastonite (Fig.3.38, b).

When summarizing the above mentioned results, it can be stated that α-C_2SH after activation can be used as an environmentally friendly cementitious material because the heat flow after 72 h of hydration was equal to 75.44 J/g, while the compressive strength after 28 days was 24.0 MPa, which matches the requirements set upon the belite and special low-heat cements (BS EN 1971-1:2000 and BS EN 14216-1:2004 (171, 172)).

Acknowledgements:

Reprinted/Adapted by permission from Springer Nature: Springer Nature; Journal of Thermal Analysis and Calorimetry / Formation and thermal stability of calcium silicate hydrate substituted with Al^{3+} ions in the mixtures with CaO/SiO_2=1.5 / T. Dambrauskas, K. Baltakys, A. Eisinas, 131:501-512. 2018 https://doi.org/10.1007/s10973-017-6321-5; License No. 4505290749022

Reprinted/Adapted by permission from Sharif University of Technology; Scientia Iranica /α-C_2SH synthesis in the mixtures with CaO/SiO_2 = 1.5 and application as a precursor for binder material / K. Baltakys, T. Dambrauskas, A. Eisinas, R. Siauciunas, 23:2800-2810. 2016https://doi.org/10.24200/sci.2016.3990

3.4. Hydrothermal synthesis of kilchoanite and application as a precursor for binder material

3.4.1. Hydrothermal synthesis

As in Section 3.1.1 it was shown in $1.5CaO–SiO_2·nH_2O–H_2O$ suspensions, after 72 hours of isothermal curing at 175 °C, kilchoanite was not formed (Fig. 3.3). In order to increase the reaction rate and avoid the formation of undesirable calcium silicate hydrates, hydrothermal synthesis was carried out at higher temperatures. After 24 hours at 190 °C of synthesis, α-C_2SH, C-S-H(I) and the traces of kilchoanite were formed (Table 3.6). It should be noted that by prolonging the duration of hydrothermal synthesis to 48 h, the formed calcium silicate hydrates become metastable and recrystallized into kilchoanite. Meanwhile, after 72 h of hydrothermal synthesis, together with kilchoanite, small intensity diffraction peaks of C_8S_5 and scawtite were identified (Fig. 3.39). The present results are in good agreement with the data obtained by Black *et al*. (40) and N. Meller *et al*.(24).

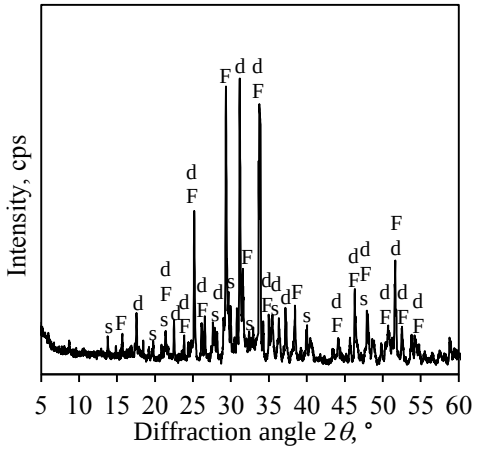

Fig. 3.39. XRD patterns of the synthesized products when the duration of hydrothermal treatment at 190 °C temperature was 72 h. Indexes: d – kilchoanite; s – scawtite; F – C_8S_5

It was examined that α-C_2SH dominates in the synthesis products after 4–16 h at 200 °C temperature (Table 3.6). Meanwhile, having extended the duration of of isothermal curing to 24 h, α-C_2SH becomes metastable and starts to recrystallize into kilchoanite, which dominates in the products after 48 h of synthesis (Fig. 3.40, a). It is worth noting that, together with kilchoanite, traces of scawtite were identified. Further, after 72 h of hydrothermal synthesis, among the synthesis products, C_8S_5 was identified (Table 3.6).

Table 3.6. Formation and stability of calcium silicate hydrates at different synthesis conditions

Synthesis condition		Compounds							
Temperature, °C	Duration, h	portlandite	C-S-H(I)	C-S-H(II)	α-C_2SH	kilchoanite	C_8S_5	scawtite	xonotlite
175	4	•	•	•	•				
	8		•	•	•				
	16		•	•	•				
	24		•		•				
	48		•		•				
	72		•		•				
190	4	•	•	•	•				
	8		•	•	•				
	16		•	•	•				
	24		•		•	?			
	48		?		•	•	?		
	72		?			•	•	?	
200	4	•	•	•	•				
	8		•	•	•				
	16		•	•	•				
	24		?		•	•			
	48		?			•		?	
	72		?			•	•	?	
210	4		•		•				
	8		•		•	•	•	•	
	16		?			•	•	•	
	24		?			•	•	?	
	48		?			•	•	?	•
	72		?			•	•	?	•
220	4		•		?	•	•	•	
	8		•			•	•	•	
	16		?			•	•	•	
	24		?			•	•	?	
	48		?			•	•	?	•
	72		?			•	•	?	•

? – the traces of compound could be present in the products

The previous results were confirmed with data from STA analysis. It was proved that kilchoanite does not contain crystallization water as thermal conversions attributed to the latter compound were not observed in the DSC curve (Fig. 3.40, b, curve 2). It should be underlined that these results are in good agreement with the data obtained by Garbev *et al*. (44), Meducin *et al*. (85) and Taylor (90). The mass losses (~0.7 %) estimated within the 80–150 °C temperature range can be ascribed to the dehydration of C-S-H(I). It should be noted that the decomposition of calcium carbonate as well as the decomposition of scawtite overlaps at ~675 °C temperature.

Additionally, it was estimated that the synthesized product loses ~0.11 % of its mass during the decomposition of recent compounds.

The FT-IR spectrum of kilchoanite after 48 h of isothermal curing is presented in Figure 3.40 c. In bending δ(Si-O-Si) and δ(O-Si-O) vibrations range, two absorption bands at ~435, ~583 cm^{-1} and the duplet at ~498, ~517 cm^{-1} were identified (167, 168). Meanwhile, a duplet at ~842, ~854 cm^{-1} and five absorption bands at ~896, ~930, ~952, ~978, ~994 cm^{-1}, which can be attributed to symmetrical ν_s(O-SiO-) stretching signals, were observed. Two absorption bands assigned to asymmetrical ν_{as}(Si-O-Si) stretching vibrations were identified at ~1045 cm^{-1}; the latter one shows that $[SiO_4]^{4-}$ tetrahedron forms a triple chains in the structure of synthesized products. It should be considered that a significant increase in the intensity of the absorption signal at ~710 cm^{-1} was observed as well, reflecting the symmetrical ν_s(Si-O-Si) stretching vibrations.

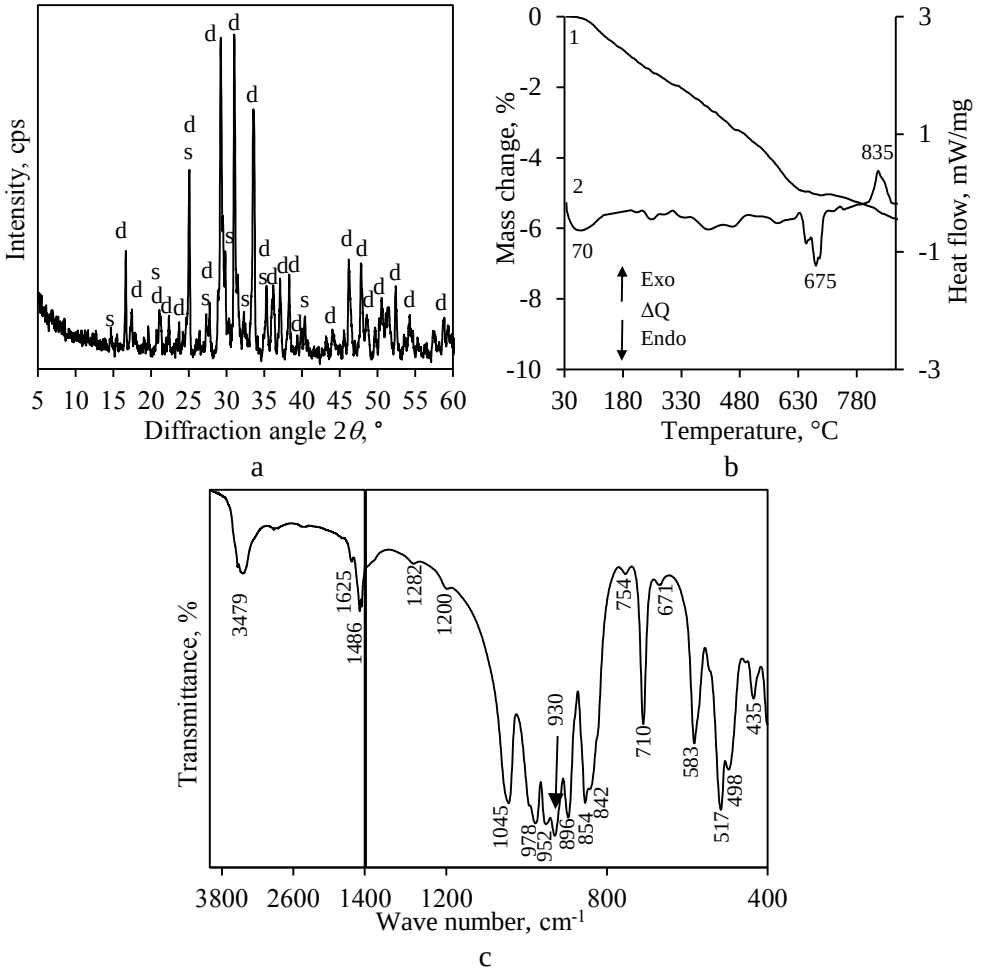

Fig. 3.40. XRD pattern (a), STA curves (b) (1 – TG; 2 – DSC) and FT-IR spectrum (c) of the synthesized products when the duration of hydrothermal treatment at 200 °C temperature was 48 h. Indexes: d – kilchoanite; s – scawtite

Furthermore, the increase of the temperature positively affects the formation of calcium silicates: these compounds were obtained at 210 °C after 8 hours, while at 220 °C after 4 hours (Fig. 3.41). It should be noted that, under these hydrothermal conditions, pure kilchoanite was not obtained (Table 3.6). In addition, by prolonging the duration of the hydrothermal synthesis to 48–72 h, a new synthesis product – xonotlite (PDF 04-016-1649; *d*-spacing – 0.324; 0.308; 0.282; 0.270 nm) was formed (Table 3.6).

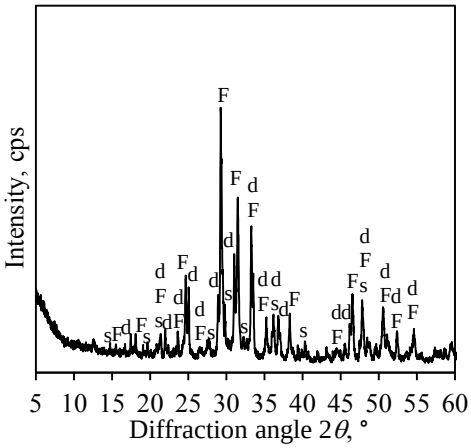

Fig. 3.41. XRD patterns of the synthesized products when the duration of hydrothermal treatment at 220 °C temperature was 4 h. Indexes: d – kilchoanite; s – scawtite; F – C_8S_5

3.4.2. Thermal stability

The literature concerning thermal stability and other parameters of synthetic kilchoanite is scarce. Thus the thermal stability of kilchoanite synthesized after 48 h at 200 °C was examined in detail. It was estimated that kilchoanite is stable till 1100 °C because the typical diffraction maximums characteristic to kilchoanite remain unchanged (Fig. 3.42, curve 2). Meanwhile, at a higher temperature (1200 °C), the latter compound is fully recrystallized to rankinite (PDF 04-015-0709; *d*-spacing – 0.317; 0.301; 0.289; 0.271 nm) (Fig. 3.42, curve 3). It was observed that scawtite and C-S-H(I) recrystallized to wollastonite, respectively, at 700 °C and 800 °C.

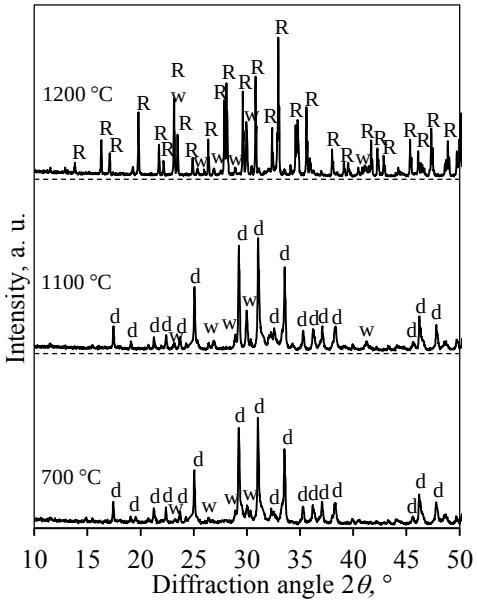

Fig. 3.42. XRD patterns of calcined products for 3 h. Indexes: R – rankinite; w – wollastonite; d – kilchoanite

The data of *in situ* XRD experiments confirmed the thermal behavior of the formed compounds (Fig. 3.43). It was estimated that kilchoanite is stable till 1120 °C and at higher temperatures (1180 °C) the latter compound is fully recrystallized to rankinite. It should be mentioned that scawtite recrystallized to wollastonite at 680 °C temperature, and C-S-H(I) recrystallized at 850 °C.

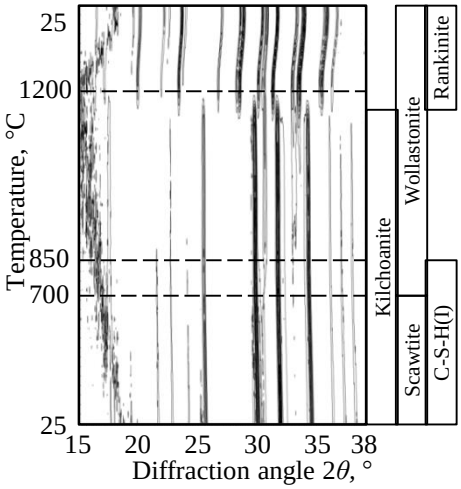

Fig. 3.43. *In situ* XRD patterns of the sample when the temperature of calcination is 25–1200 °C

The XRD results were verified with FT-IR analysis. It was determined that, after calcination at 700 °C, in the middle (1400–1500 cm^{-1}) wavenumbers range, the

absorption bands attributed to $\nu(C–O_3^{2-})$ vibrations are not detected, which refers to to scawtite and calcium carbonate (Fig. 3.44) (167, 169). Whereas having carried out calcination at 1100 °C, the FT-IR spectrum showed no significant changes; only the multiplicity and intensity of the absorption maximums are shifted. Remarkable changes are observed in the FT-IR spectrum of products when the temperature of calcination is 1200 °C. In the bending δ(Si-O-Si) and δ(O-Si-O) vibrations range, the absorption band at ~422 cm^{-1} and the triplet at ~489, ~539, ~561 cm^{-1} were identified (167, 168, 169, 173). It should be noted that, also, an absorption signal at ~710 cm^{-1}, reflecting the symmetrical ν_s(Si-O-Si) stretching vibrations, a significant shift till 656 cm^{-1}, was noticed. Meanwhile, adsorption signals at ~854, ~908 cm^{-1} and a duplet at ~953, ~987 cm^{-1}, which can be attributed to symmetrical ν(O-SiO-) stretching signals, were observed. The absorption band assigned to asymmetrical ν_{as}(Si-O-Si) stretching vibrations were identified at ~1004 cm^{-1} (Fig. 3.44).

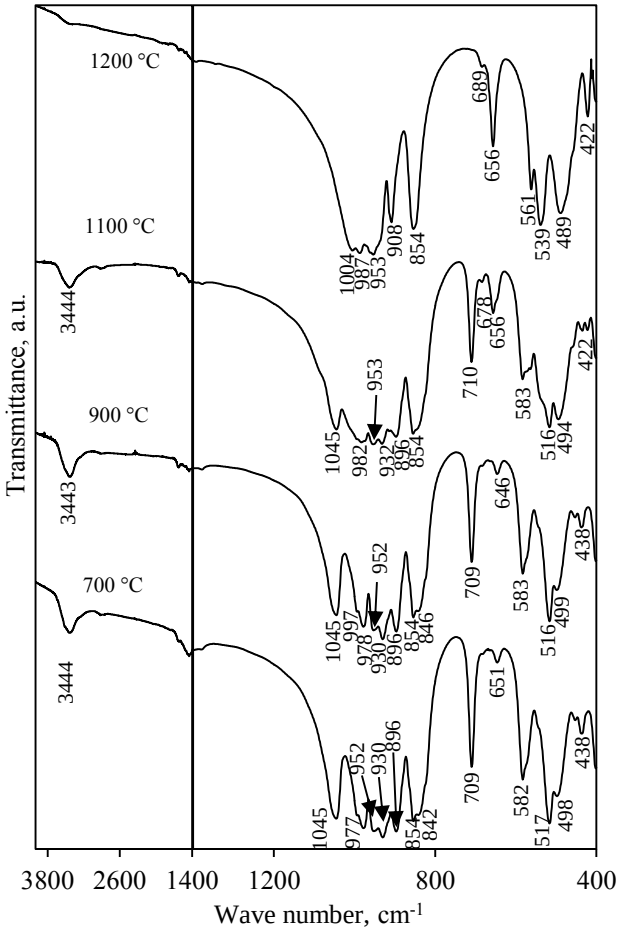

Fig. 3.44. FT-IR spectrum of calcined products

The previous results were in good agreement with the data of SEM analysis. It was determined that irregularly shaped crystals of globules are attributable to

kilchoanite (Fig. 3.45, a). This data corresponds with Meducin *et al.*'s (85) results. After calcination at 1200 °C, roughly equiaxed grains similarly sized and shaped with an average size of 2–10 nm of rankinite were detected.

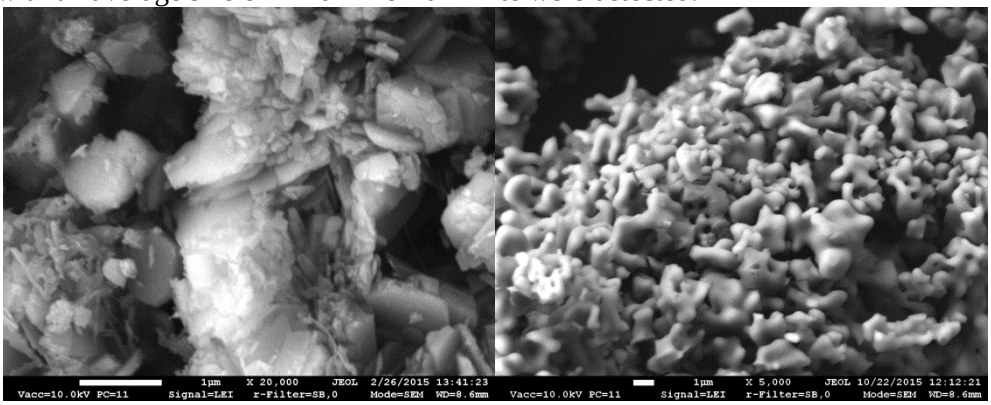

a b

Fig. 3.45. SEM micrographs: a – after hydrothermal treatment at 200 °C (x10000), b – after calcination at 1200 °C (x5000)

3.4.3. Hydration properties

In order to obtain a hydraulically active cementitious binder material, synthesized kilchoanite was mixed with quartz sand (the ratio was equal to 1:1 by mass), and the mixture was milled (950 rpm, 5 min) and thermally treated (450 °C, 1 h). The calcination temperature was chosen according to the previous results (Section 3.1.3) and literature data (15, 18, 56).

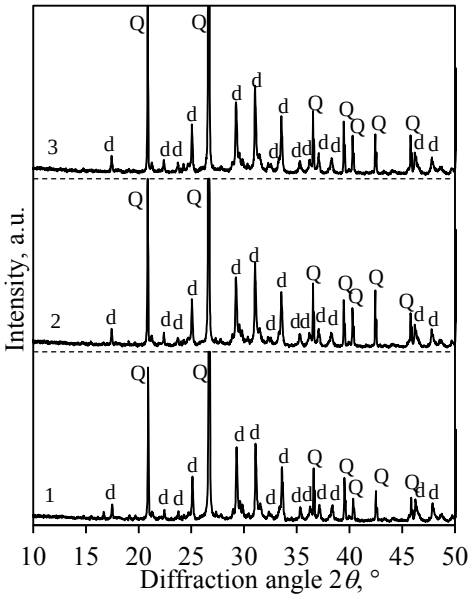

Fig. 3.46. XRD patterns of BM-k-Qbefore milling (curve 1), after milling (curve 2) and burning (curve 3). Indexes: Q – quartz; d – kilchoanite

It was determined that tribochemical activation has no influence on the BM structure. This fact was confirmed with XRD analysis: the intensity of diffraction peaks characteristic to both kilchoanite (*d*-spacing – 0.355; 0.304; 0.288; 0.267 nm) and quartz remained unchanged (Fig. 3.46, curves 1-2). In addition to this, the calorimetric curves of BM-k-Q differ from the one of OPC (159, 160, 174, 175, 176, 177, 178). The heat release curves obtained during the hydration of the BM-k-Q sample produced with kilchoanite show two distinctive peaks (Fig. 3.47, a). In cement hydration, the rate of heat evolution first starts with an initial reaction caused by the exothermic dissolution of the cement constituents. It was observed that in the initial exothermic reactions, there is a rapid evolution of the heat culminating in a peak within the first 1–2 min, and the heat flow is equal to 0.0038 W/g.

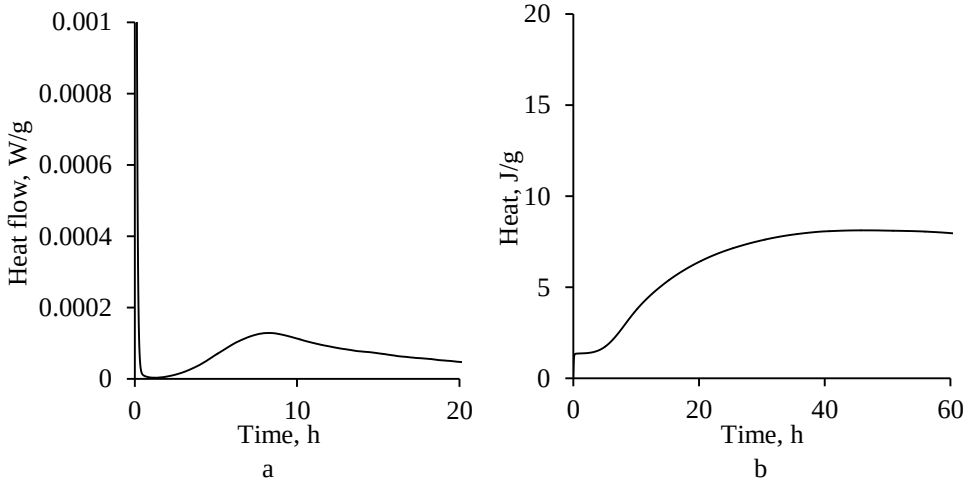

Fig. 3.47. Heat evolution rate (a) and cumulative heat (b) of BM-k-Q sample after tribochemical activation

Having performed the initial reaction, the calorimetry curves comprise a period of a slow reaction (induction period) followed by a speed-up reaction (acceleration period) (Fig. 3.47). It was observed that the induction period was prolonged to 2 h in the BM-k-Q sample. Equally important is the second exothermic reaction proceeding from 2 to 15 h (Fig. 3.47, a), and, during this process, the total amount of heat increased only to 5.3 J/g (Fig. 3.47, b). At the later stages of hydration, the calorimetric curve of BM-k-Q showed a slower continuous reaction as the rate of heat evolution was decreased. Meanwhile, the amount of the total cumulative heat after 60 hours of hydration was equal only to 7.97 J/g. Thus it can be stated that kilchoanite and the quartz sand sample after activation do not exhibit any hydraulic activity.

Acknowledgements:

Reprinted/Adapted by permission from Springer Nature: Springer Nature; Journal of Thermal Analysis and Calorimetry / A study on the thermal stability of kilchoanite synthesized under hydrothermal conditions / T. Dambrauskas, K. Baltakys, A. Eisinas, R. Siauciunas, 127:229-238.2017https://doi.org/10.1007/s10973-016-5424-8; License No. 4505290569459

3.5. Hydrothermal synthesis of hydroxyledgrewite and its properties

In the first part of Section 3.5, the mineralogical composition of the synthesis products was examined. It was determined that in the mixture (CaO/SiO_2 = 2.25), after 8 hours of isothermal curing at 200 °C, the starting materials hardly reacted: intensive diffraction maximums characteristic to portlandite and a broad basal reflection, in the 26–37° diffraction angles range, typical to dibasic semicrystalline type compounds were identified (Fig. 3.48). By prolonging the duration of the synthesis to 16 h, the interaction degree between the raw materials increased because hydroxyledgrewite (PDF No. 04-019-1437; *d*-spacing –0.303; 0.282; 0.191 nm) formed in the products (Fig. 3.48). It is worth mentioning that together with hydroxyledgrewite, the quite intensive diffraction peaks of unreacted portlandite were observed.

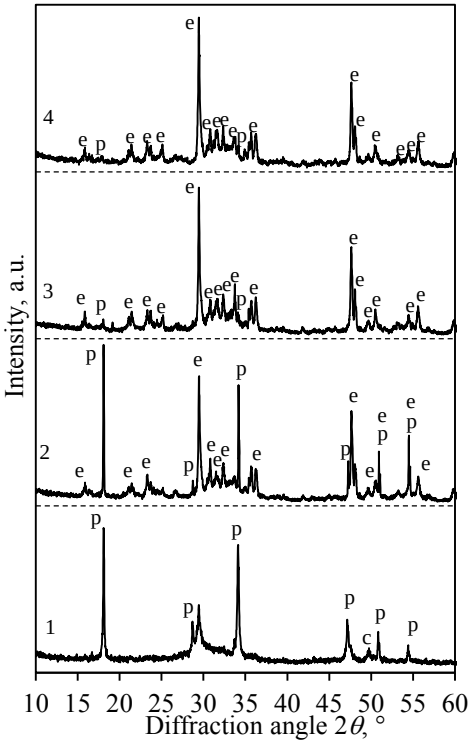

Fig. 3.48. XRD patterns of the synthesis products when the duration of the hydrothermal treatment at 200 °C temperature was, h: 1 – 8; 2 – 16; 3 – 48; 4 – 72.
Indexes: p – portlandite; c – C-S-H; e – hydroxyledgrewite

After 48 h of synthesis, only the traces of unreacted portlandite were observed (Fig. 3.48). Meanwhile, the main peak characteristics of synthesized hydroxyledgrewite also correspond to the PDF-4+ 2016 entry PDF No. 04-019-1437 (Table 3.7). It was calculated that the mean crystallite size of hydroxyledgrewite is equal to 52±3 nm (Rexp – 6.43, Rwp 11.06, GOF – 1.72). It was determined that even after 72 h of hydrothermal treatment, the traces of unreacted portlandite are present in the synthesis products (Fig. 3.48). In brief, it can be stated that the optimal

synthesis conditions for hydroxyledgrewite are CaO/SiO_2, 48 h and 200 °C. For this reason, in the further work, the hydroxyledgrewite synthesized under the optimal conditions was used to determine its properties. It is worth mentioning that the obtained results differs from the data presented in literature (1, 23, 24, 45, 58, 93); there, the hydrothermal synthesis of dibasic calcium silicates hydrates was examined in detail. In these works (1, 23, 24, 45, 58, 93), afwillite, hillebrandite, α-C_2SH and other C-S-H where synthesized; however, hydroxyledgrewite was not obtained. Presumably, the differences between the obtained results of the present thesis and those of literature arose due to the nature and reactivity of the used raw materials.

Table 3.7. The main peak characteristics of synthesized hydroxyledgrewite and entry

Estimated parameters		PDF No. 04-019-1437
2θ, deg.	*d*-spacing, nm	*d*-spacing, nm
15.897	0.557	0.558
21.469	0.414	0.414
23.337	0.381	0.381
23.690	0.375	0.375
25.185	0.353	0.354
29.293	0.305	0.304
29.462	0.303	0.303
29.644	0.301	0.300
30.799	0.290	0.289
31.496	0.284	0.286
31.652	0.282	0.282
32.363	0.276	0.276
33.743	0.265	0.266
35.695	0.251	0.251
36.227	0.248	0.248
47.577	0.191	0.191
48.026	0.189	0.189

The FT-IR spectrum of hydroxyledgrewite is presented in Figure 3.49. In bending δ(Si-O-Si) and δ(O-Si-O) vibrations range, the duplet at ~514, ~558 cm^{-1} was identified (101, 167, 168). Meanwhile, four absorption bands at ~616, ~654, ~708, ~764 cm^{-1} can be attributed to symmetrical ν_s(Si-O-Si) signals. In a higher frequency interval (800–1000 cm^{-1}), the absorption maximums can be assigned to symmetrical ν_s(O-SiO-) stretching vibrations; in this particular region, a sextet is detected. The absorption band which can be assigned to asymmetrical ν_{as}(Si-O-Si) stretching vibrations was identified at ~1040 cm^{-1}. The 3600–3400 cm^{-1} region relating to OH^- stretching vibrations displays a duplet in the spectrum of hydroxyledgrewite which consists of bands at 3471 and 3558 cm^{-1} (Fig. 3.49). It was observed that, under these experimental conditions, $\nu(CO_3^{-2})$ vibrations at 1452 cm^{-1} are clearly visible in the FT-IR spectrum. The presently mentioned vibrations appeared due to carbonation when the products were dried in an air conditioned chamber (50 °C, 24 h), and a small amount of $CaCO_3$ was formed. It is worth noting that the diffraction peaks of the presently mentioned compound were not detected in the XRD curves (Fig. 3.49).

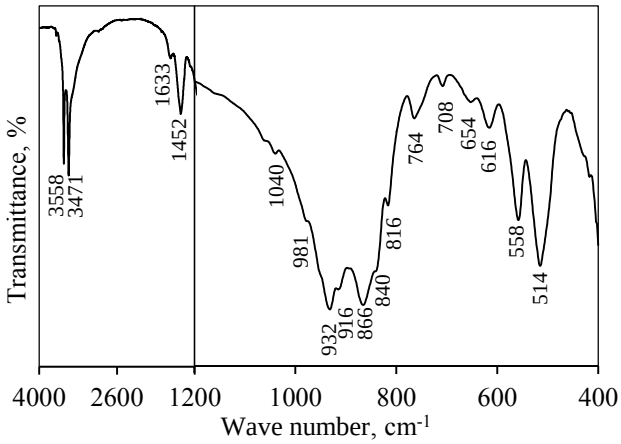

Fig. 3.49. FT-IR spectrum of synthetic hydroxyledgrewite

The thermal characteristics of hydroxyledgrewite, obtained by simultaneous thermal analysis are shown in Table 3.8 and Figure 3.50. In the DSC curve, the first endothermic effect (30–250 °C) reflects the removal of adsorption/crystallization water in the sample (Fig. 3.50). The decomposition of unreacted portlandite is observed at 451 °C temperature (Fig. 3.50, Table 3.8). Moreover, it was estimated that, during the decomposition of portlandite, the synthesis products lose ~0.36 % of mass, which is equivalent to 1.60 % of portlandite. This data is in good agreement with the XRD results; there, traces of unreacted portlandite were observed (Fig. 3.50). The decomposition of hydroxyledgrewite is observed within a wide temperature interval (620–720 °C), in which, ~2.2 % of the mass was lost. According to this data, it was calculated that 93.1 % of hydroxyledgrewite was formed. In addition, the exothermic effect at 861 °C can be assigned to the recrystallization of C_2S polymorphs.

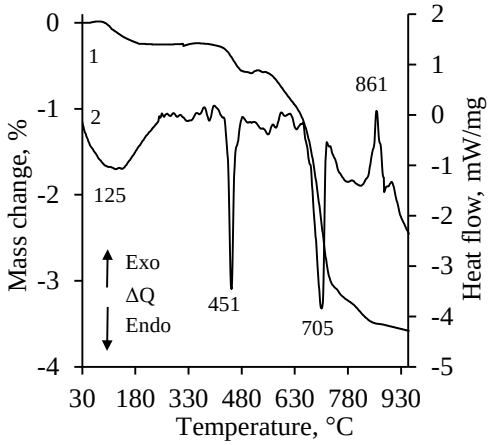

Fig. 3.50. STA curves (1 – TGA; 2 – DSC) of synthetic hydroxyledgrewite

Table 3.8. The thermal characteristics of hydroxyledgrewite

Removal of adsorption/crystallization water			Decomposition of portlandite		
Peak, °C	Δm*, %	ΔQ*, J/g	Peak, °C	Δm, %	ΔQ, J/g
125	0.25	47.11	451	0.36	10.97
Decomposition of hydroxyledgrewite			Recrystallization of C_2S polymorphs		
Peak, °C	Δm, %	ΔQ, J/g	Peak, °C	Δm, %	ΔQ, J/g
705	2.2	20.50	861	0.15	11.49

*Δm – loss on ignition; ΔQ – heat off thermal effect

The STA results were proven by an *in situ* XRD experiment. Hydroxyledgrewite was explored in a high-temperature camera MTC-hightemp within the 25–1200 °C temperature range (Fig. 3.51). It was estimated that hydroxyledgrewite is stable till 675 °C because the typical diffraction maximums characteristic to the above mentioned compound remain unchanged. Meanwhile, at a higher temperature (800 °C), the latter compound is fully recrystallized to γ-C_2S. Due to the different molar ratio between hydroxyledgrewite (2.25) and γ-C_2S (2.0), reflections of calcium oxide (PDF 00-043-1001; *d*-spacing – 0.278; 0.241 nm) are visible. Furthermore, when the temperature of calcination increases to 860 °C, γ-C_2S becomes metastable and recrystallization into α'$_L$-C_2S starts.

At 1000 °C, diffraction peaks characteristic to γ-C_2S disappeared; meanwhile, the intensity of the diffraction peaks characteristic to α'$_L$-C_2S was increased. The present results are in good agreement with the data obtained by Garbev *et al*. (16, 78, 164) and Toraya *et al*. (83). It is worth noting that α'$_L$-C_2S remained stable till 1200 °C, and transformed into β-C_2S (PDF 00-002-0843; *d*-spacing – 0.278; 0.274; 0.261; 0.240) upon subsequent cooling (500 °C).

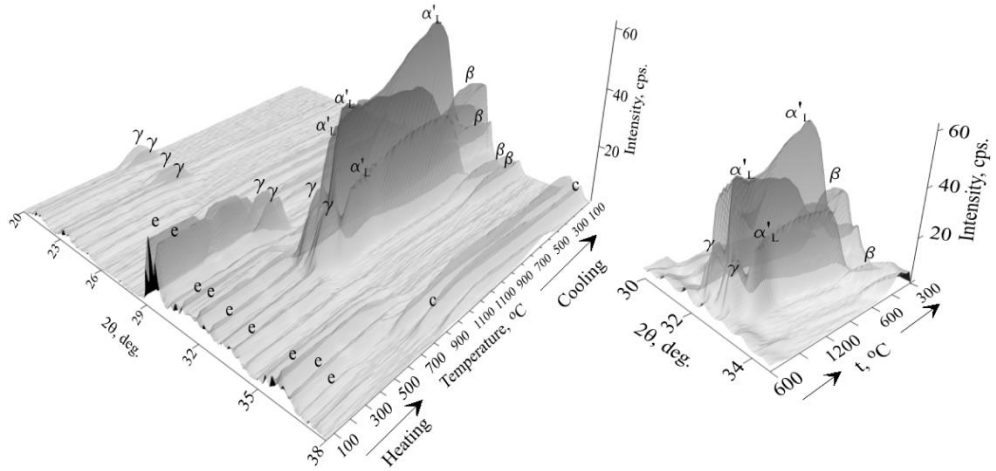

Fig. 3.51. *In situ* XRD patterns of hydroxyledgrewite when the temperature of calcination is 25–1200 °C. Indexes: e – hydroxyledgrewite, γ – γ-C_2S; α'$_L$ – α'$_L$-C_2S; β – β-C_2S; l – CaO

It is possible to assume that during experiments of hydrothermal synthesis and the calcination of hydroxyledgrewite samples, the phase formation and transformation occurred in the following sequence:

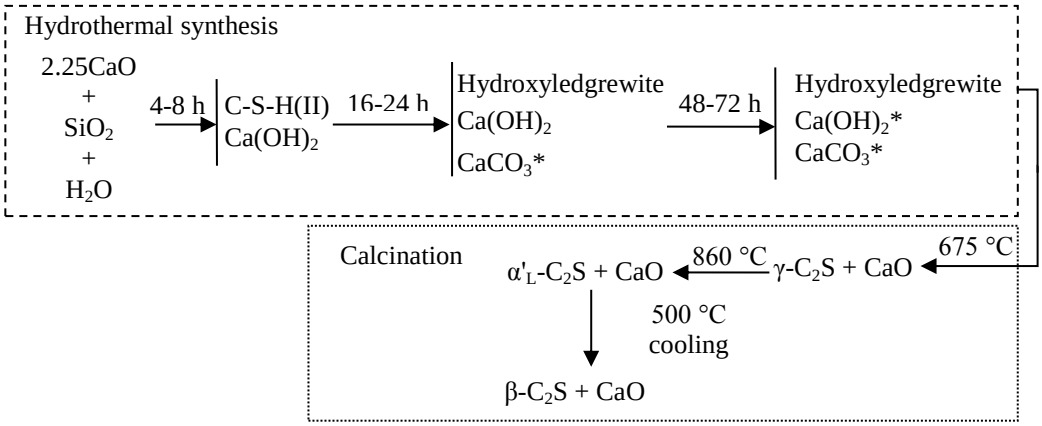

* – traces of the compound could be present in the products

One of the most important thermal parameters is the specific heat capacity (C_P), which is the heat capacity per unit molecular weight of the substance. Thus specific heat is a measure of ability of materials to absorb heat from the surroundings (179–181). The specific heat capacity of hydroxyledgrewite at a constant pressure was determined as a function of temperature by the sapphire method (Fig. 3.52) (181). According to the sapphire method, the specific heat capacity was obtained in three stages (Fig. 3.52, a): (1) the baseline was obtained by heating two empty crucibles of the same mass; (2) the second curve was recorded with the sample crucible filled with Al_2O_3; (3) and finally the third curve was recorded with a crucible filled with hydroxyledgrewite. Thus the values of C_P were calculated from equation 3.20:

$$C_P = \left(\frac{\Delta y_2 \cdot m'}{\Delta y_2 \cdot m}\right) \cdot C'_P \qquad \text{(Eq. 3.20)}$$

where: Δy_1 is the distance from the baseline curve to that of the sample; Δy_2 is the distance from the baseline curve to the one of sapphire (Al_2O_3); m' is the mass of the sapphire; m is the mass of the sample; C'_P is the specific heat capacity of Al_2O_3.

It was obtained that, at 25 °C, the C_P value of hydroxyledgrewite is equal to 0.928 J/(g·K) (Table 3.9). In the temperature range up to 320 °C, the specific heat capacities of hydroxyledgrewite increased monotonically in a continuous manner (Fig. 3.52, b). Meanwhile, in the higher temperature range up to 420 °C, C_P grows rapidly (Table 3.9, Fig. 3.52, b). It is worth highlighting that C_P values cannot be accurately determined in a higher temperature range because thermal conversions of portlandite (422–452 °C) still take place. In general, particles of hydroxyledgrewite move more vigorously at higher temperatures than at lower temperatures. Hence, a particular quantity of hydroxyledgrewite at higher temperatures requires more energy to increase the same temperature than at lower temperatures; for this reason, the specific heat capacity increases with temperature.

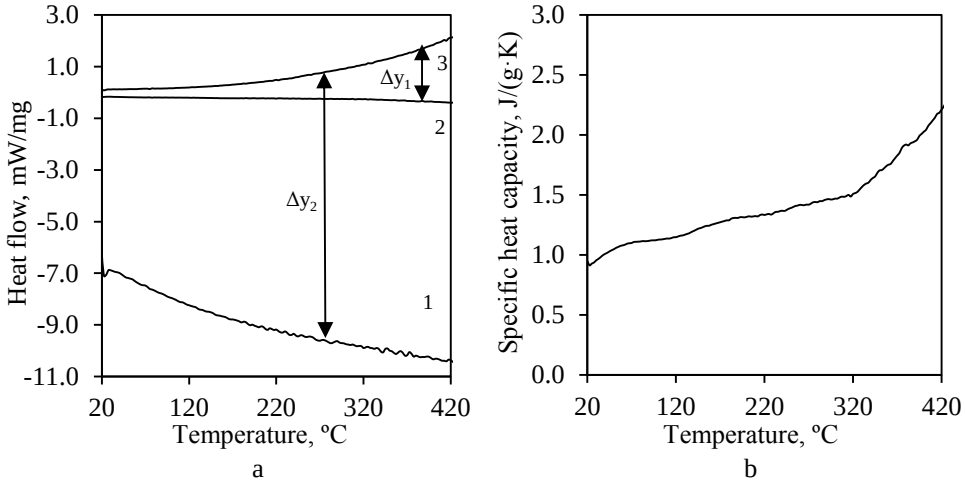

Fig. 3.52. The principal scheme of the application of the sapphire method (a): 1 – the sapphire curve; 2 – the sample curve; 3 – the baseline curve; changes of C_P (b) at 20–420 °C temperature

Table 3.9. The thermal characteristics of hydroxyledgrewite

T, °C	25	50	100	150	200	250	300	350	400	420
C_P, J/(g·K)	0.928	1.048	1.128	1.230	1.318	1.392	1.470	1.705	2.028	2.212

As it was shown previously, to achieve hydraulic activity of dibasic calcium silicates hydrates, they must be activated by milling and, subsequently, thermally treated. In this case, hydrogen bonds are destroyed, and reactive fragments are deposited in a disordered state on silicate surfaces. For this reason, hydroxyledgrewite was mixed with granite cutting waste and tribochemically activated. In order to test the effectiveness of the presently mentioned method, microcalorimetry analysis was performed. The total amount of the released heat was calculated on the grounds of a unit weight of hydroxyledgrewite, thus the rates can be compared with each other or with literature data.

Data on the heat release (J/g) of samples is presented in Figure 3.53. It was determined that in order to achieve hydraulic activity of samples, the calcination temperature of 550 °C is too low because the amount of the total cumulative heat after 72 hours of hydration was equal only to 17.05 J/g. Meanwhile, when the calcination temperature was increased to 700 °C, the amount of cumulative heat increased more than 4 times (74.34 J/g). The further increment of the calcination temperature (900 °C) yielded a negative effect on the amount of the released heat (Fig. 3.53). According to literature (17, 56, 58, 59, 67, 77, 142) and the previously obtained results, the amount of the total cumulative heat after activation of the most commonly used dibasic calcium silicate hydrate α-C_2SH, is equal to 40–230 J/g. For this reason, it is probable that hydroxyledgrewite after activation can be used as an environmentally friendly cementitious material.

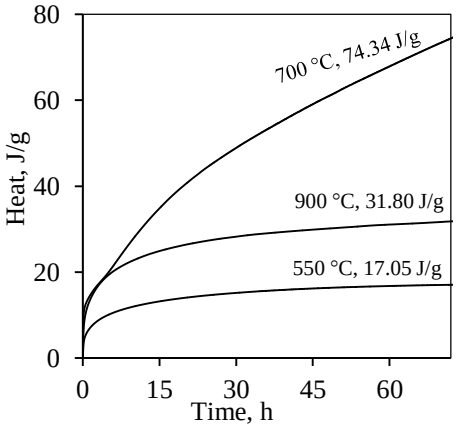

Fig. 3.53. Cumulative heat of hydroxyledgrewite samples after tribochemical activation

Acknowledgements:

Reprinted/Adapted by permission from John Wiley and Sons: John Wiley and Sons; Journal of the American Ceramic Society / Part 1: A study on the properties of synthetic hydroxyledgrewite / T. Dambrauskas, K. Baltakys, 101:3710-3718, 2018 https://doi.org/10.1111/jace.15530; License No. 4505291118551

3.6. Microstructure of synthetic and calcined α-C_2SH, kilchoanite and hydroxyledgrewite

3.6.1 Microstructure of synthetic products

The specific surface area is one of the most important characteristic of porous materials, while nitrogen adsorption/desorption is one of the main experimental techniques to determine this parameter (182–185). The N_2 adsorption/desorption isotherms of calcium silicates hydrates are presented in Figure 3.54. According to IUPAC classification, adsorption isotherms of α-C_2SH and hydroxyledgrewite correspond to the Type IV isotherm and can be described by the BET adsorption model (Figure 3.54, a and b) (183, 186, 187). This type of isotherm is presented in mesoporous materials (the pore diameter varies within the 2–50 nm range), where, at first, a monolayer is formed, then a multilayer and, finally, capillary condensation occurs. It should be noted that a characteristic feature of the Type IV isotherm is the hysteresis loop which is related with capillary condensation and pore filling at a higher relative pressure (P/P_0> 0.4). In the case of α-C_2SH and hydroxyledgrewite (Figure 3.54, a and b), the adsorption isotherms show sharp increment till P/P_0 ~0.05, which is related with the existence of micropores in the structure of the compounds. The formation of the monolayer is manifested within the range of relative pressure at ~0.05-0.35, while, at higher relative pressures (P/P_0> 0.35), the hysteresis loop occurs. It was observed that hysteresis loops do not have a plateau at P/P_0> 0.7, thus it can be classified as type H3. The presently mentioned type of the

hysteresis loop shows that pores of α-C_2SH and hydroxyledgrewite are slit-shaped, which occurs between disordered aggregates of plate-like particles. Moreover, the rapidly increasing adsorption isotherm above P/P_0 = 0.9 shows the existence of macropores.

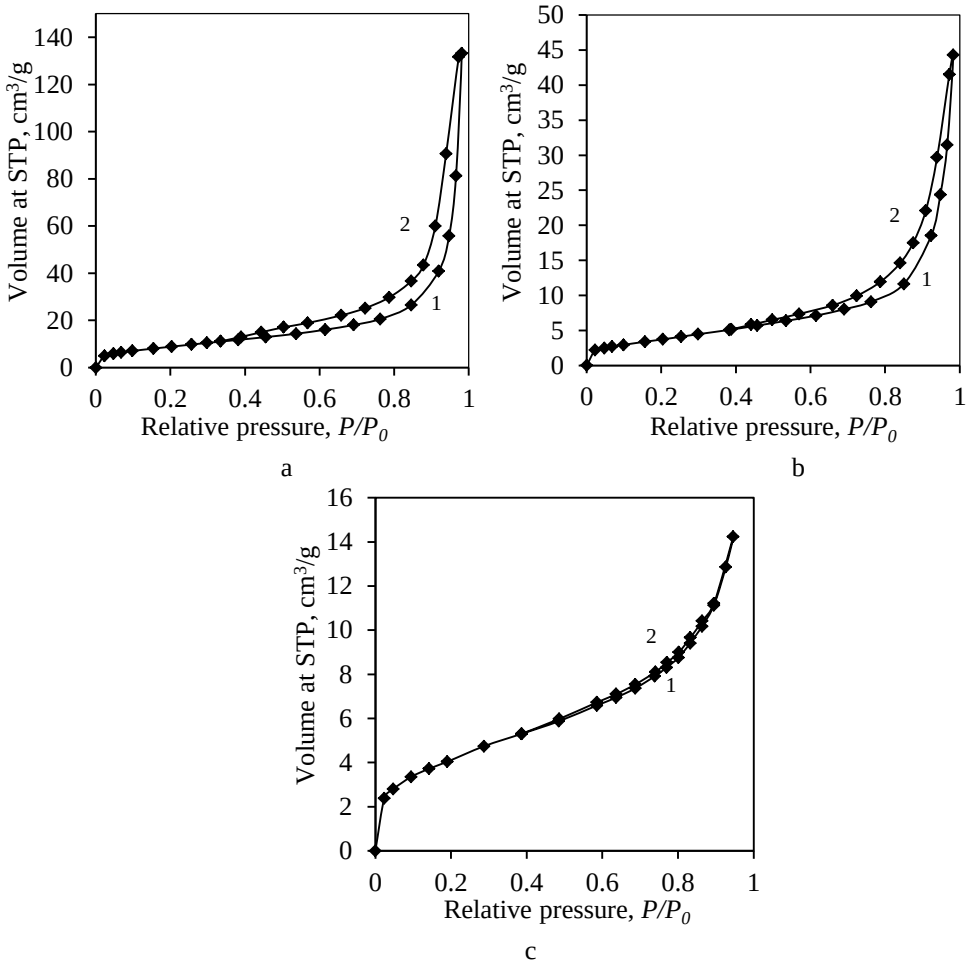

Fig. 3.54. Adsorption (1) – desorption (2) isotherms of synthetic α-C_2SH (a), hydroxyledgrewite (b) and kilchoanite (c) samples

A different tendency was observed in the kilchoanite sample: the adsorption isotherm corresponds to Type II because the isotherm does not have a hysteresis loop (183, 186, 187). Type II isotherms typically define adsorption in mesoporous materials and also can be observed in nonporous or only macroporous solids (182, 183).

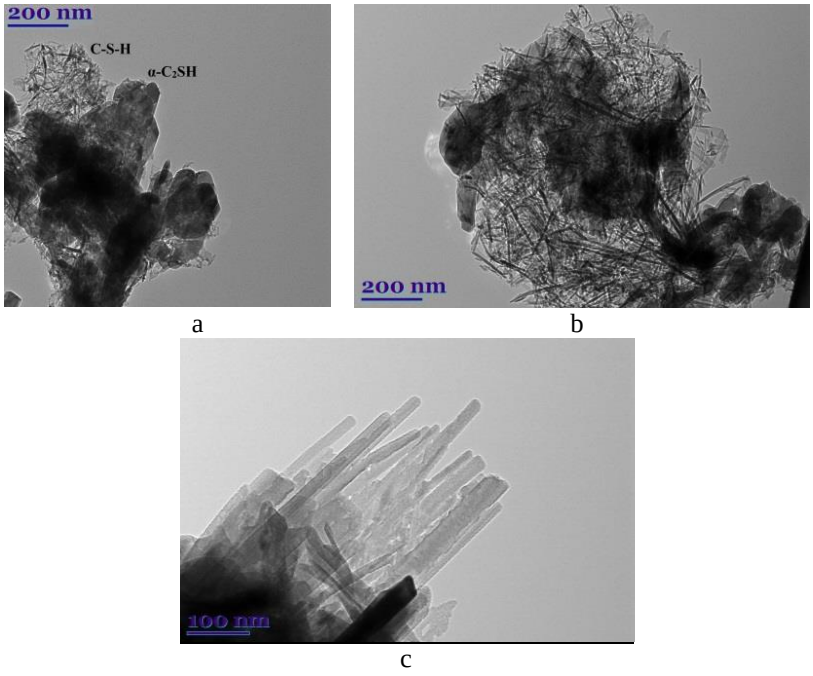

a b c

Fig. 3.55. TEM micrographs of synthetic: α-C_2SH (a), hydroxyledgrewite (b) and kilchoanite (c) samples

The obtained N_2 adsorption/desorption results were confirmed by TEM analysis (Fig. 3.55). The TEM micrograph of the α-C_2SH sample showed plate-like crystallites of α-C_2SH and disordered uncertainly shaped crystallites of semi-crystalline phase C-S-H (Fig. 3.55, a). It is worth noting that the micrograph of hydroxyledgrewite showed crystallites of a similar shape of the following size: width ~5–10 nm; length ~80–120 nm (Fig.3.55, b). It is clearly seen that between these crystallites mesopores were formed (2–10 nm), while micropores (< 2 nm) can be observed in the presently mentioned samples. Also, the TEM micrograph of kilchoanite sample showed that the crystallites of this compound are aligned, and only a few micropores and mesopores can be found (Fig. 3.55, c).

The BET equation of all the samples yields a linear plot in the range of relative pressures $0.05 \leq p/p0 \geq 0.35$ (Fig. 3.56). A straight line with the correlation coefficient R^2=0.9997 was obtained in the BET coordination $\left(1/\left(X\left[\left(P_0/P\right)-1\right]\right)\right)-\left(P_0/P\right)$. The calculated parameters are represented in Table 3.10.

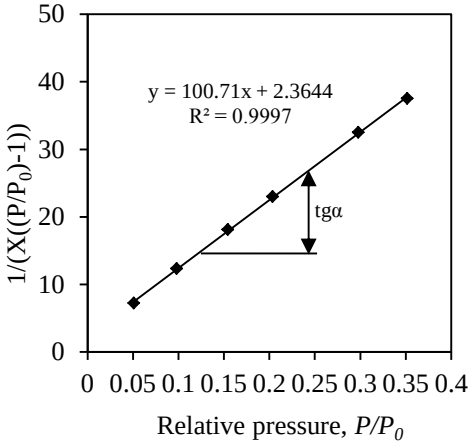

Fig. 3.56. The isotherm of N_2 adsorption at 77 K in the BET plot of α-C_2SH sample

According to the BET theory, constant C_{BET} is related to the monolayer adsorption energy and is equal to 50–300 if no weak interaction or no chemisorption occurs (182, 183, 185). In general, if the value of mentioned constant is >50, the knee of the isotherm is sharp, and Point B is fairly well defined (182, 183, 188). If the value of C_{BET} is lover than 50, Point B cannot be identified as a single point on the isotherm, and the calculated parameters obtained by using the BET equation could involve some errors. It was determined that the values of C_{BET} are higher than 50 only in the kilchoanite sample (Table 3.10). Meanwhile, α-C_2SH and hydroxyledgrewite samples showed slightly lower values (43.59 and 40.93, respectively). It is worth noting that Type II and Type IV isotherms are valid till C_{BET}> 2 (182, 188), and the BET equation can be used for surface area calculations. The calculation revealed that the capacity of monolayer X_m and values of S_{BET} of α-C_2SH sample is equal to 0.0097 g and 33.81 m^2/g, respectively (Table 3.10). Meanwhile, the samples of kilchoanite and hydroxyledgrewite showed ~2.2 times lower values of X_m (0.0044 and 0.0041 g) and S_{BET} (15.24 and 14.30 m^2/g). Also, the calculated values of the total pore volume is the highest in α-C_2SH sample ($0.206 \cdot 10^{-6}$ m^3/g), while, in the case of hydroxyledgrewite and kilchoanite, this parameter is 3 and 9 times lower.

Table 3.10. Calculated parameters of synthetic samples specific surface area (S_{BET})

Sample	Mass, g	BET equation constants		S_{BET}, m^2/g	C_{BET} constant	Capacity of monolayer X_m, g	Total pore volume, ΔV_p, m^3/g	Reliability coefficient R^2
		Slope, S = tgα	Intercept, I					
α-C_2SH	0.1004	100.71	2.364	33.81	43.59	0.0097	$0.206 \cdot 10^{-6}$	0.999
Hydroxyl-edgrewite	0.1051	237.81	5.955	14.30	40.93	0.0041	$0.069 \cdot 10^{-6}$	0.995
Kilchoanite	0.1064	225.08	3.605	15.24	63.44	0.0044	$0.022 \cdot 10^{-6}$	1.000

3.6.2 Microstructure of calcined products

It was determined that calcination exerts significant influence on the texture of the investigated samples (Figs. 3.55–3.58). The N_2 adsorption/desorption isotherms showed that, due to solid sintering, the samples do not have micropores (the adsorption isotherms do not show sharp increment till P/P_0 ~0.1) (Fig. 3.56). Furthermore, the calcined α-C_2SH and kilchoanite samples showed fairly narrow hysteresis loops, which is related with the decreasing pore volume. Meanwhile, the calcined hydroxyledgrewite sample showed a type H2 hysteresis loop which occurs when pores with narrow mouths or/and relatively uniform channel-like pores are formed in the samples.

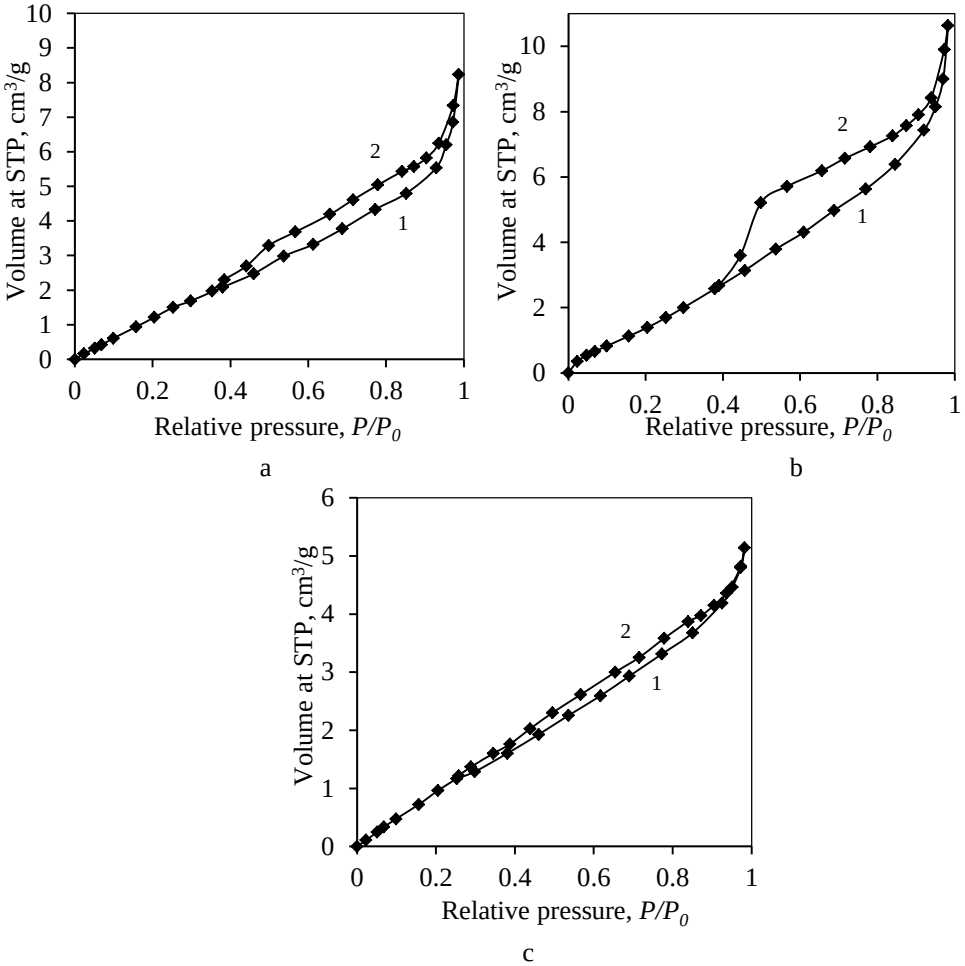

Fig. 3.57. Adsorption (1) – desorption (2) isotherms of calcined α-C_2SH (a), hydroxyledgrewite (b) and kilchoanite (c) samples

The previous results were verified with the data of TEM analysis. It is clearly seen that, during calcination, the smallest units of the investigated samples sintered, and the size of crystallites increased to 1–2 μm in α-C_2SH and kilchoanite samples

(Fig.3.55 and 3.58). It was also observed that the crystallites of the presently mentioned compounds were bounded, and only a few micropores and mesopores were formed (Fig. 3.58). Meanwhile, the micrograph of the calcined hydroxyledgrewite sample showed that particles were not fully sintered and that between the smallest units, micropores and mesopores were formed.

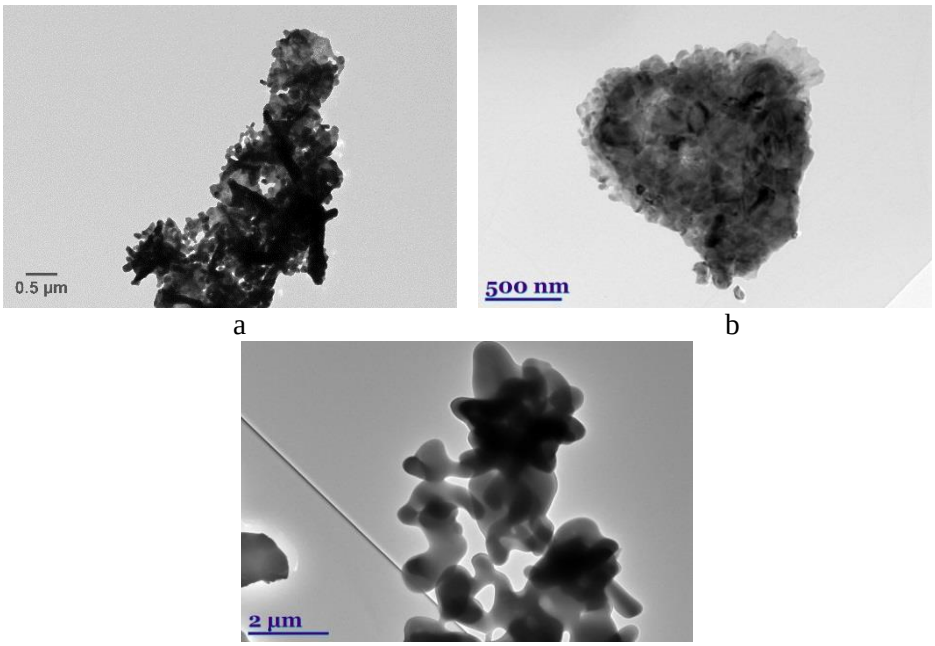

a b c

Fig. 3.58. TEM micrographs of calcined: α-C_2SH (a), hydroxyledgrewite (b) and kilchoanite (c) sample

As mentioned above, the constant C_{BET} which is related to the monolayer adsorption energy should be equal to 50–300 if no weak interaction or no chemisorption occurs. In the case of calcined samples, the values of the presently mentioned constant were 2.5–15 times lower than 50 (Table 3.11) due to a greater interaction force between the adsorbate molecules than adsorbent–adsorbate (182, 183, 187, 188). Thus the multilayer formation process is unrestricted. The calculation revealed that the capacity of monolayer X_m and the values of S_{BET} of the calcined α-C_2SH sample decreased to 0.0026 g and 9.21 m^2/g, respectively (Table 3.10 and Table 3.11). Similar results were obtained in the calcined hydroxyledgrewite sample (0.0027 g and 9.53 m^2/g), while the kilchoanite sample showed the lowest values of X_m (0.0019 g) and S_{BET} (6.55 m^2/g). It is worth noting that the same tendency was observed in the calculations of the total pore volume (Table 3.11). The decrement in the above mentioned values can be explained due to the sintering of the smallest units. The obtained results are in good agreement with the TEM data (Fig. 3.55 and Fig. 3.58).

Table 3.11. Calculated parameters of the calcined samples specific surface area (S_{BET})

Sample	Mass, g	BET equation constants		S_{BET}, m^2/g	C_{BET} constant	Capacity of monolayer X_m, g	Total pore volume, ΔV_p, m^3/g	Reliability coefficient R^2
		Slope, S = tgα	Intercept, I					
α-C_2SH 1000 °C	0.0996	260.20	118.11	9.21	3.20	0.0026	$0.013 \cdot 10^{-6}$	0.998
Hydroxyl-edgrewite 1000 °C	0.1027	347.04	18.716	9.53	19.54	0.0027	$0.018 \cdot 10^{-6}$	0.999
Kilchoanite 1200 °C	0.0901	386.14	146.22	6.55	3.64	0.0019	$0.008 \cdot 10^{-6}$	0.998

SEM analysis. SEM was applied for the visual inspection of the surface morphology (texture) and the crystalline structure. A synthetic α-C_2SH sample showed plate-like crystals of the following size: width – 25 μm, length – 60 μm (Fig. 3.59, a). Also, in the micrograph of the presently mentioned sample, the uncertainly shaped crystals of C-S-H(I) or/and C-SH(II) were observed. Meanwhile, after the calcination of the α-C_2SH sample, the SEM micrograph showed a sintered particle of a size of a few micrometers (Fig. 3.59, d).

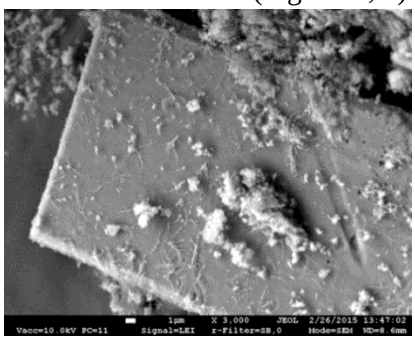
a

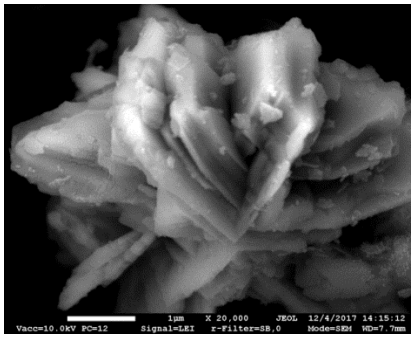
b

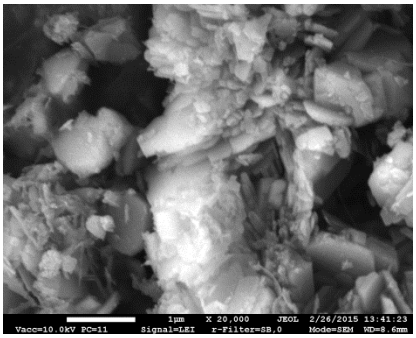
c

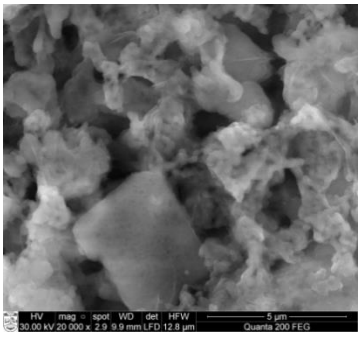
d

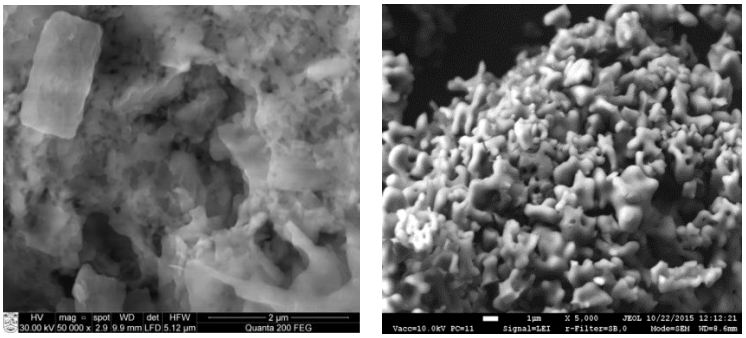

e f

Fig. 3.59. SEM micrographs of synthetic: α-C_2SH (a), hydroxyledgrewite (b) and kilchoanite (c) and calcined: α-C_2SH (d), hydroxyledgrewite (e) and kilchoanite (f) samples

In the SEM images of synthetic hydroxyledgrewite and kilchoanite samples, irregularly shaped particles of an average size of 1–6 μm were observed (Fig. 3.59, b and c), and this data is in good agreement with the results of Galuskin *et al*. (101) and Meducin *et al*. (85). Furthermore, due to the formed β-C_2S after calcination, the hydroxyledgrewite sample was found to be similar to α-C_2SH particles (Fig. 3.59, d and e). Meanwhile, in a case of the kilchoanite sample, roughly equiaxed particles similarly shaped with the average size of 2–10 nm were observed (Fig. 3.59, f).

4. Conclusions

1. It was determined that at 175 °C temperature in a $CaO–SiO_2·nH_2O–H_2O$ (CaO/SiO_2=1.5–1.75) system after 8–16 hours of hydrothermal synthesis, portlandite had fully reacted, and α-C_2SH was dominating (53–64 %) in the products by prolonging its duration till 72 h. Meanwhile, at a higher temperature (200 °C), the latter compound was found to be stable till 16 h, while, after 24 h, it got recrystallized to kilchoanite (after 48 h, the purity exceeded 95 %).

2. For the first time, hydroxyledgrewite was synthesized under hydrothermal conditions (CaO/SiO_2=2.25, 200 °C); its purity after 48 h exceeded 93.1 %. It was determined that this compound is stable till 675 °C, and at 800 °C temperature it fully recrystallizes to γ-C_2S.

3. γ-Al_2O_3 exerted significant influence on the formation mechanism and stability of the synthesis products. At the beginning of the synthesis (4–8 h), the additive retarded the formation of calcium silicate hydrates; however, it stimulated the crystallization of dicalcium silicate and calcium aluminate silicate hydrates and/or calcium aluminate hydrates which remained stable under all experimental conditions. The formation of the presently mentioned compounds was supported by thermodynamic calculations and data of instrumental analysis.

4. It was determined that α-C_2SH and α-C_2SH-Al samples are stable till 400 °C. Despite the fact that, at a higher temperature of calcination (450 °C), the crystallinity of the α-C_2SH–Al sample (40.76 %) was 1.37 times higher than that of the α-C_2SH sample (29.75 %), both samples were fully recrystallized to x-C_2S and calcium olivine. In a pure system, x-C_2S recrystallized to α'-C_2S and β-C_2S at 750 °C temperature, while at 900 °C only β-C_2S and wollastonite were identified. Meanwhile, in the α-C_2SH-Al sample, β-C_2S, kilchoanite, gehlenite and wollastonite were formed at 900 °C.

5. It was estimated that synthetic calcium silicates and/or calcium silicates hydrates formed in non-stoichiometric mixtures; after mechanochemical and thermal activation, they can be used for the manufacturing of environmentally friendly cementitious materials. It was examined that the induction period lasted 1.5 h in the α-C_2SH/quartz sample, while, in the α-C_2SH-Al/quartz sample, it was shortened to 40–50 min. It should be underlined that, after 60 hours, the total heat (90.53 J/g) of the α-C_2SH/quartz sample was not significantly different from that of α-C_2SH-Al/quartz (96.27 J/g).

6. The preparation technique for the production of a binder material whose strength values (24 MPa after 28 hydration days) match the requirements set upon belite and special low-heat cements was developed. This method combines the hydrothermal synthesis of calcium silicate hydrates and their solid-state sintering at a low temperature.

References

1. RICHARDSON, I.G. The Calcium Silicate Hydrates.*Cement and Concrete Research*, 2008, vol. 38, no. 2, pp. 137-158, ISSN 0008-8846.
2. BLACK, L. Sustainability of Construction Materials (Second Edition) J.M. KHATIB ed., Woodhead Publishing, 2016 17 - Low Clinker Cement as a Sustainable Construction Material, pp. 415-457, ISBN 9780081009956.
3. ZHANG, X., CHANG, W., ZHANG, T. and ONG, C.K. Nanostructure of Calcium Silicate Hydrate Gels in Cement Paste. *Journal of the American Ceramic Society*, 2000, vol. 83, no. 10, pp. 2600-2604, ISSN 1551-2916.
4. HARA, N., CHAN, C.F. and MITSUDA, T. Formation of 14 Å Tobermorite. *Cement and Concrete Research*, 1978, vol. 8, no. 1, pp. 113-115, ISSN 0008-8846.
5. MASSE, S., et al. High Temperature Hydration of Tricalcium Silicate, the Major Component of Portland Cement: A Silicon-29 NMR Contribution. *The Journal of Chemical Physics*, 1952, vol. 92, no. 10, pp. 1861-1866, ISSN 0021-9606.
6. Taylor H. F. W. Cement Chemistry // San Diego DA: Academic Press, 1997, vol. 2. pp. 459, ISBN 0727725920.
7. BALTAKYS, K. and SIAUCIUNAS, R. Formation of Gyrolite in the CaO-Quartz-Na_2O-H_2O System. *Materials Science Poland*, 2007, vol. 25, no. 4, pp. 1089-1100, ISSN 2083-1331.
8. BELL, N.S., VENIGALLA, S., GILL, P.M. and ADAIR, J.H. Morphological Forms of Tobermorite in Hydrothermally Treated Calcium Silicate Hydrate Gels. *Journal of the American Ceramic Society*, 1996, vol. 79, no. 8, pp. 2175-2178, ISSN 1551-2916.
9. ZULUMYAN, N., et al. A Low-Temperature Method of the B-Wollastonite Synthesis.*Journal of Thermal Analysis and Calorimetry*, 2015, vol. 122, no. 1, pp. 97-104, ISSN 1388-6150.
10. KALLA, P., et al. Durability Studies on Concrete Containing Wollastonite. *Journal of Cleaner Production*, 2015, vol. 87, pp. 726-734, ISSN 0959-6526.
11. MAGALLANES-PERDOMO, M., et al. Bone-Like Forming Ability of Apatite–wollastonite Glass Ceramic. *Journal of the European Ceramic Society*, 2011, vol. 31, no. 9, pp. 1549-1561, ISSN 0955-2219.
12. SOMTÜRK, S.M., et al. Effect of Wollastonite Extender on the Properties of Exterior Acrylic Paints.*Progress in Organic Coatings*, 2016, vol. 93, pp. 34-40, ISSN 0300-9440.
13. ABD RASHID, R., SHAMSUDIN, R., ABDUL HAMID, M.A. and JALAR, A. Low Temperature Production of Wollastonite from Limestone and Silica Sand through Solid-State Reaction. *Journal of Asian Ceramic Societies*, 2014, vol. 2, no. 1, pp. 77-81, ISSN 2187-0764.
14. AÏTCIN, P.C., and FLATT. R.J. Science and Technology of Concrete Admixtures. Elsevier Ltd, 2016, ISBN 9780081006962.
15. GARTNER, E. and HIRAO, H. A Review of Alternative Approaches to the Reduction of CO_2 Emissions Associated with the Manufacture of the Binder Phase in Concrete. *Cement and Concrete Research*, 2015 vol. 78, Part A. pp. 126-142, ISSN 0008-8846.
16. GARBEV, K., GASHAROVA, B. and STEMMERMANN, P. A Modular Concept of Crystal Structure Applied to the Thermal Transformation of α-C_2SH. *Journal of the American Ceramic Society*, 2014, vol. 97, no. 7, pp. 2286-2297, ISSN 1551-2916.
17. STEMMERMANN, P., GARBEV, K., SCHWEIKE, U. and BEUCHLE, G. Belite-Based Binder Production Method. WO2007017142. 2007.
18. ISHIDA, H., SASAKI, K. and MITSUDA, T. Highly Reactive - Dicalcium Silicate: I, Hydration Behavior at Room Temperature. *Journal of the American Ceramic Society*, 1992, vol. 75, no. 2, pp. 353-358, ISSN 1551-2916.

19. BLACK, L., et al. X-Ray Photoelectron Spectroscopic Investigation of Nanocrystalline Calcium Silicate Hydrates Synthesised by Reactive Milling. *Cement and Concrete Research*, 2006, vol. 36, no. 6, pp. 1023-1031, ISSN 0008-8846.
20. CHEN, J.J., THOMAS, J.J., TAYLOR, H.F.W. and JENNINGS, H.M. Solubility and Structure of Calcium Silicate Hydrate. *Cement and Concrete Research*, 2004, vol. 34, no. 9, pp. 1499-1519, ISSN 0008-8846.
21. HARTMANN, A., BUHL, J.-CH. and VAN BREUGEL, K. Structure and Phase Investigations on Crystallization of 11 Å Tobermorite in Lime Sand Pellets. *Cement and Concrete Research*, 2007, vol. 37, no. 1, pp. 21-31, ISSN 0008-8846.
22. NONAT, A. The Structure and Stoichiometry of C-S-H.*Cement and Concrete Research*, 2004, vol. 34, no. 9, pp. 1521-1528, ISSN 0008-8846.
23. HONG, S.-Y. and GLASSER, F.P. Phase Relations in the $CaO–SiO_2–H_2O$ System to 200 °C at Saturated Steam Pressure. *Cement and Concrete Research*, 2004, vol. 34, no. 9, pp. 1529-1534, ISSN 0008-8846.
24. MELLER, N., KYRITSIS, K. and HALL, C. The Mineralogy of the $CaO–Al_2O_3–SiO_2–H_2O$ (CASH) Hydroceramic System from 200 to 350 °C.*Cement and Concrete Research*, 2009, vol. 39, no. 1, pp. 45-53, ISSN 0008-8846.
25. ILJINA, A., et al. the Stability of Formed CaF_2 and its Influence on the Thermal Behavior of C–S–H in CaO–silica Gel Waste-H_2O System. *Journal of Thermal Analysis and Calorimetry*, 2017, vol. 127, no. 1, pp. 221-228, ISSN 1388-6150.
26. CHURAKOV, S.V. and MANDALIEV, P. Structure of the Hydrogen Bonds and Silica Defects in the Tetrahedral Double Chain of Xonotlite. *Cement and Concrete Research*, 2008, vol. 38, no. 3, pp. 300-311, ISSN 0008-8846.
27. ZOU, J., et al. Structure, Morphology and Mechanism Research on Synthesizing Xonotlite Fiber from Acid-Extracting Residues of Coal Fly Ash and Carbide Slag. *Materials Chemistry and Physics*, 2016, vol. 172, pp. 121-128, ISSN 0254-0584.
28. CAO, J., LIU, F., LIN, Q. and ZHANG, Y. Hydrothermal Synthesis of Xonotlite from Carbide Slag. *Progress in Natural Science*, 2008, vol. 18, no. 9, pp. 1147-1153, ISSN 1002-0071.
29. SHAW, S., CLARK, S.M. and HENDERSON, C.M.B. Hydrothermal Formation of the Calcium Silicate Hydrates, Tobermorite ($Ca_5Si_6O_{16}(OH)_2 \cdot 4H_2O$) and Xonotlite ($Ca_6Si_6O_{17}(OH)_2$): An in Situ Synchrotron Study. *Chemical Geology*, 2000, vol. 167, no. 1–2, pp. 129-140, ISSN 0009-2541.
30. ISMAIL, H., SHAMSUDIN, R. and ABDUL HAMID, M.A. Effect of Autoclaving and Sintering on the Formation of B-Wollastonite. *Materials Science and Engineering: C*, 2016, vol. 58, pp. 1077-1081, ISSN 0928-4931.
31. TURKMEN, O., KUCUK, A. and AKPINAR, S. Effect of Wollastonite Addition on Sintering of Hard Porcelain. *Ceramics International*, 2015, vol. 41, no. 4, pp. 5505-5512, ISSN 0272-8842.
32. LI, H.C., et al. Influence of Different Amount of Na_2O Additive on the Structure, Mechanical Properties and Degradability of Bioactive Wollastonite. *Ceramics International*, 2016, vol. 42, no. 1, part B, pp. 1439-1445, ISSN 0272-8842.
33. YAZDANI, A., REZAIE, H.R. and GHASSAI, H. Investigation of Hydrothermal Synthesis of Wollastonite using Silica and Nano Silica at Different Pressures. 2010;11(3):348–53. *Journal of Ceramic Processing Research*, 2010, vol. 11, no. 3, pp. 348-453, ISSN 1229-9162.
34. YANG, K., JUNG, Y., CHO, M. and TAE, S. Effect of Supplementary Cementitious Materials on Reduction of CO_2 Emissions from Concrete. *Journal of Cleaner Production*, 2015, vol. 103, pp. 774-783, ISSN 0959-6526.

35. GEORGESCU, M., et al. Highly Reactive Dicalcium Silicate Synthesised by Hydrothermal Processing. *Cement and Concrete Composites*, 2000, vol. 22, no. 5, pp. 315-319, ISSN 0958-9465.
36. TANTAWY, M.A., et al. Low Temperature Synthesis of Belite Cement Based on Silica Fume and Lime. *International Scholarly Research Notices*, 2014, vol. 2014, pp. 1-10, ISSN 2356-7872.
37. MELLER, N., HALL, C. and PHIPPS, J.S. A New Phase Diagram for the $CaOAl_2O_3SiO_2H_2O$ Hydroceramic System at 200 °C.*Materials Research Bulletin*, 2005, vol. 40, no. 5, pp. 715-723, ISSN 0025-5408.
38. DING, J., et al. A Novel Process for Synthesis of Tobermorite Fiber from High-Alumina Fly Ash.*Cement and Concrete Composites*, 2016, vol. 65, pp. 11-18, ISSN 0958-9465.
39. GALVÁNKOVÁ, L., MÁSILKO, J., SOLNÝ, T. and ŠTĚPÁNKOVÁ, E. Tobermorite Synthesis Under Hydrothermal Conditions. *Procedia Engineering*, 2016, vol. 151, pp. 100-107, ISSN 1877-7058.
40. BLACK, L., et al. Characterisation of Crystalline C-S-H Phases by X-Ray Photoelectron Spectroscopy. *Cement and Concrete Research*, 2003, vol. 33, no. 6, pp. 899-911, ISSN 0008-8846
41. KLIMESCH, D.S. and RAY, A. DTA-TGA Evaluations of the $CaO–Al_2O_3–SiO_2–H_2O$ System Treated Hydrothermally. *Thermochimica Acta*, 1999, vol. 334, no. 1–2. pp. 115-122 ISSN 0040-6031.
42. MOON, J., YOON, S. and MONTEIRO, P.J.M. Mechanical Properties of Jennite: A Theoretical and Experimental Study. *Cement and Concrete Research*, 2015, vol. 71, pp. 106-114, ISSN 0008-8846.
43. BONACCORSI, E., MERLINO, S. and TAYLOR, H.F.W. The Crystal Structure of Jennite, $Ca_9Si_6O_{18}(OH)_6{\cdot}8H_2O$. *Cement and Concrete Research*, 2004, vol. 34, no. 9, pp. 1481-1488, ISSN 0008-8846.
44. GARBEV, K., BLACK, L., BEUCHLE, G. and STEMMERMANN, P. Inorganic Polymers in Cement Based Materials. Wasser- Und Geotechnologie (Nachrichten Aus Dem Institut Für Technische Chemie), 2002, vol. 1, no. 2, pp. 19-30.
45. SIAUCIUNAS, R. and BALTAKYS, K. Formation of Gyrolite during Hydrothermal Synthesis in the Mixtures of CaO and Amorphous SiO_2 or Quartz. *Cement and Concrete Research*, 2004, vol. 34, no. 11, pp. 2029-2036, ISSN 0008-8846.
46. RÓŻYCKA, A., KOTWICA, Ł and MAŁOLEPSZY, J. Synthesis of Single Phase Gyrolite in the CaO-Quartz-Na_2O-H_2O System. *Materials Letters*, 2014, vol. 120, pp. 166-169, ISSN 0167-577X.
47. BALTAKYS, K. and SIAUCIUNAS, R. Influence of Gypsum Additive on the Gyrolite Formation Process. *Cement and Concrete Research*, 2010, vol. 40, no. 3, pp. 376-383, ISSN 0008-8846.
48. ILJINA, A., BALTAKYS, K. and EISINAS, A. The Influence of Hydrothermal Treatment Duration on Gyrolite Synthesis.*Romanian Journal of Materials*, 2015, vol. 45, no. 3, pp. 240-249, ISSN 2457-502X.
49. BALTAKYS, K., ILJINA, A. and BANKAUSKAITE, A. Thermal Properties and Application of Silica Gel Waste Contaminated with F^- Ions for C-S-H Synthesis. *Journal of Thermal Analysis and Calorimetry*, 2015, vol. 121, no. 1, pp. 145-154, ISSN 1388-6150.
50. HORGNIES, M., et al. The Effects of Seeding C_3S Pastes with Afwillite.*Cement and Concrete Research*, 2016, vol. 89, pp. 145-157, ISSN 0008-8846.
51. MARTÍN-SEDEÑO, M.C., et al. Stability and Oxide Ion Conductivity in Rare-Earth Aluminium Cuspidines. *Journal of Solid State Chemistry*, 2006, vol. 179, no. 11, pp. 3445-3455, ISSN 0022-4596.

52. CASASOLA, R., PÉREZ, J.M. and ROMERO, M. Effect of Fluorine Content on Glass Stability and the Crystallisation Mechanism for Glasses in the SiO_2–CaO–K_2O–F System. *Journal of Non-Crystalline Solids*, 2013, vol. 378, pp. 25-33, ISSN 0022-3093.
53. CHEN, X., et al. Novel Alkali Free Bioactive Fluorapatite Glass Ceramics. *Journal of Non-Crystalline Solids*, 2014, vol. 402, pp. 172-177, ISSN 0022-3093.
54. SEO, M., et al. Non-Isothermal Melt Crystallization of Cuspidine in CaO–SiO_2–CaF_2 Based Glasses. *Journal of Non-Crystalline Solids*, 2015, vol. 412, pp. 58-65, ISSN 0022-3093.
55. AL-HARBI, O.A. and HAMZAWY, E.M.A. Stable Wollastonite-Cuspidine Glass-Ceramic using Inexpensive Raw Materials. *Silicon*, 2014, vol. 6, no. 4, pp. 257-264, ISSN 1876-990X.
56. STEMMERMANN, P., SCHWEIKE, U. and GARBEV K. Celitement – a Sustainable Prospect for the Cement Industry. *Cement International 8*, 2010, vol. 8, no. 5, pp. 52-66, ISSN 1610-6199.
57. STEMMERMANN, P., BEUCHLE, G. and GARBEV, K. Celitement® - A New Sustainable Hydraulic Binder Based on Calcium Hydrosilicates. 13th International Congress on the Chemistry of Cement, Madrid, Spain, 2011, ISBN 978-84-7292-400-0
58. SIAUCIUNAS, R., GENDVILAS, R., MIKALIUNAITE, J., URBONAS L. Heat Flow and Strength Properties of Perspective Hydraulic Binder Material. *Journal of Thermal Analysis and Calorimetry*, 2015, vol. 121, pp. 57-65, ISSN 1388-6150
59. SIAUCIUNAS, R., MIKALIUNAITE, J., URBONAS, L. and BALTAKYS, K. Tribochemical and Thermal Activation of α-C_2S Hydrate as Precursor for Cementitious Binders. *Journal of Thermal Analysis and Calorimetry*, 2014, vol. 118, pp. 817-823, ISSN 1388-6150.
60. BLACK, L., GARBEV, K. and STUMM, A. Structure, Bonding and Morphology of Hydrothermally Synthesised Xonotlite. *Advances in Applied Ceramics*, 2009, vol. 108, no. 3, pp. 138-144, ISSN 1743-6753.
61. MERLINO, S., BONACCORSI, E., ARMBRUSTER, T. The Real Structures of Clinotobermorite and Tobermorite 9 Å: OD Character, Polytypes and Structural Relationships. *European Journal of Mineralogy*, 2000, vol. 12, pp. 411-429, ISSN 0935-1221.
62. BLACK, L., et al. X-Ray Photoelectron Spectroscopy of Aluminium-Substituted Tobermorite. *Cement and Concrete Research*, 2005, vol. 35, no. 1, pp. 51-55, ISSN 0008-8846.
63. MATSUI, K., et al. In Situ Time-Resolved X-Ray Diffraction of Tobermorite Formation in Autoclaved Aerated Concrete: Influence of Silica Source Reactivity and Al Addition.*Cement and Concrete Research*, 2011, vol. 41, no. 5, pp. 510-519, ISSN 0008-8846.
64. FROST, R.L., MAHENDRAN, M., POOLOGANATHAN, K. and XI, Y. Raman Spectroscopic Study of the Mineral Xonotlite $Ca_6Si_6O_{17}(OH)_2$-A Component of Plaster Boards. *Materials Research Bulletin*, 2012, vol. 47, no. 11, pp. 3644-3649, ISSN 0025-5408.
65. CHAN, C.F. and MITSUDA, T. Formation of 11 Å Tobermorite from Mixtures of Lime and Colloidal Silica with Quartz. *Cement and Concrete Research*, 1978, vol. 8, no. 2, pp. 135-138, ISSN 0008-8846.
66. SAHU, S. and DECRISTOFARO, N. Part One of a Two - Part Series Exploring the Chemical Properties and Performance Results of Sustainable Solidia Cement ™ and Solidia Concrete ™. *Solidia Cement*, 2013, pp. 1-12.
67. GARBEV, K., BEUCHLE, G. and SCHWEIKE, U. Hydration Behavior of Celitement®: Kinetics, Phase Composition, Microstructure and Mechanical Properties. 13th International Congress on the Chemistry of Cement, Madrid, Spain, 2011, ISBN 978-84-7292-400-0.

68. TAYLOR, H.F.W., BESSEY, G.E. Review of Hydrothermal Reactions in the System Lime-Silica-Water. *Magazine of Concrete Research*, 1950, vol. 2, pp. 15, ISSN 0024-9831.
69. HELLER, L. The Thermal Decomposition of the Hydrated Calcium Silicates, Proceedings of Third International Symposium on the Chemistry of Cement (London 1952). Cement and Concrete Association, 1954, pp. 237.
70. RYSKIN, Y.I. and STAVITSKAYA, G.P. Spectroscopic Investigation of the Hydrogen Bond in Acid Silicates and Phosphates. *Optika I Spektroskopiya*, 1960, vol. 8, no. 9, pp. 606, ISSN 0030-4034.
71. HELLER, L. The Structure of Dicalcium Silicate α-Hydrate.*Acta Crystallographica*, 1952, vol. 5, pp. 724-728, ISSN 2053-2733.
72. KALOUSEK, G.L, LOGIUDICE, J.S., and DODSON, V.H. Studies on the Lime-Rich Crystalline Solid Phases in the System Lime-Silica-Water. *Journal of American Ceramic Society*, 1952, vol. 37, pp. 7-13, ISSN 0002-7820.
73. MIDGLEY H.G., CHOPRA, S.K. Hydrothermal Reactions in the Lime-Rich Part of the System $CaO\text{-}SiO_2\text{-}H_2O$. *Magazine of Concrete Research*, 1960, vol. 34, pp. 19-26, ISSN 0024-9831.
74. IMLACH, B.V., TAYLOR, .H.F.W. Prolonged Hydrothermal Treatment of Cement Mixes I. Curing in Water Under Saturated Steam Pressure at 140-170 ºC. *Transactions and Journal of the British Ceramic Society*, 1972, vol. 71, pp. 71, ISSN 0307-7357.
75. TAYLOR, H.F.W. The Calcium Silicate Hydrates // the Chemistry of Cements, London, 1964, Edited by H.F.W. Taylor (Academic Press, London, 1964). 1964, pp. 167.
76. MITSUDA, T., KOBAYAKAWA, S. and TORAYA, H. Characterization of Hydrothermally Formed CSH // the 8th International Congress on the Chemistry of Cement, Rio De Janeiro, 1986, ISBN 978-84-7292-400-0.
77. ISHIDA, H., YAMAZAKI, S., SASAKI, K., OKADA, Y., MITSUDA, T. α-Dicalcium Silicate Hydrate – Preparation, Decomposed Phase and its Hydration. *Journal of the American Ceramic Society*, 1993, vol. 76, pp. 1707-1712, ISSN 1551-2916.
78. GARBEV, K., et al. First Observation of $\alpha\text{-}Ca_2[SiO_3(OH)](OH)\text{-}Ca_6[Si_2O_7][SiO_4](OH)_2$ Phase Transformation upon Thermal Treatment in Air. *Journal of the American Ceramic Society*, 2008, vol. 91, no. 1, pp. 263-271, ISSN 1551-2916.
79. YANO, T., et al. Structure of Alpha-Dicalcium Silicate Hydrate. *Acta Cystallographica Section C-Crystal Structure Communications*, 1993, vol. 49, pp. 1555-1559, ISSN 2053-2296.
80. BUTT, J.M., et al. The Formation of Calcium Hydrosilicates and its Characterization.*Silikattechn*, 1961, vol. 12, pp. 281.
81. HU, X., YANAGISAWA, K., ONDA, A., KAJIYOSHI, K. Stability and Phase Relations of Dicalcium Silicate Hydrates Under Hydrothermal Conditions. *Journal of the Ceramic Society of Japan*, 2006, vol. 114, pp. 174-179, ISSN 1882-0743.
82. MIYAZAKI, M., et al. Crystallographic Data of a New Phase of a Dicalcium Silicate. *Journal of American Ceramic Society*, 1998, vol. 81, no. 5, pp. 1339-1349, ISSN 1551-2916.
83. TORAYA H., Y.S. Simulated Annealing Structure Solution of a New Phase of Dicalcium Silicate Ca_2SiO_4 and the Mechanism of Structural Changes from α-Dicalcium Silicate Hydrate to Dicalcium Silicate Via the New Phase. *Acta Crystallographica*, 2002, vol. B58, pp. 613-621, ISSN 2053-2296.
84. MARSH R.E. A Revised Structure for α-Dicalcium Silicate Hydrate.*Acta Crystallographica*, 1994, vol. C50. pp. 996-997, ISSN: 2053-2296
85. MÉDUCIN, F., et al. Calcium Silicate Hydrates Investigated by Solid-state High Resolution ^{1}H and ^{29}Si Nuclear Magnetic Resonance. *Cement and Concrete Research*, 2007, vol. 37, no. 5, pp. 631-638, ISSN 0008-8846.

86. AGRELL, S. O. and GAY. P. Kilchoanite, a Polymorph of Rankinite. *Nature*, 1961, vol. 189, pp. 743-743, ISSN 0028-0836.
87. PETSCHNIG, L. and KAHLENBERG, V. Structural Reinvestigation of Synthetic Kilchoanite a $Ca_3Si_2O_7$ Polymorph. Universität Innsbruck, Innrain 52, A-6020 Innsbruck, Österreich. Mitt.Österr.Miner.Ges., 2012, vol. 158. pp. 59-65.
88. ROY, M. Studies in the System $CaO-Al_2O_3-SiO_2-H_2O$ IV; Phase Equilibria in the High-Lime Portion of the System $CaO-SiO_2-H_2O$. *The American Mineralogist*, 1958, vol. 43, no. 11-12, pp. 1009-1028, ISSN 0003-004X.
89. MITSUDA, T. Low-Temperature Synthesis of Kilchoanite from Quartz-LimeMixtures by a New Method. *Mineralogical Journal*, 1972, vol. 7, no. 1.pp. 108-114, ISSN 1881-4174.
90. TAYLOR, H.F.W. The Crystal Structure of Kilchoanite, $Ca_6(SiO_3)(Si_3O_{10})$, with some Comments on Related Phases. *Mineralogical Magazine*, 1971, vol. 38, pp. 26-31, ISSN 0026-461X.
91. MITSUDA, T., ASAMI, J., MATSUBARA, Y. and TORAYA, H. Hydrothermal Formation of γ-Dicalcium Silicate from Lime-Silica Mixtures using a Rapid-Heating Method and its Reaction to Give Kilchoanite Or Calciochondrodite. *Cement and Concrete Research*, 1985, vol. 15, no. 4, pp. 613-621, ISSN 0008-8846.
92. SPEAKMAN, K., TAYLOR, H.F.W., BENNETT, J.M., and GARD, J.A. Hydrothermal Reactions of γ-Dicalcium Silicate. *Journal of the Chemical Society A: Inorganic, Physical, Theoretical*, 1967, pp. 1052-1060.
93. YANAGISAWA, K., HU, X., ONDA, A. and KAJIYOSHI, K. Hydration of B-Dicalcium Silicate at High Temperatures under Hydrothermal Conditions. *Cement and Concrete Research*, 2006, vol. 36, no. 5, pp. 810-816, ISSN 0008-8846.
94. TAYLOR, H.F.W. The Chemistry of Cements // Academic Press, London and New York, 1964, vol. 1, ISBN 0126839026.1.
95. KRAUS, W., and NOLZE, G. POWDER CELL - a Program for the Representation and Manipulation of Crystal Structures and Calculation of the Resulting X-Ray Powder Patterns. *Journal of Applied Crystallography*, 1996, vol. 29, no. 3, pp. 301-303, ISSN 1600-5767.
96. HENRY, M. Retrosynthesis in Inorganic Crystal Structures: Application to Nesosilicate and Inosilicate Networks. *Coordination Chemistry Reviews*, 1998, vol. 178-180, part 2, pp. 1109-1163, ISSN 0010-8545.
97. ROY, D. M. and HARKER, R. I. Phase Equilibria in the System $CaO-SiO_2-H_2O$ // Fourth International Symposium on the Chemistry of Cement. Washington, USA, 1960.
98. ROY, D.M., GARD, J.A., NICOL, A.W. and TAYLOR, H.F.W. New Data for the Calcium Silicate "Phase Z."*Nature*, 1960, vol. 188, pp. 1187-1188, ISSN 1476-4687.
99. ROMO-CASTAÑEDA, J., et al. Thermodynamic Modeling of Mineralogical Phases Formed by Continuous Casting Powders.*Thermochimica Acta*, 2011, vol. 512, no. 1-2, pp. 129-133, ISSN 0040-6031.
100. JUNG, I., LEHMANN, J. and JAK, E. Treatise on Process Metallurgy S. SEETHARAMAN ed., Boston: Elsevier, 2014 Chapter 5.3 - Applications, pp. 675-798, ISBN 9780080969848.
101. GALUSKIN, E. V., et al. Edgrewite $Ca_9(SiO_4)_4F_2$ - Hydroxyledgrewite $Ca_9(SiO_4)_4(OH)_2$, a New Series of Calcium Humite-Group Minerals from Altered Xenoliths in the Ignimbrite of Upper Chegem Caldera, Northern Caucasus, Kabardino-Balkaria, Russia. *American Mineralogist*, 2012, vol. 97, pp. 1998-2006, ISSN 0003-004X.
102. GALUSKIN, E.V., et al. Chegemite, $Ca_7(SiO_4)_3(OH)_2$ - a New Calcium Mineral of the Humite-Group from the Northern Caucasus, Kabardino-Balkaria, Russia. *European Journal of Mineralogy*, 2009, vol. 21, pp. 1045-1059, ISSN 0935-1221.
103. GALUSKIN, E.V. et al. Pavlovskyite $Ca_8(SiO_4)_2(Si_3O_{10})$ - a New Mineral of Altered Silicate-Carbonate Xenoliths from the Two Russian Type Localities: Birkhin Massif, Baikal

Lake Area and Upper Chegem Caldera, North Caucasus. *American Mineralogist*, 2012, vol. 97, pp. 503-512, ISSN 0003-004X.
104. GAINES, R.V., SKINNER, H.C.W., FOORD, E.E., MASON, B., ROSENZWEIG, A. Dana's New Mineralogy: The System of Mineralogy of James Dwight Dana and Edward Salisbury Dana 8th Edition. 8th ed. Wiley-Interscience, 1997, ISBN 0471193100.
105. THOMPSON, J.B. Biopyriboles and Polysomatic Series. *American Mineralogist*, 1978, vol. 63, pp. 239-249, ISSN 0003-004X.
106. OLIVIER, J.G.J., MAENHOUT, G.J., MUNTEAN, M. and PETERS, J.A.H.W. Trends in Global CO2 Emissions: 2015 Report. Hague: PBL Netherlands Environmental Assessment Agency, 2015.
107. OLIVIER, J.G.J., SHURE, K.M. and PETERS, J.A.H.W. Trends in Global CO2 and Total Greenhouse Gas Emissions: 2017 Report. PBL Netherlands Environmental Assessment Agency, 2017.
108. JANSSENS-MAENHOUT, G., et al. Fossil CO_2& GHG Emissions of all World Countries. JRC Science for Policy Report, 2017.
109. BARCELO, L., KLINE, J., WALENTA, G. and GARTNER, E. Cement and Carbon Emissions. *Materials and Structures*, 2014, vol. 47, no. 6, pp. 1055-1065, ISSN 1871-6873.
110. SINGH, N.B., KALRA, M., KUMAR, M. and RAI, S. Hydration of Ternary Cementitious System: Portland Cement, Fly Ash and Silica Fume. *Journal of Thermal Analysis and Calorimetry*, 2015, vol. 199, no. 1, pp. 381-389, ISSN 1388-6150.
111. XU, J., FLEITER, T., EICHHAMMER, W. and FAN, Y. Energy Consumption and CO2 Emissions in China's Cement Industry: A Perspective from LMDI Decomposition Analysis. *Energy Policy*, 2012, vol. 50, pp. 821-832, ISSN 0301-4215.
112. Energy Technology Perspectives 2010, Scenario and Strategies to 2050. Paris: International Energy Agency. 2010, ISBN 978-92-64-08597-8
113. BENHELAL, E., ZAHEDI, G., SHAMSAEI, E. and BAHADORI, A. Global Strategies and Potentials to Curb CO_2 Emissions in Cement Industry. *Journal of Cleaner Production*, 2013, vol. 51, pp. 142-161, ISSN 0959-6526.
114. Concrete CO_2 Fact Sheet. National Ready Mixed Concrete Association; 2012.NRMCA Publication Number 2PCO2.
115. ABDUL-WAHAB, S.A., AL-RAWAS, G.A., ALI, S. and AL-DHAMRI, H. Impact of the Addition of Oil-Based Mud on Carbon Dioxide Emissions in a Cement Plant. *Journal of Cleaner Production*, 2016, vol. 112, part 5, pp. 4214-4225, ISSN 0959-6526.
116. PENG, J.H., et al. Modeling of Carbon Dioxide Measurement on Cement Plants. *Advanced Materials Research*, 2013, vol. 610-613, pp. 2120-2128, ISSN 1662-8985.
117. MILLER, S.A., JOHN, V.M., PACCA, S.A. and HORVATH, A. Carbon Dioxide Reduction Potential in the Global Cement Industry by 2050. *Cement and Concrete Research*, 2018, vol. 114, pp. 115-124, ISBN 0008-8846.
118. MADDALENA, R., ROBERTS, J.J. and HAMILTON, A. Can Portland Cement be Replaced by Low-Carbon Alternative Materials? A Study on the Thermal Properties and Carbon Emissions of Innovative Cements.*Journal of Cleaner Production*, 2018, vol. 186, no. 10, pp. 933-942, ISBN 0959-6526.
119. LIU, Z., WANG, Z., YUAN, M.Z. and YU, H.B. Thermal Efficiency Modelling of the Cement Clinker Manufacturing Process. *Journal of the Energy Institute*, 2015, vol. 88, no. 1, pp. 76-86, ISSN 1743-9671.
120. KHURANA, S., BANERJEE, R. and GAITONDE, U. Energy Balance and Cogeneration for a Cement Plant. *Applied Thermal Engineering*, 2002, vol. 22, no. 5, pp. 485-494, ISSN 1359-4311.

121. MADLOOL, N.A., SAIDUR, R., HOSSAIN, M.S. and RAHIM, N.A. A Critical Review on Energy use and Savings in the Cement Industries. *Renewable and Sustainable Energy Reviews*, 2011, vol. 15, no. 4, pp. 2042-2060, ISSN 1364-0321.
122. FELLAOU, S. and BOUNAHMIDI, T. Evaluation of Energy Efficiency Opportunities of a Typical Moroccan Cement Plant: Part I. Energy Analysis. *Applied Thermal Engineering.*2017, vol. 155, no. 25, pp. 1161-1172, ISBN 1359-4311.
123. ALTUN, O. Energy and Cement Quality Optimization of a Cement Grinding Circuit. *Advanced Powder Technology*, 2018, vol. 29, no. 7, pp. 1713-1723, ISBN 0921-8831.
124. WANG, J., MU, M. and LIU, Y. Recycled Cement. *Construction and Building Materials*, 2018, vol. 190, no. 30, pp. 1124-1132, ISBN 0950-0618.
125. XU, J., FLEITER, T., FAN, Y. and EICHHAMMER, W. CO_2 Emissions Reduction Potential in China's Cement Industry Compared to IEA's Cement Technology Roadmap Up to 2050. *Applied Energy*, 2014, vol. 130, pp. 592-602, ISSN 0306-2619.
126. UWASU, M., HARA, K. and YABAR, H. World Cement Production and Environmental Implications. *Environmental Development*, 2014, vol. 10, pp. 36-47, ISBN 2211-4645.
127. SHARMA, R. Cement Industry Trends Report. The Energy and Resources Institute 2017, 2017.
128. IMBABI, M.S., CARRIGAN, C. and MCKENNA, S. Trends and Developments in Green Cement and Concrete Technology. *International Journal of Sustainable Built Environment*, 2012, vol. 1, no. 2, pp. 194-216, ISBN 2212-6090.
129. BIERNACKI, J.J., et al. Cements in the 21st Century: Challenges, Perspectives, and Opportunities. *Journal of the American Ceramic Society*, 2017, vol. 100, no. 7, pp. 2746-2773, ISSN 0002-7820.
130. GARTNER, E. and SUI, T. Alternative Cement Clinkers. *Cement and Concrete Research*, 2018, vol. 114, pp. 27-39, ISBN 0008-8846.
131. SÁNCHEZ-HERRERO, M.J., FERNÁNDEZ-JIMÉNEZ, A. and PALOMO, Á. Alkaline Hydration of C_2S and C_3S. *Journal of the American Ceramic Society*, 2016, vol. 99, no. 2, pp. 604-611, ISSN 0002-7820.
132. GENDVILAS, R., SIAUCIUNAS, R. and BALTAKYS, K. Quantitative Thermal Analysis of α-C_2SH as a Precursor for Low-Energy Cements. *Journal of Thermal Analysis and Calorimetry*, 2015, vol. 121, no 1, pp. 155-162, ISSN 1388-6150.
133. SINYOUNG, S., KUNCHARIYAKUN, K., ASAVAPISIT, S. and MACKENZIE, K.J.D. Synthesis of Belite Cement from Nano-Silica Extracted from Two Rice Husk Ashes. *Journal of Environmental Management*, 2017, vol. 190, pp. 53-60, ISBN 0301-4797.
134. CHRYSAFI, R., PERRAKI, T. and KAKALI, G. Sol-gel Preparation of $2CaO{\cdot}SiO_2$. *Journal of the European Ceramic Society*, 2007, vol. 27, no. 2-3, pp. 1707-1710, ISBN 0955-2219.
135. THOMAS, J.J., GHAZIZADEH, S. and MASOERO, E. Kinetic Mechanisms and Activation Energies for Hydration of Standard and Highly Reactive Forms of β-dicalcium Silicate (C_2S). *Cement and Concrete Research*, 2017, vol. 100, pp. 322-328, ISBN 0008-8846.
136. WESSELSKY, A. and JENSEN, O.M. Synthesis of Pure Portland Cement Phases. *Cement and Concrete Research*, 2009, vol. 39, no. 11, pp. 973-980, ISBN 0008-8846.
137. CHATTERJEE, A.K. Future Technological Options: Part II. *Cement and Concrete Research*, 1996, vol. 26, no. 8, pp. 1227-1237, ISSN 0008-8846.
138. CHATTERJEE, A.K. High Belite cements-Present Status and Future Technological Options: Part I. Cement and Concrete Research, 1996, vol. 26, no. 8, pp. 1213-1225, ISBN 0008-8846.

139. CHEN, Y., et al. Characterization of Mortars from Belite-Rich Clinkers Produced from Inorganic Wastes. *Cement and Concrete Composites*, 2011, vol. 33, no. 2, pp. 261-266, ISBN 0958-9465.
140. GARTNER, E. Industrially Interesting Approaches to "low-CO_2" Cements. *Cement and Concrete Research*, 2004, vol. 34, no. 9, pp. 1489-149, ISSN 0008-8846.
141. GARBEV, K., et al. Preparation of a Novel Cementitious Material from Hydrothermally Synthesized C–S–H Phases. *Journal of the American Ceramic Society*, 2014, vol. 97, no. 7, pp. 2298-2307, ISSN 0002-7820.
142. LINK, T., BELLMANN, F., LUDWIG, H.M. and BEN HAHA, M. Reactivity and Phase Composition of Ca_2SiO_4 Binders made by Annealing of Alpha-Dicalcium Silicate Hydrate. *Cement and Concrete Research*, 2015, vol. 67, pp. 131-137, ISSN 0008-8846.
143. GENDVILAS, R. and SIAUCIUNAS, R. Hydrothermal Synthesis of α-C_2S Hydrate at 175 °C. Chemistry and chemical technology of inorganic materials: proceedings of scientific conference chemistry and chemical technology. Kaunas: Technologija, 2012, p. 21-25, ISSN 2029-9222.
144. SIAUCIUNAS, R., STANKEVICIUTE, M., GENDVILAS, R. and BALTAKYS, K. Heat Release during the Hydration of Calcinated α-C_2SH and its Mixture with Killalaite. *Journal of Thermal Analysis and Calorimetry*, 2017, vol. 127, no. 1, pp. 163-171, ISSN 1388-6150.
145. GENDVILAS, R. and SIAUCIUNAS, R. Hydrothermal Synthesis of α-C_2S Hydrate in Stirred Suspensions at 200°C. Proceedings of the BaltSilica, 2014, p. P-2. Poznan, Poland, ed., ISBN 9788362783014.
146. SIAUCIUNAS, R., BALTAKYS, K., GENDVILAS, R. and PRICHOCKIENE, E. Synthesis of Low-Energy Cement Based on α-C_2SH. Proceedings of 34th annual cement and concrete science conference.Sheffield : The University of Sheffield, UK ed. 2014.
147. ISHIDA, H., MABUCHI, K., SASAKI, K. and MITSUDA, T. Low-Temperature Synthesis of β-Ca_2SiO_4 from Hillebrandite. *Journal of the American Ceramic Society*, 1992, vol. 75, no. 9, pp. 2427-2432, ISSN 1551-2916.
148. MUNIZ, F.T.L., MIRANDA, M.A.R., MORILLA DOS SANTOS, C. and SASAKI, J.M. The Scherrer Equation and the Dynamical Theory of X-Ray Diffraction.*Acta Crystallographica Section A*, 2016, vol. 72, no. 3, pp. 385-390, ISSN 2053-2733.
149. BURTON, A.W., ONG, K., REA, T. and CHAN, I.Y. On the Estimation of Average Crystallite Size of Zeolites from the Scherrer Equation: A Critical Evaluation of its Application to Zeolites with One-Dimensional Pore Systems. *Microporous and Mesoporous Materials*, 2009, vol. 117, no. 1-2, pp. 75-90, ISBN 1387-1811.
150. DINNEBIER, R.E., et al. Powder Diffraction. The Royal Society of Chemistry.ISBN - 978-0-85404-231-9.
151. BLANC, P., BOURBON, X., LASSIN, A. and GAUCHER, E.C. Chemical Model for Cement-Based Materials: Temperature Dependence of Thermodynamic Functions for Nanocrystalline and Crystalline C–S–H Phases. *Cement and Concrete Research*, 2010, vol. 40, no. 6, pp. 851-866, ISSN 0008-8846.
152. Babushkin V. I., Matveev G. M. and Mchedlow-Petrossyan O. P. Thermodynamics of Silicates. Moscow: 1986. ISSN 1060-0396.
153. MATSCHEI, T., LOTHENBACH, B. and GLASSER, F.P. Thermodynamic Properties of Portland Cement Hydrates in the System $CaO–Al_2O_3–SiO_2–CaSO_4–CaCO_3–H_2O$. *Cement and Concrete Research*, 2007, vol. 37, no. 10, pp. 1379-1410, ISSN 0008-8846.
154. LOTHENBACH, B. and WINNEFELD, F. Thermodynamic Modelling of the Hydration of Portland Cement. *Cement and Concrete Research*, 2006, vol. 36, no. 2, pp. 209-226, ISSN 0008-8846.

155. RIVAS-MERCURY, J.M., PENA, P., DE AZA, A.H. and TURRILLAS, X. Dehydration of $Ca_3Al_2(SiO_4)_Y(OH)_{4(3-y)}$ ($0<Y<0.176$) studied by neutron thermodiffractometry. *Journal of the European Ceramic Society*, 2008, vol. 28, no 9, pp. 1737-1748, ISBN 0955-2219.
156. DILNESA, B.Z., et al. Synthesis and Characterization of Hydrogarnet $Ca_3(Al_xFe_{1-x})_2(SiO_4)_Y(OH)_{4(3-y)}$. *Cement and Concrete Research*, 2014, vol. 59, pp. 96-111, ISSN 0008-8846.
157. JAPPY, T.G. and GLASSER, F.P. Synthesis and Stability of Silica-Substituted Hydrogarnet $Ca_3Al_2Si_{3-x}O_{12-4x}(OH)_{4x}$. *Advances in Cement Research*, 1991, vol. 4, no. 13, pp. 1-8, ISSN 0951-7197.
158. MAHESWARAN, S., KALAISELVAM, S., PALANI, G.S. and SASMAL, S. Investigations on the Early Hydration Properties of Synthesized β-Belites Blended Cement Pastes. *Journal of Thermal Analysis and Calorimetry*, 2016, vol. 125, no. 1, pp. 53-64, ISSN 1388-6150.
159. SHI, C. and DAY, R.L. Some Factors Affecting Early Hydration of Alkali-Slag Cements. *Cement and Concrete Research*, 1996, vol. 26, no. 3, pp. 439-447, ISSN 0008-8846.
160. GRUYAERT, E., ROBEYST, N., DE BELIE, N. Study of the Hydration of Portland Cement Blended with Blast-Furnace Slag by Calorimetry and Thermogravimetry. *Journal of Thermal Analysis and Calorimetry*, 2010, vol. 102, no. 3, pp. 941-951, ISSN 1388-6150.
161. DE WEERDT, K., et al. Hydration Mechanisms of Ternary Portland Cements Containing Limestone Powder and Fly Ash. *Cement and Concrete Research*, 2011, vol. 41, no. 3, pp. 279-291, ISSN 0008-8846.
162. PACEWSKA, B., WILIÅ„SKA, I. and BUKOWSKA, M. Hydration of Cement Slurry in the Presence of Spent Cracking Catalyst. *Journal of Thermal Analysis and Calorimetry*, 2000, vol. 60, no. 1, pp. 71-78, ISSN 1388-6150.
163. EVJU, C. Initial Hydration of Cementitious Systems using a Simple Isothermal Calorimeter and Dynamic Correction. *Journal of Thermal Analysis and Calorimetry*, 2003, vol. 71, no. 3, pp. 829-840, ISSN 1388-6150.
164. GARBEV, K., et al. Structural Features of C-S-H(I) and its Carbonation in Air. A Raman Spectroscopic Study. Part I: Fresh Phases. *Journal of the American Ceramic Society*, 2007, vol. 90, no. 3, pp. 900-907, ISSN 1551-2916.
165. TAYLOR H.F.W. Hydrated Calcium Silicates: Part V. the Water Content of Calcium Silicate Hydrate (I). *Journal of the Chemical Society*, 1953. pp. 163-167.
166. GARD, J.A. and TAYLOR, H.F.W. Calcium Silicate Hydrate (II) ("C-S-H(II)"). *Cement and Concrete Research*, 1976, vol. 6, no. 5. pp. 667-677 ISSN 0008-8846.
167. SIAUCIUNAS R, BALTAKYS K, BALTUSNIKAS A. Instrumental Analysis of Silicate Materials. Kaunas: Vitae Litera, 2007, ISBN 978-9955-686-36-1.
168. CHUKANOV, NV. Infrared Spectra of Mineral Species. New York and London: Springer, 2014, ISBN 978-94-007-7128-4.
169. DUMITRU, M.D., MILJKOVIC, D., SCOREI, R.I., ROTARU, P. FT-IR and Raman Spectroscopic Analysis of a Calcium Fructoborate Sample. *Physic AUC*, 2010, vol. 20, no. 1, pp. 113-119.
170. HOU, D., ZHAO, T., JIN, Z. and LI, Z. Structure, Reactivity and Mechanical Properties of Water Ultra-Confined in the Ordered Crystal: A Case Study of Jennite. *Microporous and Mesoporous Materials*, 2015, vol. 204, pp. 106-114, ISSN 1387-1811.
171. BS EN 14216: 2004. Cement - Composition, Specifications and Conformity Criteria for very Low Heat Special Cements. European Commitee for Standartization (CEN). Brussels, Belgium 2004.

172. BS EN 1971-1: 2000. Cement - Part 1:Composition, Spesification and Conformity Criteria. British Standards Institution (BSI). London, United Kingdom 2004.
173. CIPRIOTI, S.V. and CATAURO, M. Synthesis, Structural and Thermal Behavior Study of Four Ca-Containing Silicate Gel-Glasses. *Journal of Thermal Analysis and Calorimetry*, 2016, vol. 123, no. 3, pp. 2091-2101, ISSN 1388-6150.
174. MELCHERT, M.B.M. et al. Simultaneous Solidification of Two Catalyst Wastes and their Effect on the Early Stages of Cement Hydration.*Journal of Thermal Analysis and Calorimetry*, 2011, vol. 105, no. 2, pp. 625-633, ISSN 1388-6150.
175. BULLARD, J.W., et al. Mechanisms of Cement Hydration.*Cement and Concrete Research*, 2011, vol. 41, no. 12, pp. 1208-1223, ISSN 0008-8846.
176. MOSTAFA, N.Y. and BROWN, P.W. Heat of Hydration of High Reactive Pozzolans in Blended Cements: Isothermal Conduction Calorimetry. *Thermochimica Acta*, 2005, vol. 435, no. 2.pp. 162-167, ISSN 0040-6031.
177. HAN, F., ZHANG, Z., WANG, D. AND YAN, P. Hydration Kinetics of Composite Binder Containing Slag at Different Temperatures. *Journal of Thermal Analysis and Calorimetry*, 2015, vol. 121, pp. 815-827, ISSN 1388-6150.
178. KLEMCZAK, B. AND BATOG, M. Heat of Hydration of Low-Clinker Cements. *Journal of Thermal Analysis and Calorimetry*, 2016, vol. 123, pp. 1351-1360, ISSN 1388-6150.
179. NAUMOV, V.N. and MUSIKHIN, A.E. Fundamental Characteristics of Solids from Low-Temperature Heat Capacity. *Computational Materials Science*, 2017, vol. 130. pp. 257-267, ISSN 0927-0256.
180. REDKIN, A., et al. Isobaric Heat Capacity of Molten Halide Eutectics. *Journal of Thermal Analysis and Calorimetry*, 2017, vol. 128, no. 1, pp. 621-626, ISSN 1388-6150.
181. ZADAVICIUTE, S., BANKAUSKAITE, A., BALTAKYS, K. and EISINAS, A. The Study of C_p Determination of Hydrotalcite Intercalated with Heavy Metal Ions. *Journal of Thermal Analysis and Calorimetry*, 2018, vol. 131, no. 1, pp. 521-527, ISSN 1388-6150.
182. NADERI, M. Progress in Filtration and Separation S. TARLETON ed., Oxford: Academic Press, 2015 Chapter Fourteen - Surface Area: Brunauer–Emmett–Teller (BET), 2015, pp. 585-608, ISBN 9780123847461.
183. ROUQUEROL, F. et al. Adsorption by Powders and Porous Solids Principles, Methodology and Applications. 2nd ed. academic press, 2012, ISBN 978-0-12-598920-6.
184. ALOTHMAN, A.Z. A Review: Fundamental Aspects of Silicate Mesoporous Materials. *Materials*, 2012, vol. 5, no. 12, pp. 2874-2902, ISBN 1996-1944.
185. LADAVOS, A.K., et al. The BET Equation, the Inflection Points of N2 Adsorption Isotherms and the Estimation of Specific Surface Area of Porous Solids.*Microporous and Mesoporous Materials*, 2012, vol. 151, pp. 126-133, ISSN 1387-1811.
186. BALTAKYS, K., SIAUCIUNAS, R. and KITRYS, S. Surface Microstructure and Specific Surface Area of Pure and Na Substituted Gyrolites. *Materials Science-Poland*, 2008, vol. 26, no. 3, pp. 633-645, ISSN 2083-1331.
187. KELLER, J.U. AND STAUDT, R. Gas Adsorption Equilibria Experimental Methods and Adsorptive Isotherms. Springer US, 2005, ISBN 978-0-387-23598-1.
188. GREGG, S.J. AND SING, K.S.W. Adsorption, Surface Area and Porosity. Berichte Der Bunsengesellschaft Für Physikalische Chemie, 1982, vol. 86, no. 10, pp. 957-957, ISSN 0005-9021.

LIST OF SCIENTIFIC PUBLICATIONS

Articles published in journals indexed in the Clarivate Analytics Web of Sciense with Impact Factor

1. Baltakys, Kęstutis; Eisinas, Anatolijus; Dambrauskas, Tadas. The influence of aluminum additive on the alpha-C_2S hydrate formation process // Journal of thermal analysis and calorimetry. ISSN 1388-6150.2015, vol. 121, iss. 1, p. 75-84.
2. Baltakys, Kęstutis; Dambrauskas, Tadas; Eisinas, Anatolijus; Šiaučiūnas, Raimundas. α-C_2SH synthesis in the mixtures with CaO/SiO_2=1.5 and application as a precursor for binder material // Scientia Iranica C. ISSN 1026-3098. 2016, vol. 23, iss. 6, p. 2800-2810.
3. Dambrauskas, Tadas; Baltakys, Kęstutis; Eisinas, Anatolijus; Šiaučiūnas, Raimundas. A study on the thermal stability of kilchoanite synthesized under hydrothermal conditions // Journal of thermal analysis and calorimetry. ISSN 1388-6150.2017, vol. 127, iss. 1, p. 229-238.
4. Dambrauskas, Tadas; Baltakys, Kęstutis; Škamat, Jelena; Kudžma, Andrius. Hydration peculiarities of high basicity calcium silicate hydrate samples // Journal of Thermal Analysis and Calorimetry. ISSN 1388-6150.2018, Vol. 131, iss. 1, p. 491-499.
5. Dambrauskas, Tadas; Baltakys, Kęstutis; Eisinas, Anatolijus. Formation and thermal stability of calcium silicate hydrate substituted with Al^{3+} ions in the mixtures with CaO/SiO_2 = 1.5 // Journal of Thermal Analysis and Calorimetry. ISSN 1388-6150.2018, Vol. 131, iss. 1, p. 501-512.
6. Dambrauskas, Tadas; Baltakys, Kęstutis. Part 1: A study on the properties of synthetic hydroxyledgrewite // Journal of the American Ceramic Society. ISSN 0002-7820.2018, vol. 101, iss. 8, p. 3710-3718.

Publications in other international databases

1. Baltakys, Kęstutis; Dambrauskas, Tadas; Eisinas, Anatolijus. The synthesis of α-C_2S hydrate substituted with Al^{3+} ions in mixture with CaO/SiO_2= 1.75 // Solid state phenomena: Powdered substances and particulate matter in industry and environmental. ISSN 1012-0394. 2016, vol. 244, p. 26-33.

Articles published in conference proceedings

1. Dambrauskas, Tadas; Baltakys, Kęstutis; Eisinas, Anatolijus. Formation and thermal stability of calcium silicate hydrate substituted with Al^{3+} ions in the mixtures with CaO/SiO_2 = 1.5 // Proceedings of international conference of thermal analysis and calorimetry in Russia (RTAC-2016), 16-23 September, 2016, Saint-Petersburg, Russia. 2016. ISBN 9785742254478. p. 199-201.
2. Dambrauskas, Tadas; Baltakys, Kęstutis; Škamat, Jelena; Kudžma, Andrius. Hydration peculiarities of high basicity calcium silicate hydrate samples //

Proceedings of international conference of thermal analysis and calorimetry in Russia (RTAC-2016), 16-23 September, 2016, Saint-Petersburg, Russia. 2016. ISBN 9785742254478. p. 197-199.

Patents registered at National patent office

1. Šiaučiūnas, Raimundas; Baltakys, Kęstutis; Eisinas, Anatolijus; Dambrauskas, Tadas. Bevandenių kalcio silikatų gamybos būdas ir tuo būdu gautas bevandenis kalcio silikatas = Anhydrous calcium silicate production method and thus obtained anhydrous calcium silicate / applicant: Kaunas University of Technology. LT 6284 B. 2016-05-25.42 p.

Publications of International Scientific Conferences

1. Baltakys, Kestutis; Dambrauskas, Tadas. Kilchoanite, α-C_2SH and hydroxyledgrewite: hydrothermal synthesis and thermal stability // BaltSilica 2018: 8th international conference on silicate materials, May 30 – June 1, 2018, Riga, Latvia. Riga: RTU Publishing House. ISSN 2243-6057. 2018, I1, p. 20-21.
2. Knabikaite, Inga; Palou, Martin T.; Baltakys, Kestutis; Dambrauskas, Tadas. Phase transformation in $CaO-SiO_2-Al_2O_3-H_2O$ system under hydrothermal conditions at 200 °C at the CaO/SiO_2 ratio 1.5 // BaltSilica 2018: 8th international conference on silicate materials, May 30 - June 1, 2018, Riga, Latvia. Riga: RTU Publishing House. ISSN 2243-6057. 2018, P31, p. 121-122.
3. Дамбраускас, Т.; Балтакис, К.; Шяучюнас, Р.; Мечай, А. Свойства вяжущего на основе αC_2SH и кварца // Сотрудничество - катализатор инновационного роста : сборник материалов 3-го Белорусско-Прибалтийского форума (Минск, 19-20 октября 2017 г.). Минск: Белорусский национальный технический университет, 2017. ISBN 9789855831304. p. 73-74.
4. Dambrauskas, Tadas; Baltakys, Kęstutis. Microcalorimetric study on α-C_2SH and quartz samples // 18th international conference-school Advanced materials and technologies, 27-31 August 2016, Palanga, Lithuania. Kaunas: Kauno technologijos universitetas. ISSN 1822-7759.2016, p. 125.
5. Dambrauskas, Tadas; Baltakys, Kęstutis. The effect of calcium-based compounds on the formation of calcium silicate hydrates // BaltSilica 2016: 7th Baltic conference on silicate materials, 26-27 May 2016, Kaunas, Lithuania. Kaunas: Kauno technologijos universitetas. ISSN 2243-6057.2016, p. 75.
6. Baltakys, Kęstutis; Dambrauskas, Tadas; Eisinas, Anatolijus. The synthesis of α-C_2S hydrate substituted with Al^{3+} ions in mixture with CaO/SiO_2 = 1.75 // Particulate solids in science, industry and the environment 2015. Kosice: Technical University of Kosice, 2015. ISBN 9788055322032.p. 40.
7. Baltakys, Kęstutis; Dambrauskas, Tadas; Eisinas, Anatolijus; Šiaučiūnas, Raimundas. A study on the thermal stability of kilchoanite synthesized under hydrothermal conditions // 3rd Central and Eastern European conference on

thermal analysis and calorimetry, CEEC-TAC3: 25-28 August 2015, Ljubljana, Slovenia. Rostock: Greifswald, 2015. ISBN 9783940237347.p. 295.

Acknowledgments

There are no proper words to convey my deep gratitude and respect for my supervisor professor Kęstutis Baltakys for his support and encouragement during this doctoral project. It was a real privilege to have a supervisor who not only cared so much about my work, shared his scientific knowledge but also showedhis extraordinary human qualities.

I would also like to thank R. Šiaučiūnas, S. Kitrys and A. Eisinas for their support, professional comments and valuable remarks. I am grateful to all of my friends and colleagues from the Department of Silicate Technology, and especially to A. Bankauskaitė for her continued support and friendship. They all contributed to the success of this project in very different ways.

I would like to thank the Research Council of Lithuania and Kaunas University of Technology not only for providing the funding, but also for giving me the opportunity to attend conferences.

I deeply thank my family who believed in me and wanted the best for me. Finally, I would like to thank my wife Vaida Dambrauskienė who never asked me to give up working or even enquired how long I planned to work; she has always loved me and supported every choice of mine. Thank you so much, my dear.

SL344. 2019-03-20, 13,75 leidyb. apsk. l. Tiražas 18 egz. Užsakymas 68
Išleido Kauno technologijos universitetas, K. Donelaičio g. 73, 44249 Kaunas
Spausdino leidyklos „Technologija“ spaustuvė, Studentų g. 54, 51424 Kaunas